AEC RESEARCH AND DEVELOPMENT REPORT

ORNL-2685
C-84 - Reactors-Special
Features of Aircraft Reactors

Cy. 22A

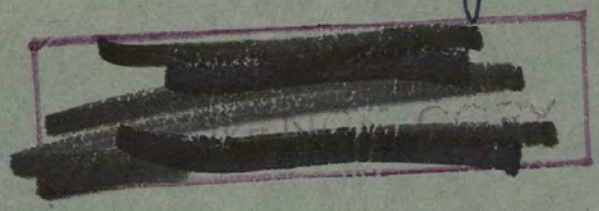

ANP MATERIALS MEETING

NOVEMBER 16-18, 1954

OAK RIDGE NATIONAL LABORATORY
operated by
UNION CARBIDE CORPORATION
for the
U.S. ATOMIC ENERGY COMMISSION

[redacted]

ORNL-2685

This document consists of 168 pages.
Copy 22 of 212 copies. Series A.

Contract No. W-7405-eng-26

METALLURGY DIVISION

ANP MATERIALS MEETING

NOVEMBER 16-18, 1954

DATE ISSUED

MAR 12 1959

OAK RIDGE NATIONAL LABORATORY
Oak Ridge, Tennessee
operated by
UNION CARBIDE CORPORATION
for the
U.S. ATOMIC ENERGY COMMISSION

[redacted]

[redacted]

FORWARD

The following papers were presented by members of the Metallurgy Division of the Oak Ridge National Laboratory at the ANP Materials Meeting, Wright Air Development Center, Dayton, Ohio, November 16-18, 1954. The papers presented at this meeting originally were to be published in a Proceedings, but this plan was later abandoned. Since much of the material has not appeared in print elsewhere, we are taking this opportunity to disseminate the information as it was presented in 1954.

[redacted]

CONTENTS

[redacted]

[redacted]

MATERIALS FOR PUMP BEARINGS, VALVES, AND SEALS FOR FLUORIDES AND SODIUM

W. H. Cook
E. E. Hoffman

In searching for materials for bearings, valves, and seals for operation in molten fluoride salt or sodium systems at elevated temperatures, metals and metal alloys were found to be unsatisfactory. The metals and metal alloys are not satisfactory because of their high wear rates, galling, and self-welding. The hard, refractory ceramics and cermets appear to be possible materials for solving these problems. As a result of the lack of ductility and low impact strength of the ceramics, the cermets seem to offer the most promise for these applications. The most common commercial cermets are metal carbides with a metal binder. Even if no ceramics are found which are satisfactory for pump shaft bearings, valves, or seals, they have many other potential reactor applications, and the corrosion resistance of these materials in the environments of interest is essential information. The tests to be discussed are a part of the initial corrosion investigation, and how these materials might be used in the fabrication of the pump units themselves was not an objective of these screening tests in fluoride and sodium.

Tests:

The screening tests were conducted in the following manner. The specimens were loaded into Inconel containers along with the sodium or fluoride bath. Fluorides 27, 30, and 44 used in these tests are various compositions of the $NaF-ZrF_4-UF_4$ ternary system. The loading and sealing of the containers was always done in a helium-atmosphere dry box to avoid contamination of the bath material. Inconel containers were chosen because, at the time, it seemed most probable that a nickel-base alloy of the Inconel type would be used for the plumbing

[redacted]

in the circulating-fuel-reactor experiment. The tests were either static or dynamic and were conducted for 100-hr test periods at 1500°F. In the dynamic tests, the specimen was retained in the hot-zone region of an Inconel tube, while the tube rocked up and down in a "seesaw"-type furnace. In this test, the bath travels from one end of the tube to the other as the furnace rocks. The ends of the tube are held at different temperatures to simulate, in a crude fashion, the temperature differentials which are to be encountered in an actual reactor system. In these tests, the hot zone is held at 1500°F and the cold zone at 1200°F, giving a 300°F temperature differential.

The extent of corrosion was determined by weight and dimensional changes, macroscopic examination, and whenever possible, microscopic examinations. Chemical and x-ray analyses were made where necessary on the corrosion media and the specimens. The most reliable criterion for evaluation was microscopic examination of as-received and tested specimens and this was used where possible.

Ceramics:

Most of the ceramics were statically tested in fluorides and sodium because static corrosion was usually severe enough to make a classification on this basis possible. Table I is a list of the borides, carbides, nitrides, oxides, silicates, and miscellaneous ceramics tested in fluorides and sodium. These materials underlined by a solid line had good resistance; good resistance being arbitrarily defined as less than 0.5% dimensional or weight change or less than 2 mils attack where microscopic examination was possible. Those materials which had fair resistance are underlined by a dashed line and were attacked from 2 to 5 mils. Those not underlined had poor resistance and were partially or completely dissolved.

TABLE 1 CERAMICS TESTED IN SODIUM AND FLUORIDES AT 1500°F FOR 100 HOURS

Sodium	Fluoride No. 44	Sodium	Fluoride No. 44
		Barium Titanate $BaTiO_3$	-
-	TiB_2 *		
-	ZrB_2 *	Cordierite $Mg_2Al_4Si_5O_{18}$	-
	Mo_2B *		
B_4C	B_4C	Spinel $Mg\ Al_2O_4$**	Spinel $Mg\ Al_2O_4$ 2/**
SiC	SiC		
TiC	TiC	Fosterite $Mg_2\ SiO_4$	-
ZrC	ZrC		
Cr_3C_2	Cr_3C_2	Zircon $Zr\ SiO_4$	-
-	WC 1/		
BN	BN	Porcelain	-
TiN	TiN		
Si_3N_4	Si_3N_4	Silica Glass	-
	-	Pyrex Glass	-
		Lead Glass	-
BeO			
MgO**	MgO**	Graph-i-tite	Graph-i-tite 2/
Al_2O_3***	Al_2O_3**		
TiO_2	-		
ZrO_2	ZrO_2		
HfO_2	-		
Sm_2O_3	Sm_2O_3		
Gd_2O_3	-		
ThO_2			

1/ This material was tested in fluoride No. 27 rather than fluoride No. 44
2/ This material was tested in fluoride No. 30 and also fluoride No. 44
* This material was dynamically tested.
** The specimen was taken from a synthetic single crystal.
*** Specimens were from a synthetic single crystal of α-Al_2O_3 and a sintered Al_2O_3 shape.

[redacted]

As may be seen in Table I, all the carbides tested in sodium had good resistance with the exception of B_4C. All the nitrides tested in sodium had good resistance. Five of the oxides tested had good resistance to sodium, while Sm_2O_3 had only fair resistance to attack.

In the fluoride tests, the borides of titanium and zirconium and the carbides of titanium, silicon, chromium, and tungsten had good corrosion resistance. Zirconium carbide, boron nitride, titanium nitride and Si_3N_4 had only fair resistance. Graph-i-tite, which is a high-density-type graphite prepared by repeated tar impregnation and firing, had good resistance to the fluoride salt but poor resistance to sodium. As may be seen in Fig. 1 (Y-13282), the fluoride salt did have a tendency to penetrate the Graph-i-tite in a narrow band along the surface.

These tests indicated that the corrosion resistance of ceramic specimens could be increased by avoiding glassy phases. In other words, well-crystallized samples were found to possess the maximum corrosion resistance. Corrosion resistance was also found to improve with reductions in the porosity of the specimens, as might be expected.

Cermets:

Silicon carbide impregnated with silicon represents a physical transition between ceramics and cermets in that it is a ceramic, SiC, bonded with a non-metal, silicon, in a manner similar to that of the true cermets. Tests on this material in sodium and fused fluoride salt result in very heavy attack due to removal of the silicon as may be seen in Fig. 2 (Y-13596). The silicon carbide grains were not attacked in either the sodium or the fluoride test.

In seeking cermets with good wearing qualities plus high strength at elevated temperatures, the cermets most readily available and with established

[redacted]

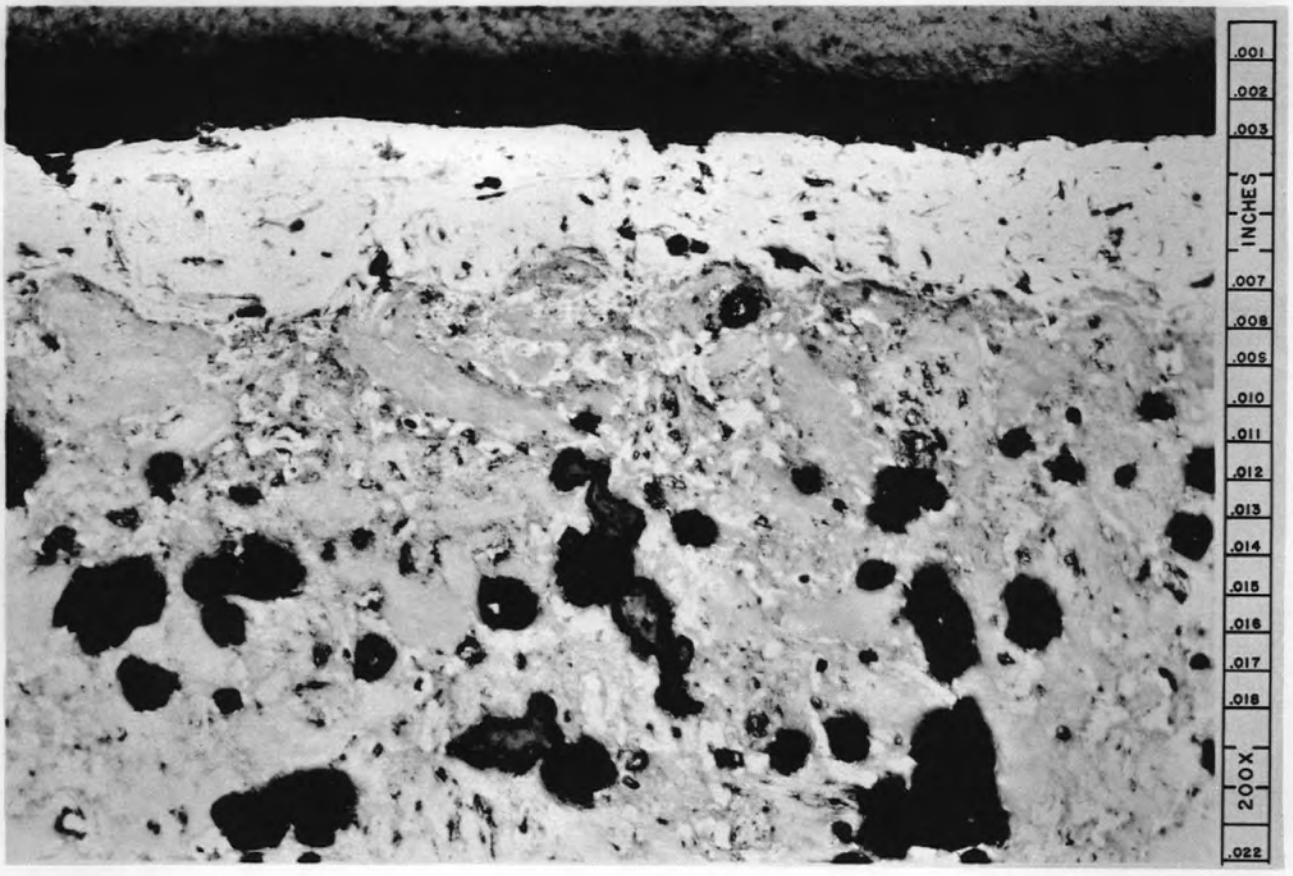

Fig. 1 (Y-13282) Penetration of Graph-i-tite by Fluoride No. 44 During 100-hr Test at 1500°F. The penetration was erratic from 0 to 5 mils. Unclassified - [redacted] with caption.

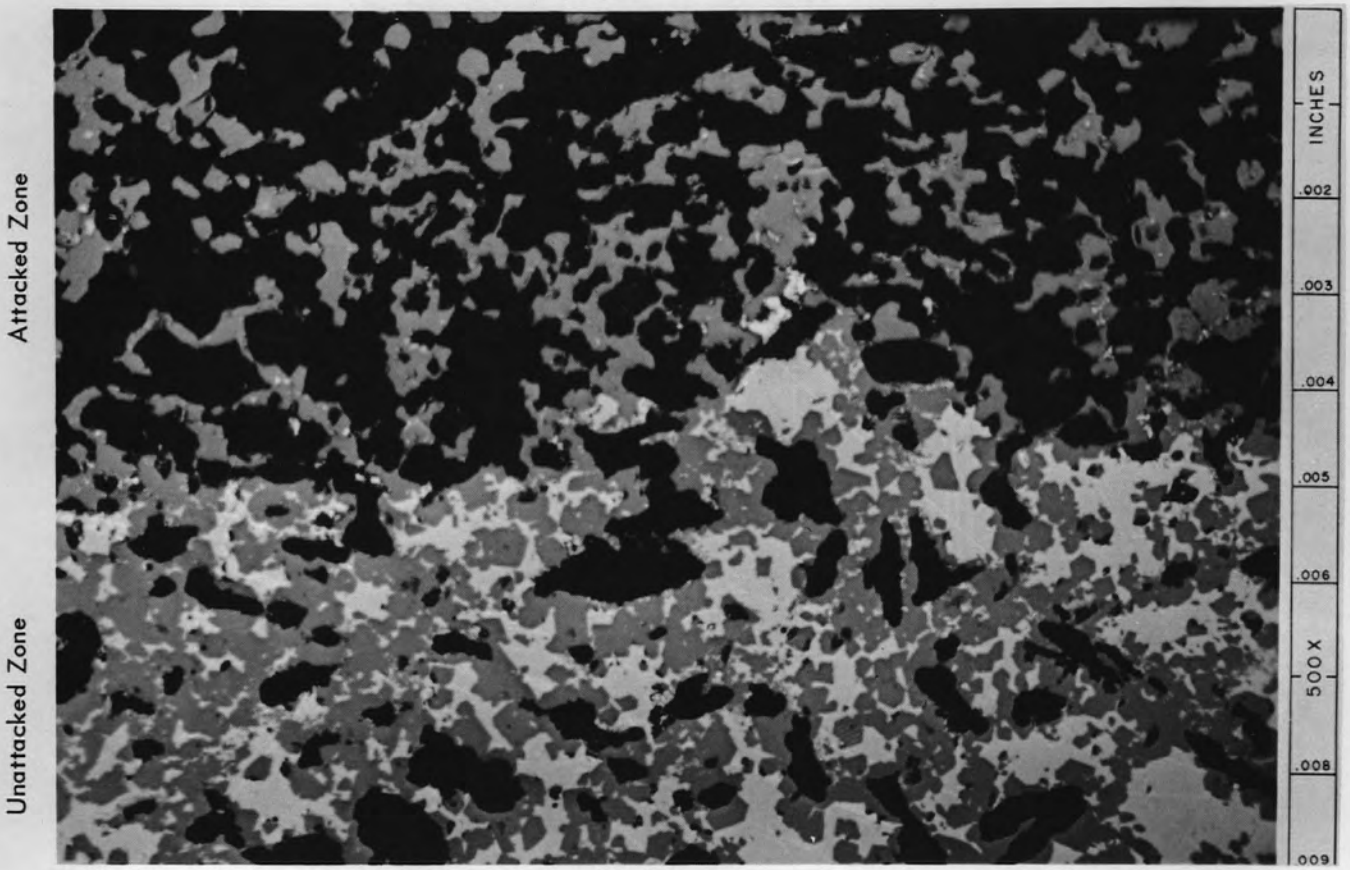

Fig. 2 (Y-13596) SiC-Si (Durhy) Tested in Fluoride No. 44. The top half of the picture is the attacked zone; note that the silicon (the light white phase) has been removed. The gray material is SiC and the black areas are voids. Unclassified - [redacted] with caption.

[redacted]

fabrication techniques were the cutting tools and associated materials. The basic materials in this category are tungsten carbide with cobalt binder and titanium carbide with either cobalt or nickel binder. In the static tests of ceramic materials, the tungsten carbide and titanium carbide specimens were not attacked by either sodium or fluoride No. 44. Consequently, all subsequent tests were dynamic in an effort to determine, at least, the relative corrosion resistance of the various cermets. The fluoride pump bearings, valves, and seals have been of primary interest; therefore, very few tests have been conducted on these materials in sodium.

Table IIa lists some of the tungsten carbide cermets commercially available plus three recently developed cermets that have been dynamically tested. The first column on the left gives the commercial designation of these cermets; the depth of attack in mils is given for each corrosive bath. With the exception of the 23 Al_2O_3-77 Cr and the 83 Cr_3C_2 - 2 WC - 15 Ni, none of these cermets were attacked. Figure 3 (Y-12679, Y-12680) shows the "before and after test" appearance of the 97.5 WC - 2.5 Co (D4675).

Although tungsten carbide cermets had satisfactory corrosion resistance in these tests, the fact that titanium carbide is lighter, harder, more oxidation resistant, and in cutting tools has higher "welding-in" temperatures than tungsten carbide, makes it more attractive as a possible material for the pump bearings, valves, or seals. The cobalt-bonded and nickel-bonded titanium carbide cermets that have been corrosion tested are listed in Table IIb. As may be seen in the table, nearly all the tests have been performed in fluoride 30 and 44. The fluoride 44 tests are the latest and, therefore, these results are the most reliable. Both the technique used to polish the specimens prior to

[redacted]

TABLE II CERMETS DYNAMICALLY TESTED IN FLUORIDES AND SODIUM

(a)

Designation	Composition	Fluoride: Na	14	27	30	44
		Depth of attack, mils				
K. D4675 [1]	97.5 WC - 2.5 Co				1	0
A. Grade AA [2]	97 WC - 3Co				0	
V. Grade 2A7 [3]	95.5 WC - 4.5 Co				0	
A. Grade A	94 WC - 6 Co				0	
V. Grade 2A3	89 WC - 11 Co				0	
C. 44A [4]	94 WC - 6 Co			0*		
C. 55A	87 WC - 13 Co			0*		
V. Grade EE	80 WC - 10 TiC-10Co				0	
V. Grade EH	54 WC - 40 TiC-6 Co				0	
A. Grade GG	60 WC - 28 TaC-12Co			1		
C. 907	74 WC - 20 TaC-6 Co			0*		
M. LT-1 [5]	23 Al_2O_3 - 77 Cr			failed		
C. 608	83 Cr_3C_2-2WC-15NI			4		
----	80 ZrC-20Fe	0*	0*			

(b)

Designation	Composition	Fluoride: Na	14	27	30	44
		Depth of attack, mils				
K138A	65 TiC-20 Co-15NbTaTiC$_3$				½-1	
(1) [6]	50 TiC-50 Co-base binder				½-2	
(4)	48 TiC-52 Co-base binder				1	
K150A	80 TiC-10 Ni-10NbTaTiC$_3$				1	0
K151A	70 TiC-20 Ni-10NbTaTiC$_3$				1½-2	0
K152B	64 TiC-30 Ni-6NbTaTiC$_3$				6	0
K153B	54 TiC-40 Ni-6NbTaTiC$_3$				2	0
K161B	TiC Ni Mo				4-7	0
K162B	64 TiC-25 Ni-5Mo-6NbTiC$_3$				3	
---	65 TiC-20Ni-15NbTaC$_2$	0*	0*	5*	0	
FS-27	43 TiC-50Ni-7Cr_3C_2				9	0
(5)	48 TiC-52Ni-base binder				2-5	
(8)	48 TiC-52Ni-base binder				0	
(10)	47 TiC-53Ni-base binder				2	
					5	

1/ All designations prefixed with a "K" are materials of Kennametal Inc., Latrobe, Pa.
2/ All designations prefixed with an "A" are materials of Adamas, Harrison, N. J.
3/ All designations prefixed with a "V" are materials of Vascoloy Ramet.
4/ All designations prefixed with a "C" are materials of Carboloy, Detroit, Mich.
5/ This is a metamic specimen.
6/ All designations of numerals enclosed in brackets denote Sintercast Corp., Yonkers, N. Y.
* This is a static test result.

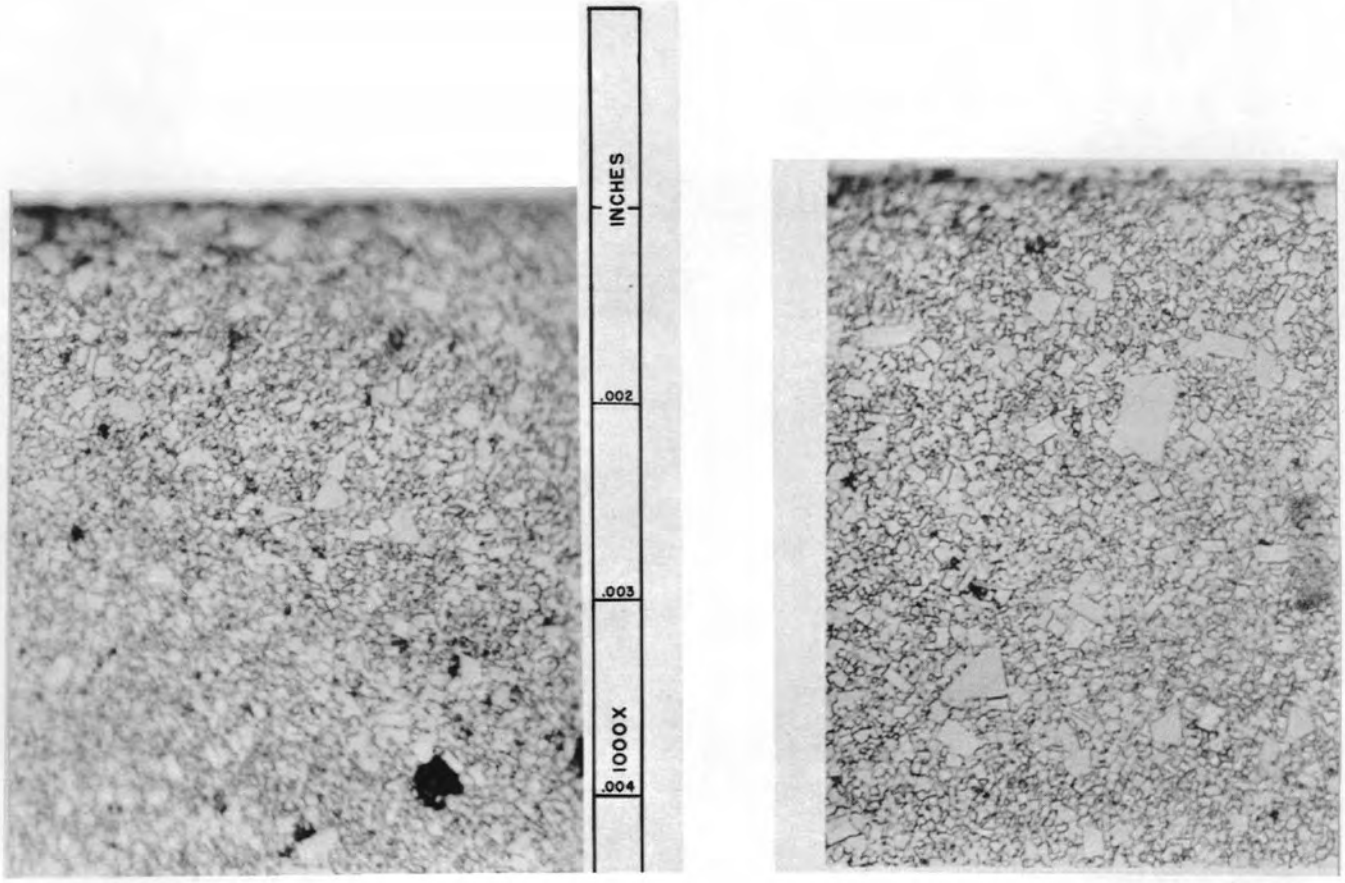

Y-12679 1000 X
$KOH-K_3Fe(CN)_6$
As-Received

Y-12680 1000 X
$KOH-K_3Fe(CN)_6$
Tested in
Fluoride No. 44

Fig. 3 D-4675 (97.5 WC - 2.5 Co) Specimens Nickel Plated to Protect Edges During Metallographic Polishing. Unclassified [redacted] with caption.

examination and increased purity of the fluoride fuels used have contributed to this apparent improvement in corrosion resistance. All the titanium carbide-nickel bonded specimens indicated in the fluoride 44 column have been tested dynamically, employing several different temperature gradients, and none were found to be attacked. Typical structures and the appearance of the specimens before and after test may be seen in Fig. 4 (Y-13586), (Y-13587). This is the Kennametal cermet K162B with a composition of 64% TiC-25% Ni-5%Mo-6% $NbTaTiC_3$. It is now planned to increase the severity of the dynamic tests until (1) the cermets can be classified corrosion-wise, and (2) if possible, determine the nature of the corrosion.

After a material has passed the sodium and fluoride corrosion tests, further evaluation of it for pump bearings, valves, and seals are made by W. C. Tunnell of the Oak Ridge National Laboratory's Experimental Engineering Group. The testing apparatus, the Bearing Materials Compatibility Tester, shown in Fig. 5, consists of a:

> "2-3/4-inch-diameter, 1/2-inch-thick plate specimen of one material that rotates against a 1/2-inch-diameter stationary pin of another or the same material. The end surface of the pin is ground to a 1/2-inch-radius cylinder to approximate line contact along a radial line of the rotating plate at a mean radius of 1 inch from its center. [redacted] contact pressure between the plate and pin is maintained by means of an external coil spring and a sliding shaft.[1]"

In tests, it was found that a load of ten pounds was necessary to break through the hydromatic film. This, then, gave an estimated stress in the line of

[1] ANP Quarterly Progress Report, December 10, 1953, ORNL-1649, p 25.

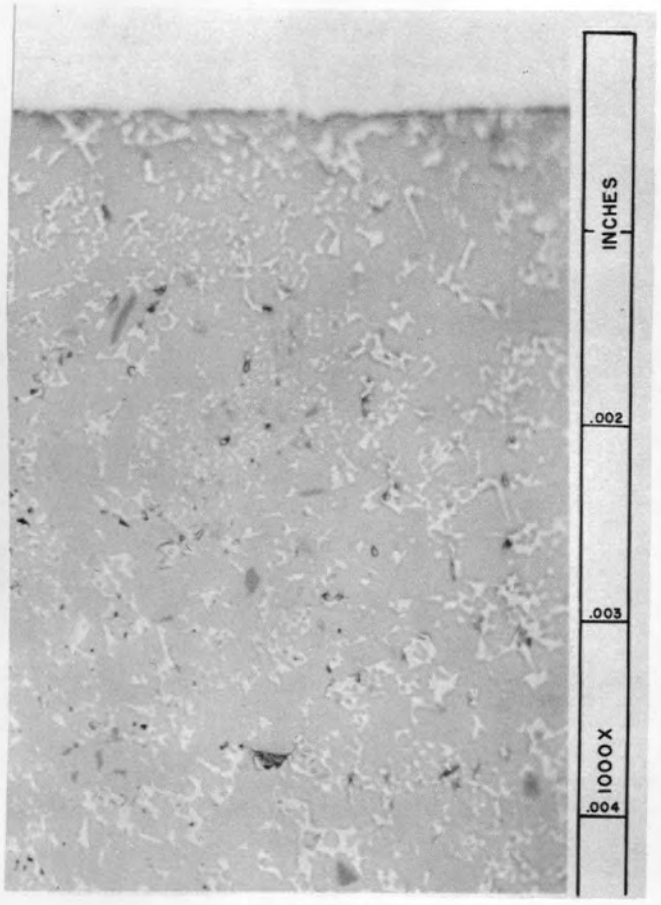

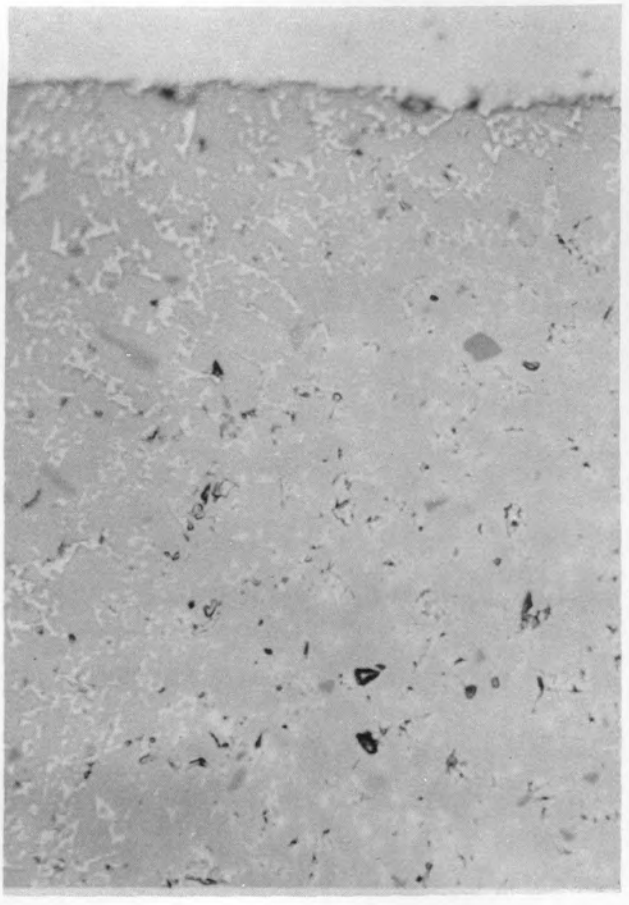

Y-13586 1000X
No Etch As-Received

Y-13587 1000X
No Etch Tested in Fluoride No. 44

Fig. 4 K162B (64% TiC-25% Ni-5% Mo-6% NbTaTiC_3) Specimens Nickel Plated to Protect Edges During Metallographic Polishing. Unclassified [redacted] with caption.

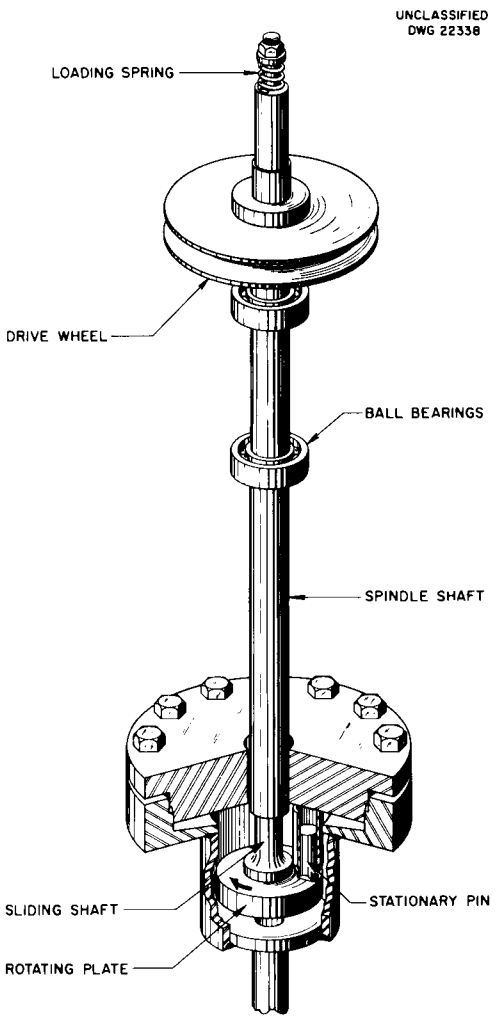

Fig. 5 (CF-2698) Bearing Materials Compatibility Tester

contact of approximately 15,000 psi. The rate of rotation is 850 RPM which gives a sliding speed of approximately 7.4 feet per second. During a two-hour test period the pin and rotating plate are submerged in the molten media, sodium or fluorides, at a temperature of 1200°F. At the conclusion of the tests the plate and pin were examined for wear and corrosion. As a result of this test, tungsten carbide and titanium carbide cermets appear to be the most promising possible bearing materials tested to date.

EFFECT OF ENVIRONMENT ON CREEP PROPERTIES OF HIGH TEMPERATURE ALLOYS

R. B. Oliver
D. A. Douglas
J. H. DeVan

The selection of the best material for the construction of a high-temperature reactor of the circulating-fuel type is one of the most difficult problems which confronts the Aircraft Nuclear Propulsion Program. The specifications for such an alloy are very restrictive in that it must have economical nuclear properties; it must have good fabrication characteristics; it must have adequate high-temperature strength; and as a corollary to this, it must be compatible with the various liquid metals, gases, and fused salts with which it will be in contact. Most of the alloys commonly used for high temperature applications fail to meet one or more of the above requirements, and through a process of elimination, a nickel-base alloy (Inconel) was selected as a promising material. For the past several years, the Metallurgy Division at the Oak Ridge National Laboratory has been evaluating the potentialities of this alloy. In line with this program, the Mechanical Testing Group has been studying its high-temperature strength. Since Inconel is no stranger to high-temperature applications, there are considerable data on its creep strength already available in the literature. Unfortunately, almost all of these data are based on tests in air, and it is considered most unwise to use such information for design purposes when the actual operating conditions involve reducing and corrosive environments.

Figure 6 illustrates the validity of this thought. It can be seen that not only the reducing and corrosive environments, but also a neutral environment (argon) results in much shorter rupture times than is experienced in air. Figure 7 is a cutaway view of the test chamber used for the creep tests in gaseous atmospheres.

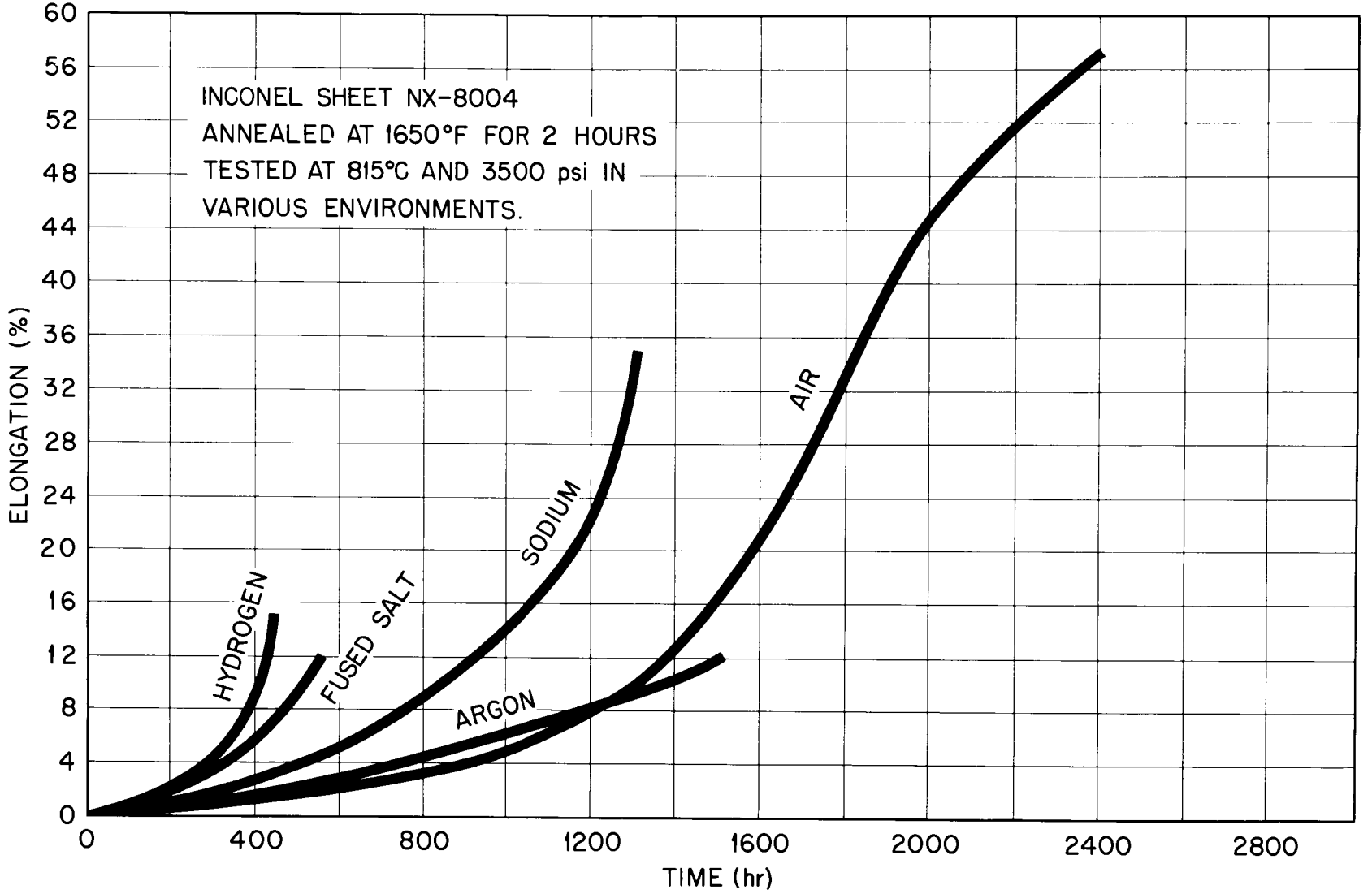

Fig. 6 (Y-14035) Strain vs. Time Plot for Inconel in Several Environments.
Classification [redacted]

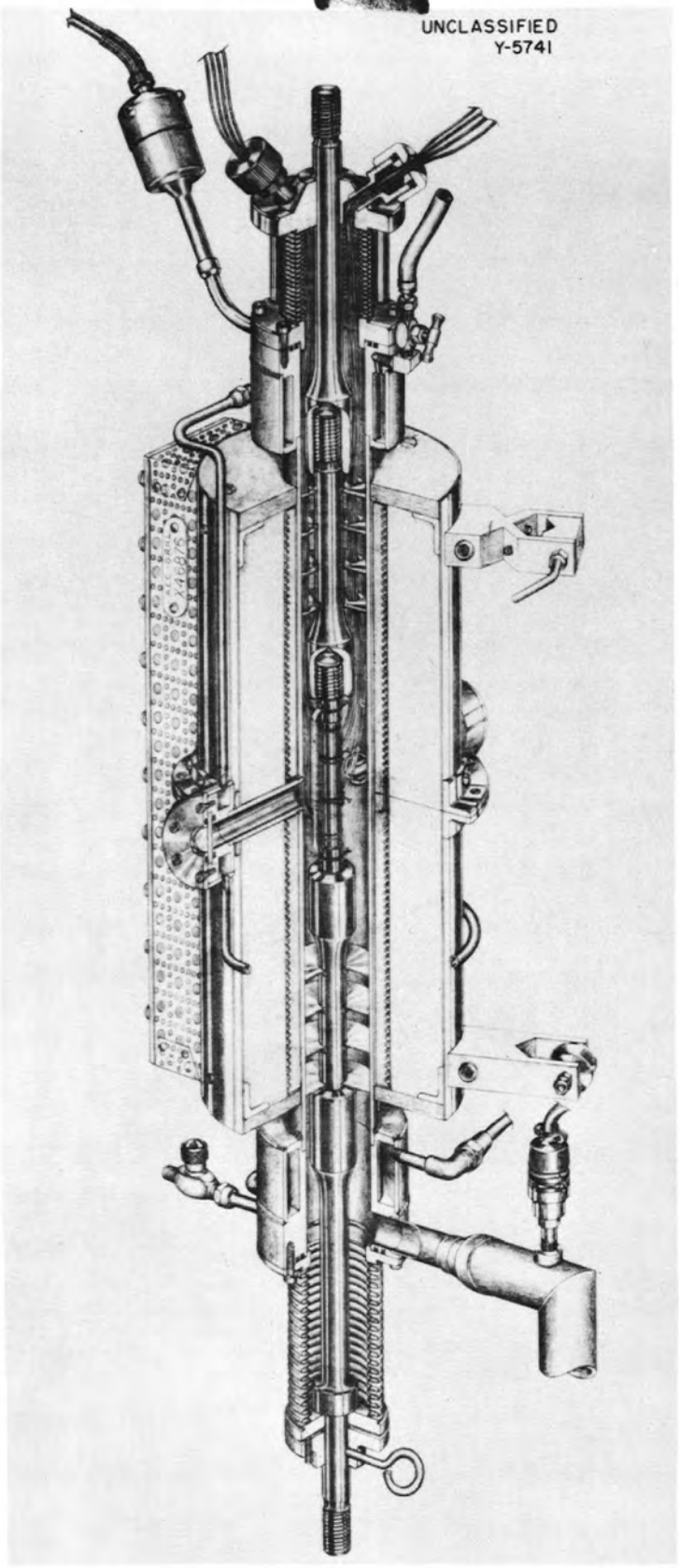

Fig. 7 (Y-5741) Creep Testing Chamber for High Purity Gaseous Environments.

[redacted]

Figure 8 shows the component parts of the test apparatus used for testing specimens in liquid-metal and fused-salt environments. Figure 9 is a plot of stress-rupture data for Inconel in the fused fluoride salts, which are the fuel carrier in the circulating-fuel reactor. Both the stress and time parameters are plotted on log scales so that a wide range of values can be shown. Such a plot is commonly referred to as a "design curve", and for any given stress it enables one to predict at what time a certain strain will be reached or when failure will occur. Calculations of service stresses for the circulating fuel reactor estimate a maximum stress of about 1000 psi. The rupture curve from this plot shows a substantial safety factor in the direction of either stress or time.

Figure 10 compares the rupture life of Inconel specimens in the fused salts and in argon at 1300, 1500, and 1650°F. It can be seen that the specimens tested in the salts show shorter rupture life than those tested in argon. This decrease in strength is the result of the corrosive effect of fluorides on Inconel. The effect of such important variables as temperature and stress on this corrosion rate is of considerable interest to us. The data shown here indicate that the least reduction in rupture life has been at 1300°F. Thus, it would appear that the corrosion rate of Inconel in the fused salts is somewhat temperature-dependent. However, the effect of the other variable, stress, is more difficult to analyze.

Figure 11 shows two pieces of Inconel--one from the gage of a test specimen, and one from an unstressed coupon which was hung next to the specimen during test. The stressed specimen appears to show considerably more attack, as evidenced by the depth of the void formation. This would lead one to believe that stress accelerates the corrosion. This test was at 3500 psi, and the specimens were exposed to the salt at 1500°F for 550 hr.

[redacted]

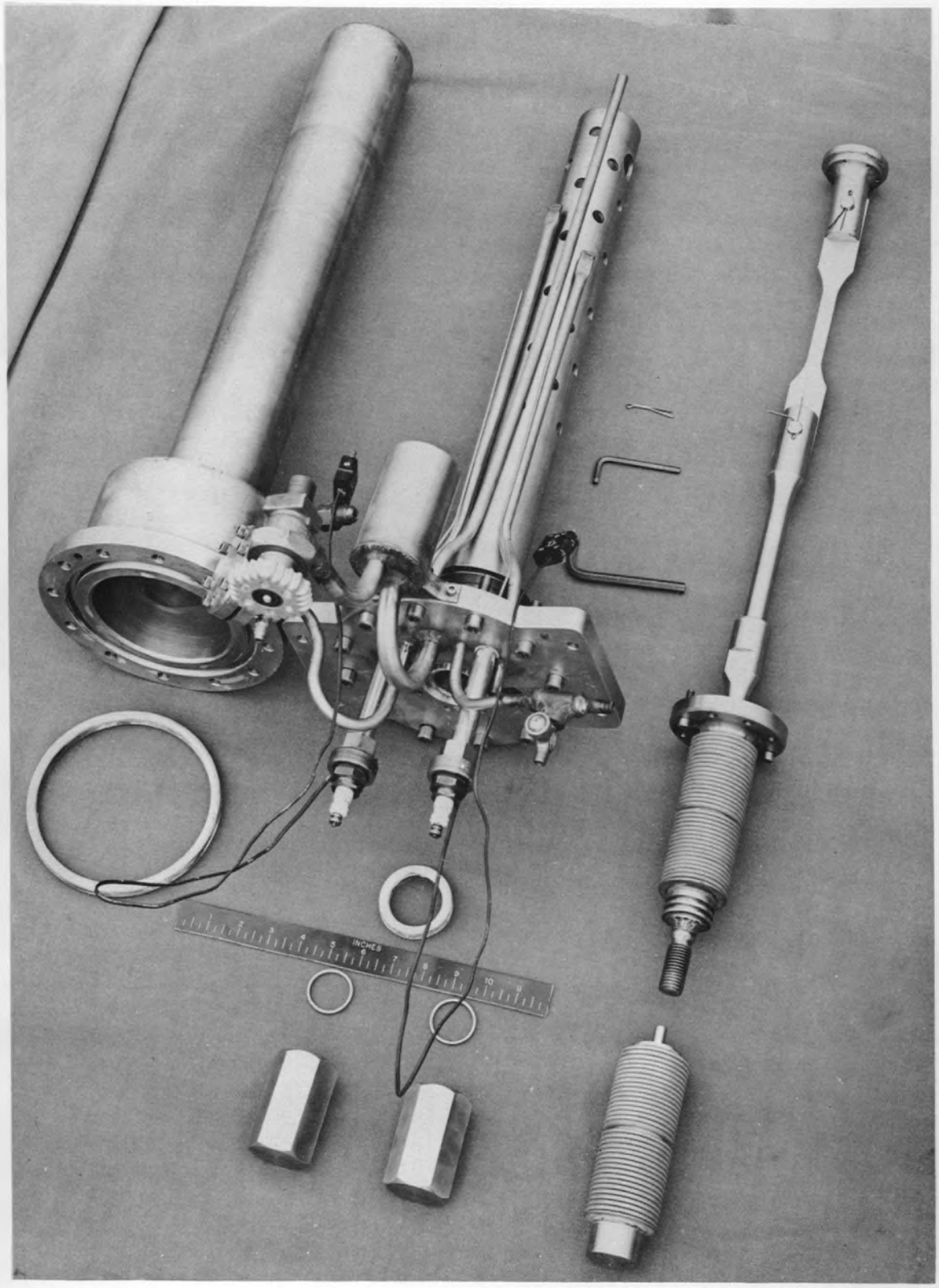

Fig. 8 (Y-5620) Component Parts of Creep Testing Chamber for Liquid-Metal Environments. Unclassified.

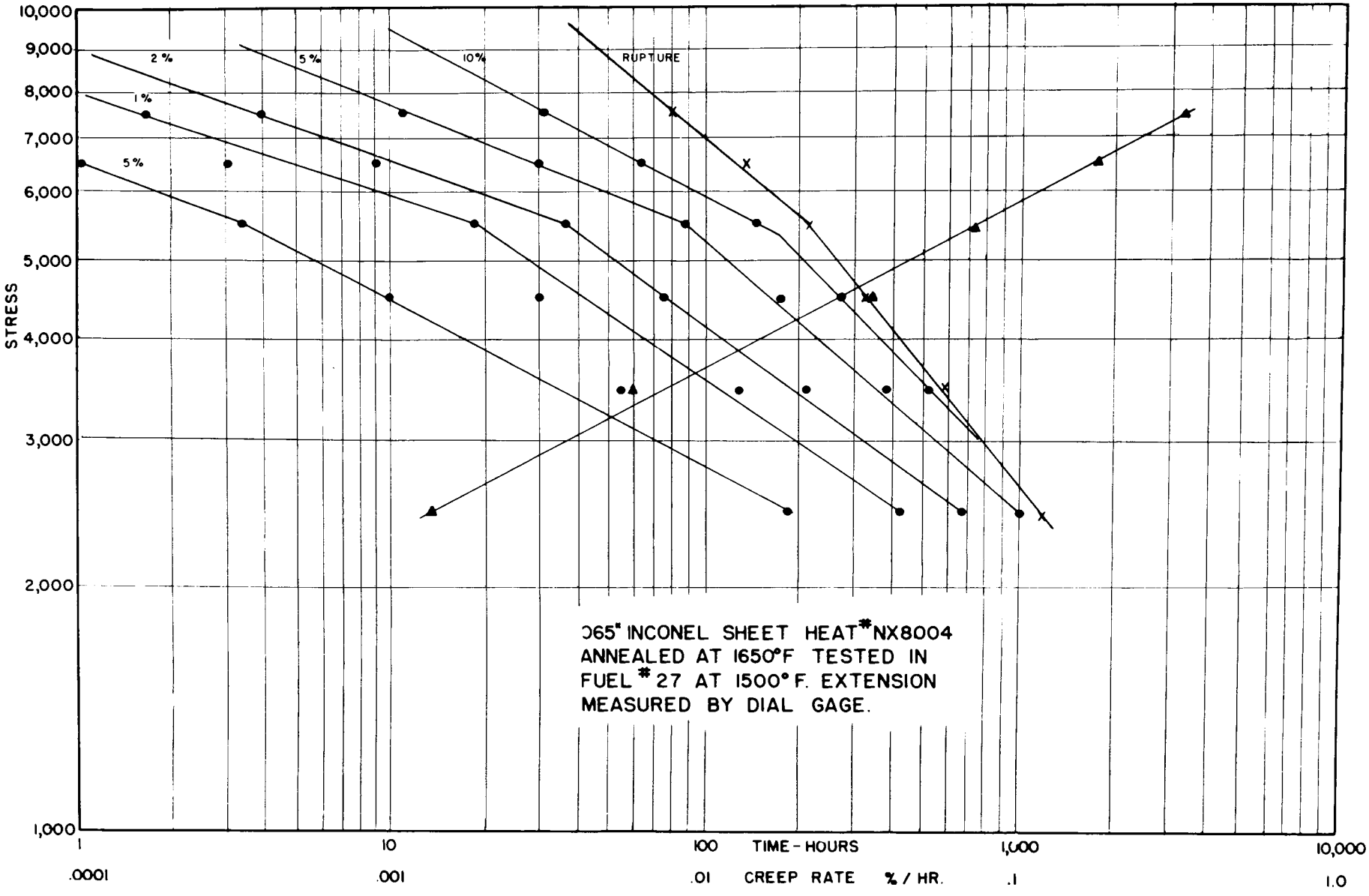

Fig. 9 (Y-9832) Design Curve for Inconel at 1500°F in a Fused Salt Environment. [redacted] with caption.

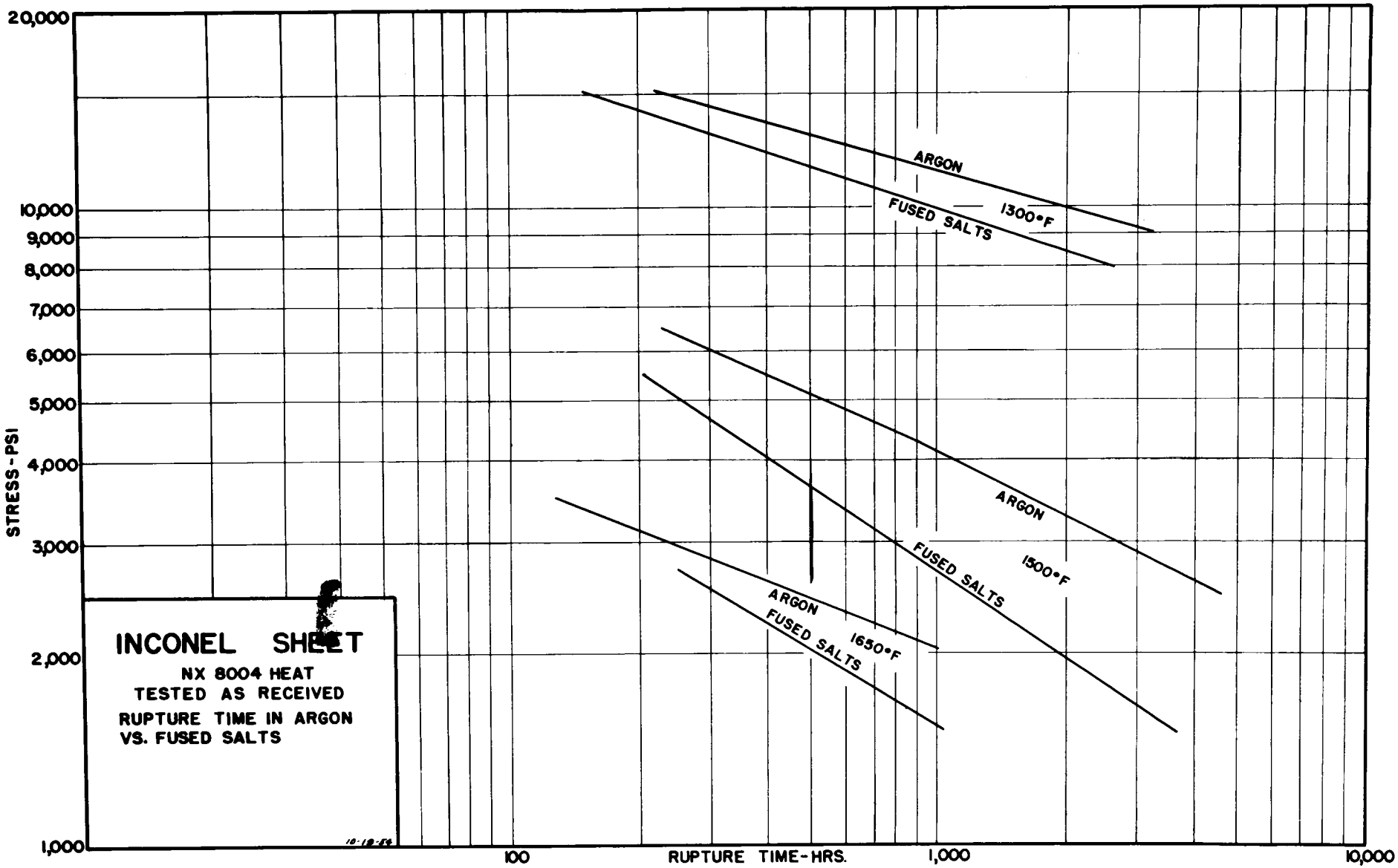

Fig. 10 (Y-13441) A Comparison of Rupture Life of Inconel in Fused Salt and Argon at 1300, 1500, and 1650°F.
Classification [redacted]

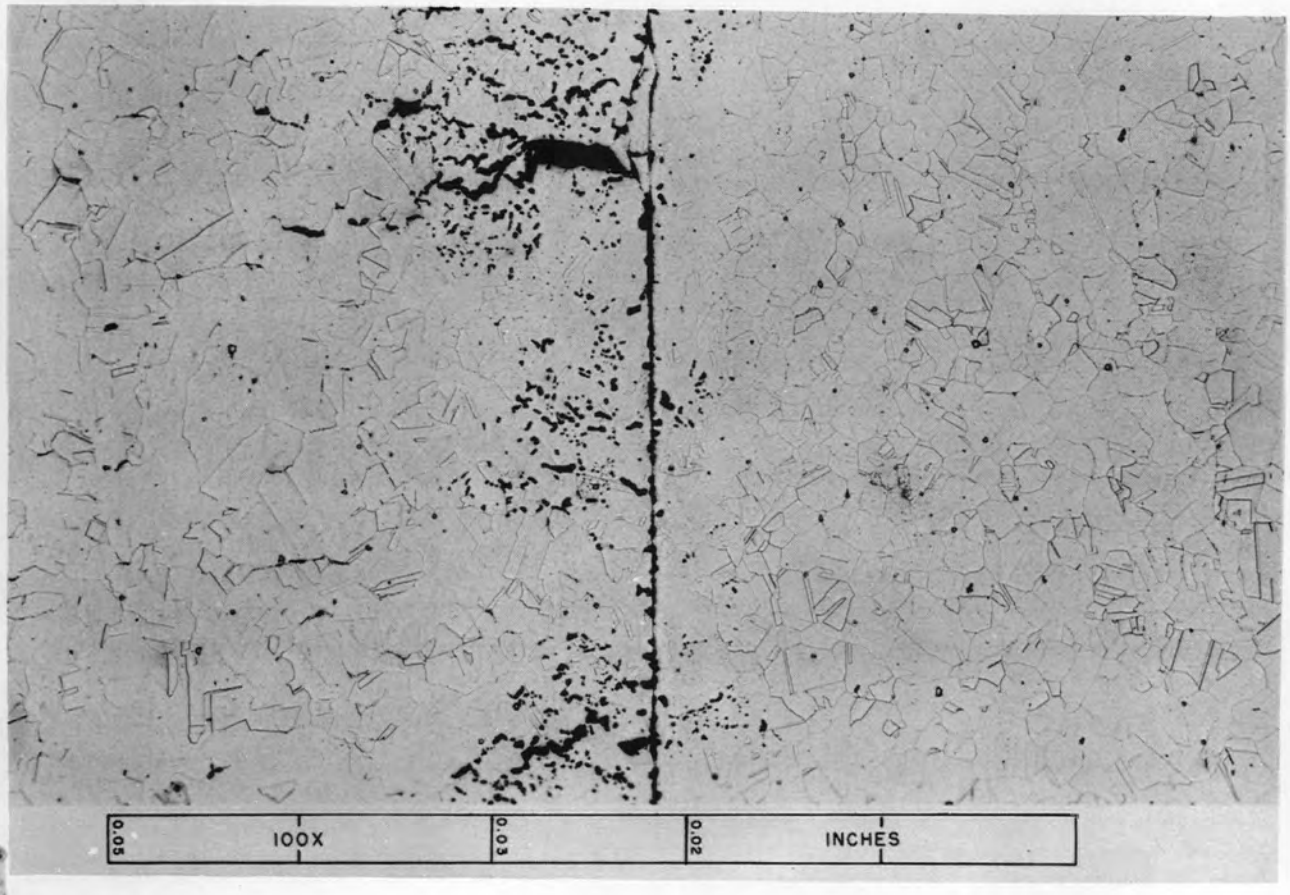

Stressed Specimen Surface

Unstressed Specimen Surface

Fig. 11 (Y-10016) Inconel Specimen Stressed at 3500 PSI in Fused Salts at 1500°F, Ruptured in 550 Hr. Unclassified [redacted] with caption.

[redacted]

However, in Figure 12, which again shows a stressed and unstressed specimen, very little difference in the depth of void formation can be seen. In this test, the specimen was stressed to only 1500 psi, and the two specimens were exposed to the salt at 1500°F for 5500 hr. Since it is generally acknowledged that stress tends to accelerate diffusion, we could give an explanation for the apparent change in corrosion rate with stress based on the diffusion rate of chromium. However, the Corrosion Groups have considerable data which indicate that fluoride corrosion is not controlled by the diffusion rate of chromium, but rather by the availability of impurities in the fused salts. Although we cannot satisfactorily explain the various effects of stress, we feel that in view of the low stresses calculated for the reactor, this variable will have no appreciable effect on the corrosion rate.

Let us now discuss another environmental problem, that of sodium. When one considers that there will be more metal surface in the reactor exposed to sodium than there is to fused salts, one begins to worry about the effect of this environment on the high-temperature strength of Inconel. Figure 6 shows that, comparatively speaking, sodium is a more detrimental environment to Inconel than argon, but not as bad as the fused salts. Figure 13 is a photomicrograph of the specimen from this test. It is evident that considerable decarburization has occurred, but there is no evidence of corrosion. The loss in strength is probably explained by the loss of carbides which tend to inhibit creep. The next Figure (Figure 14) is a photomicrograph of another specimen which showed much better creep strength when tested in sodium. It is clear from this picture that no decarburization has occurred. Considerable work has been done by the Corrosion Group on this problem of decarburization of Inconel by sodium and although no

[redacted]

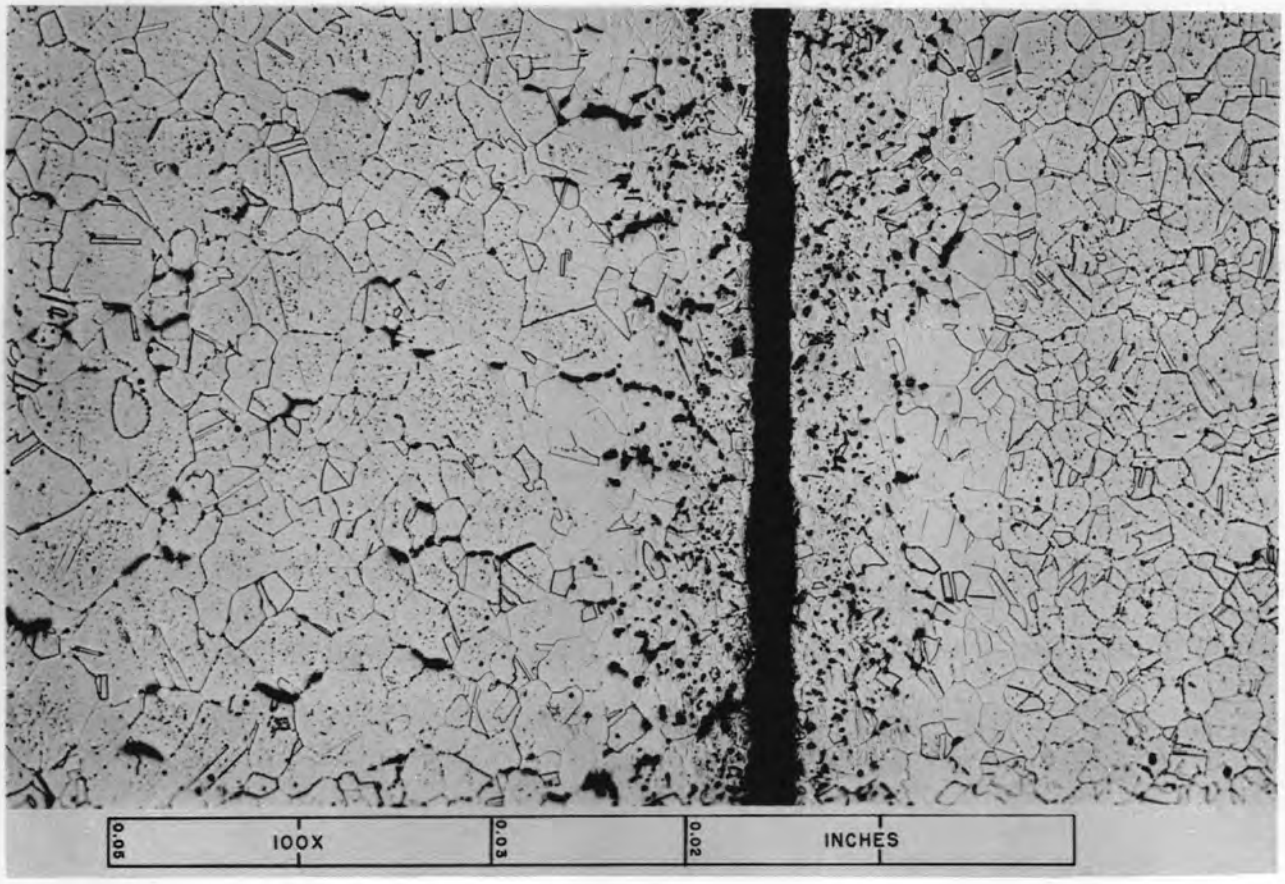

Stressed Specimen Surface

Unstressed Specimen Surface

Fig. 12 (Y-12374) Inconel Specimen Stressed at 1500 PSI in Fused Salts at 1500°F, Ruptured in 5500 Hr. Unclassified - [redacted] with caption.

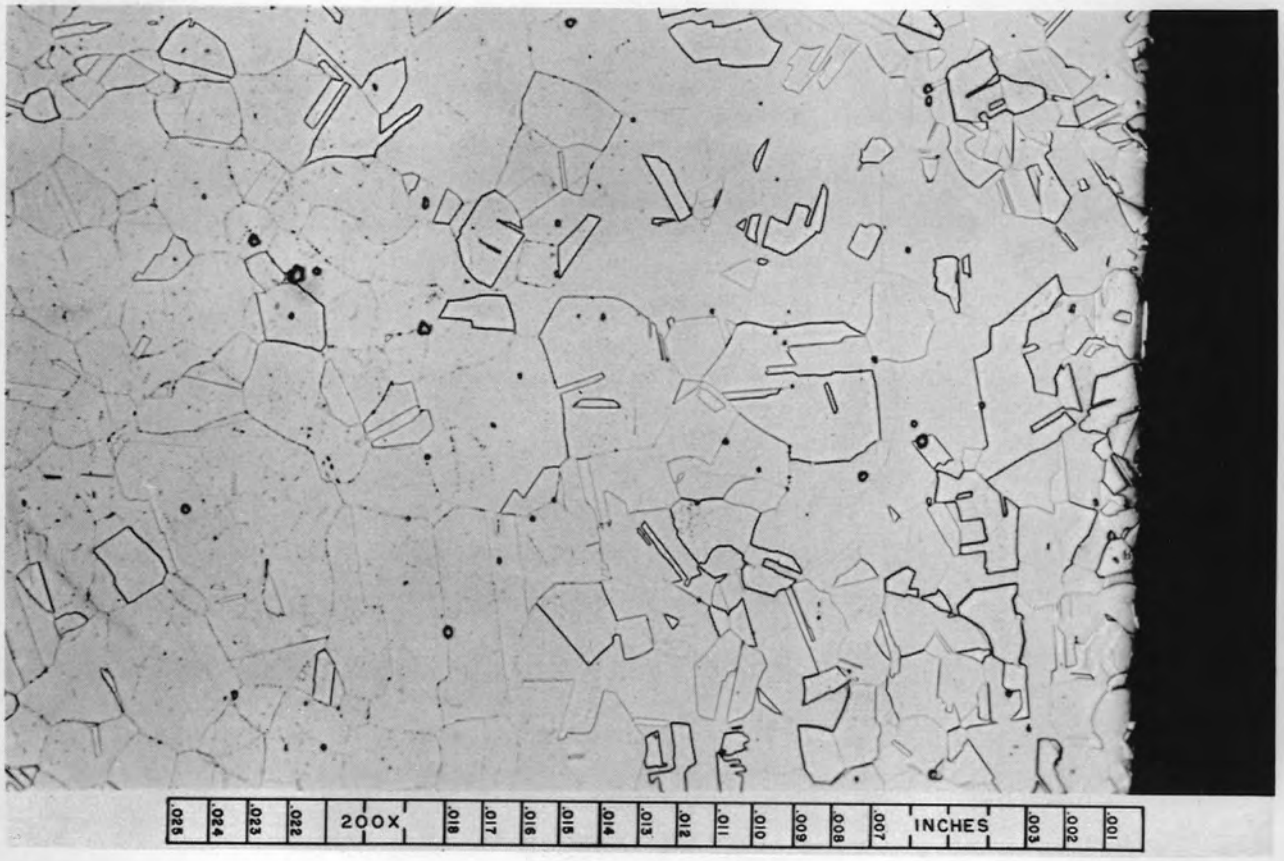

Fig. 13 (Y-10817) Inconel Specimen Stressed at 3500 PSI in Sodium at 1500°F, Ruptured in 1300 Hr. Evidence of considerable decarburization can be seen. Unclassified.

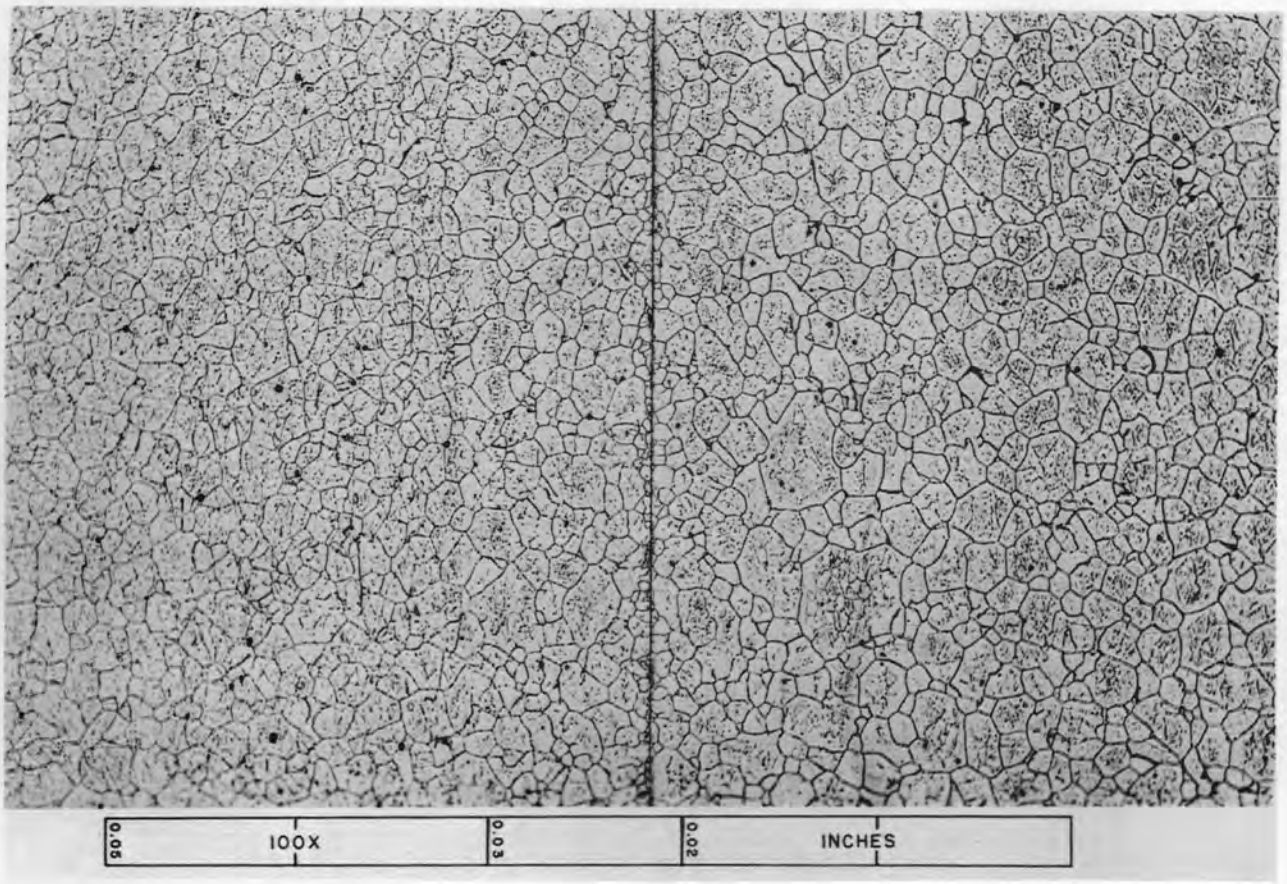

Unstressed Specimen Surface

Stressed Specimen Surface

Fig. 14 (Y-13468) Inconel Specimen Tested in Purer Sodium at 1500° F. No evidence of decarburization can be seen. Unclassified.

[redacted]

rigorous proofs can be offered, one explanation is that sodium oxide acts as the decarburizing agent, probably by the formation of a sodium carbonate. Conversely, if sodium becomes contaminated in any manner with carbon, the sodium carbonate thus formed will act as a carburizing agent. Either of these conditions is undesirable, and it appears that the purity of the sodium used in the reactor must be carefully controlled. If this can be done, Inconel appears to be quite compatible with sodium.

Previously, we have been discussing the results of tests in which a material was stressed in the conventional uniaxial manner. However, in the circulating-fuel type of reactor the majority of the component parts consist of tubing. The stresses in these parts are not pure tensile ones, and it was felt that some effort should be made to explore the effect of multiaxial stresses on the high-temperature strength of Inconel. Figure 15 illustrates one apparatus used for these tests. The outside shell is used as a container for the fused salts, sodium, or other environments. The tubular specimen is stressed by internal gas pressure. The resulting stresses are mainly hoop and axial, with the hoop stress being twice the axial stress. Several investigators who have studied the effect of multiaxial stress on mechanical properties have discovered that when the stress ratio is in the range of 2-to-1, the material will have very poor ductility. Since rupture will occur with less deformation, the stress-rupture life of a material is drastically reduced. The next Figure (Fig. 16) shows a plot of stress vs time-to-rupture of pipe and tubing in fused salts at 1500°F. As one might expect, the heavy-wall pipe has better rupture life than the thin-wall tubing in the corrosive environment. The curve on the left is distressing in that even for the low operating stresses calculated for the reactor, the rupture time is so short that the comfortable safety factor which was indicated by the tensile tests has disappeared.

[redacted]

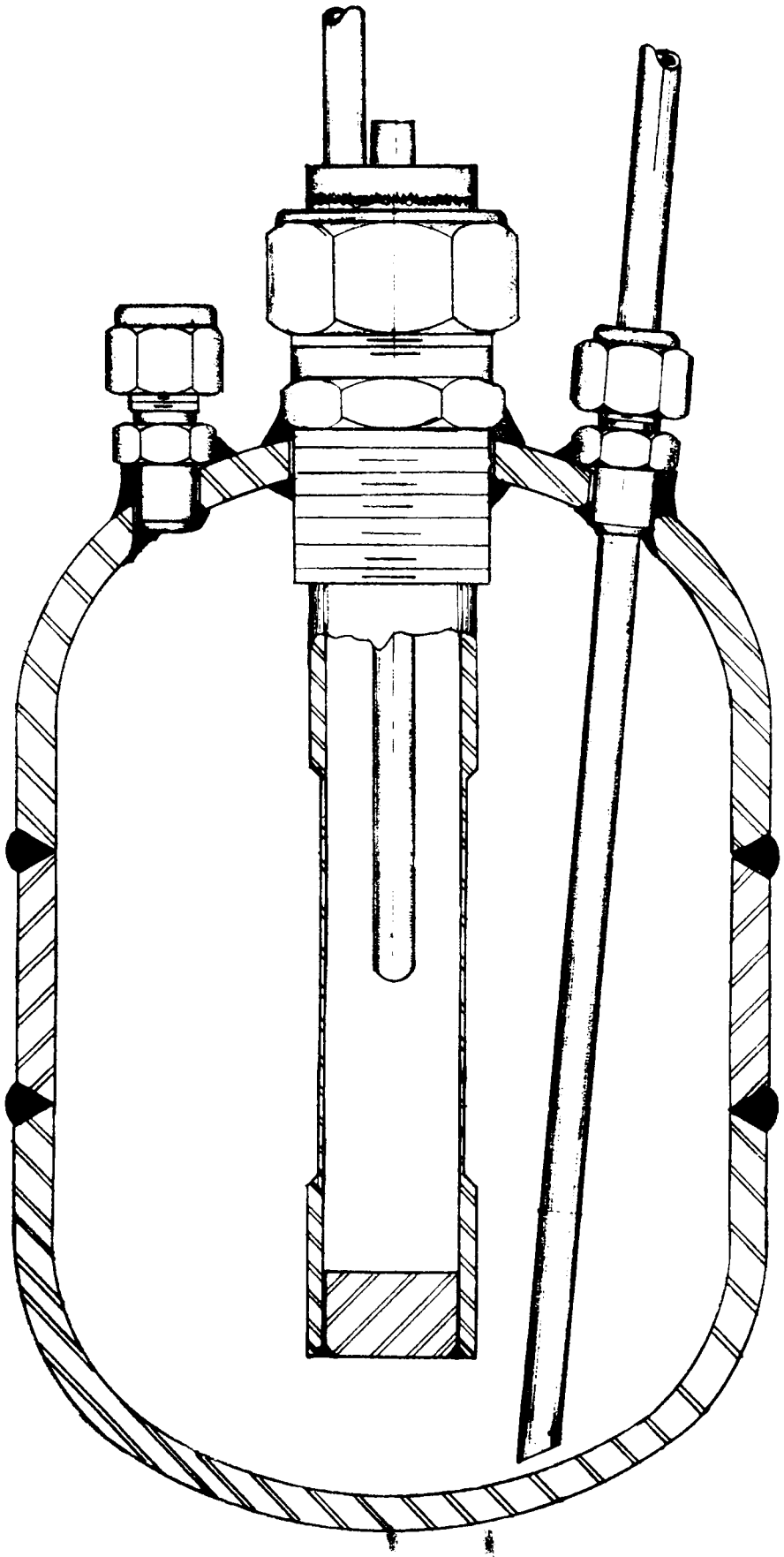

Fig. 15 (Y-13570) Test Apparatus for Multiaxial Stress Creep Tests in Gaseous or Liquid Metal Environments. Unclassified.

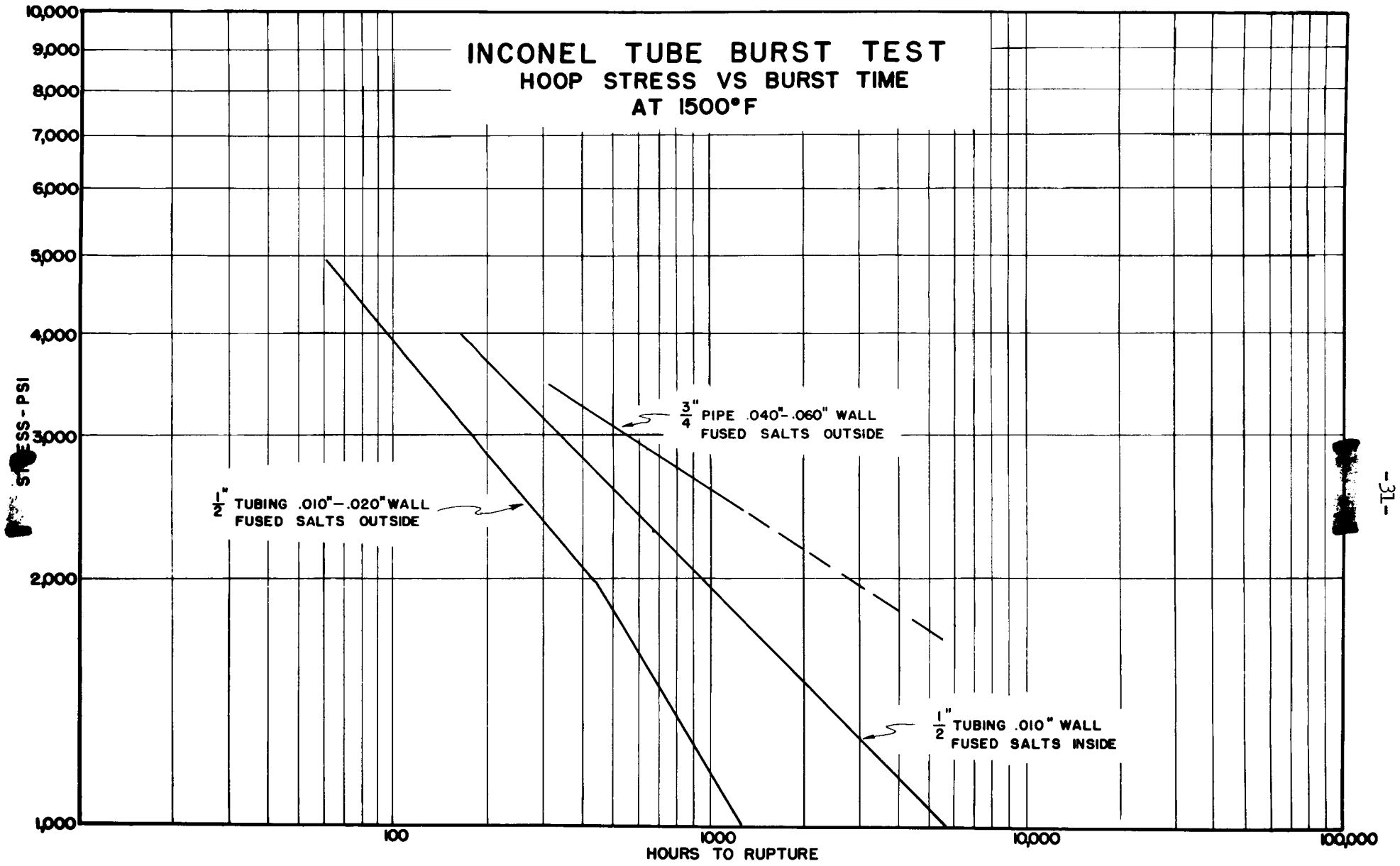

Fig. 16 (Y-13127) Rupture Curves for Inconel Tube-Burst Tests in Fused Salts at 1500°F.
Classification [redacted]

We can still be optimistic in that we know of no place in the reactor where the stress ratio will be 2-to-1, so that we feel that these data are slightly more pessimistic than is warranted. However, we also feel that the uniaxial tensile data are more optimistic than is the actual case so that, although we have bracketed the area of interest, we cannot as yet deal in specific figures. Present plans include the study of rupture life in terms of various stress ratios.

You may have noted that Figure 16 shows two rupture curves for the thin-wall tubing quite widely separated. The legend indicates that one test condition had the fused salt outside the tube; whereas, in the other, the salt was inside the tubular specimen. The reason for the difference in test results can be shown by Figs. 17 and 18. Figure 17 shows that very little, if any, corrosion of the specimen has occurred. This specimen was tested with fused salts inside so that the volume of salt used was quite small. Figure 18 shows a very marked corrosive attack. This specimen was tested with fused salts surrounding it, in which case a very large volume of salt could be used. Since the corrosion which occurs in these tests is due to the reduction by chromium of the impurities in the fluorides, it follows that when a large area of metal is exposed to a relatively small volume of salt, very little attack will be noted. It is important, therefore, in designing such test facilities, to provide a sufficient volume of fused salt in relation to the metal surface area to enable the corrosive action to continue for the full period of the test.

In conclusion, we may say that the material people at the Oak Ridge National Laboratory believe that with the presently proposed operating conditions of stress, temperature and time, Inconel provides a reasonable safety factor as a structural material. However, we also believe that the tube-burst-type test, rather than the tensile creep test, should be used as the guide for defining the limits of operating conditions when tubular components are involved.

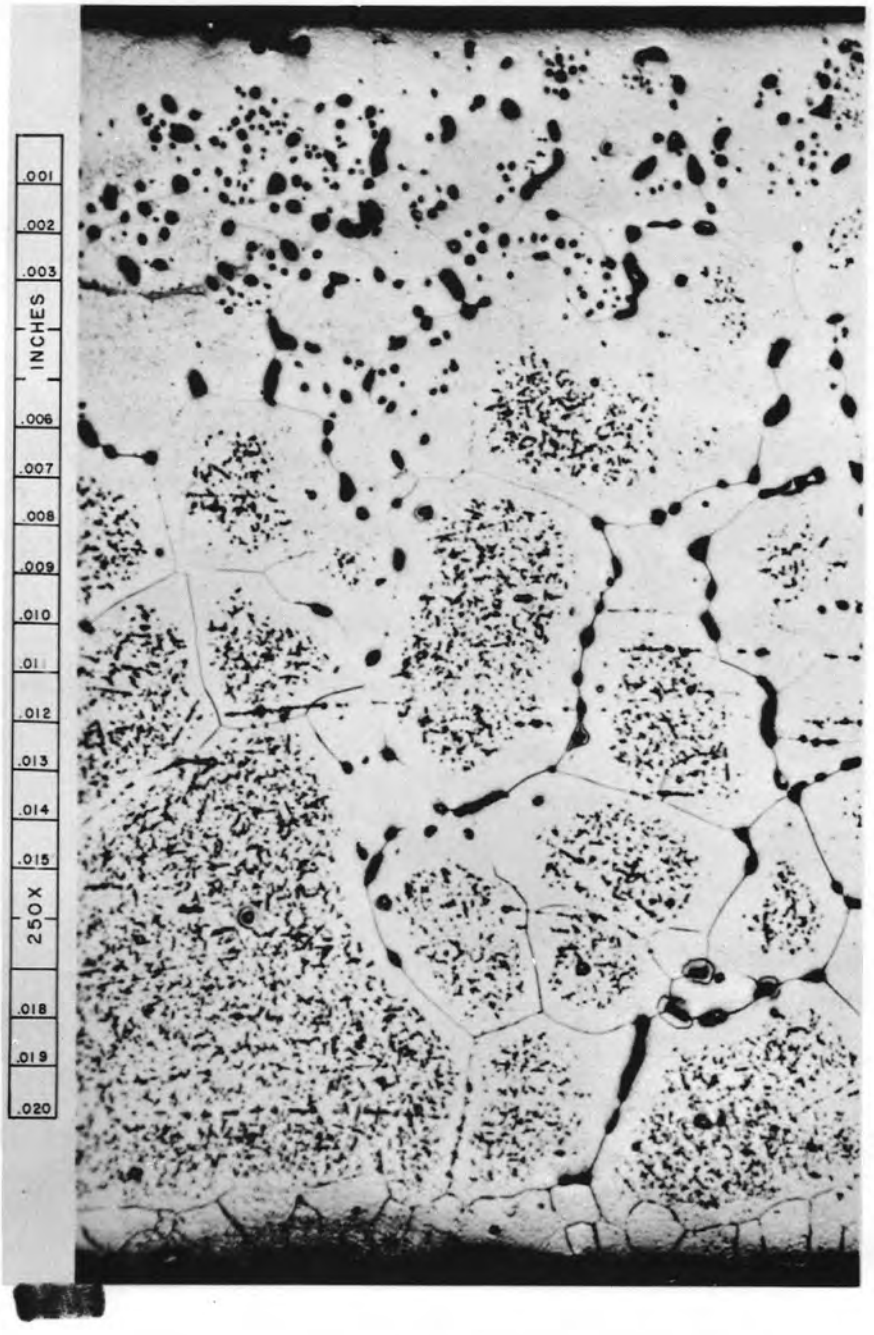

Fig. 17 (Y-12528) Surface of Tube in Contact with the Fused Salts. The Inconel specimen was tested with fused salts surrounding the tube. Unclassified [redacted] with caption.

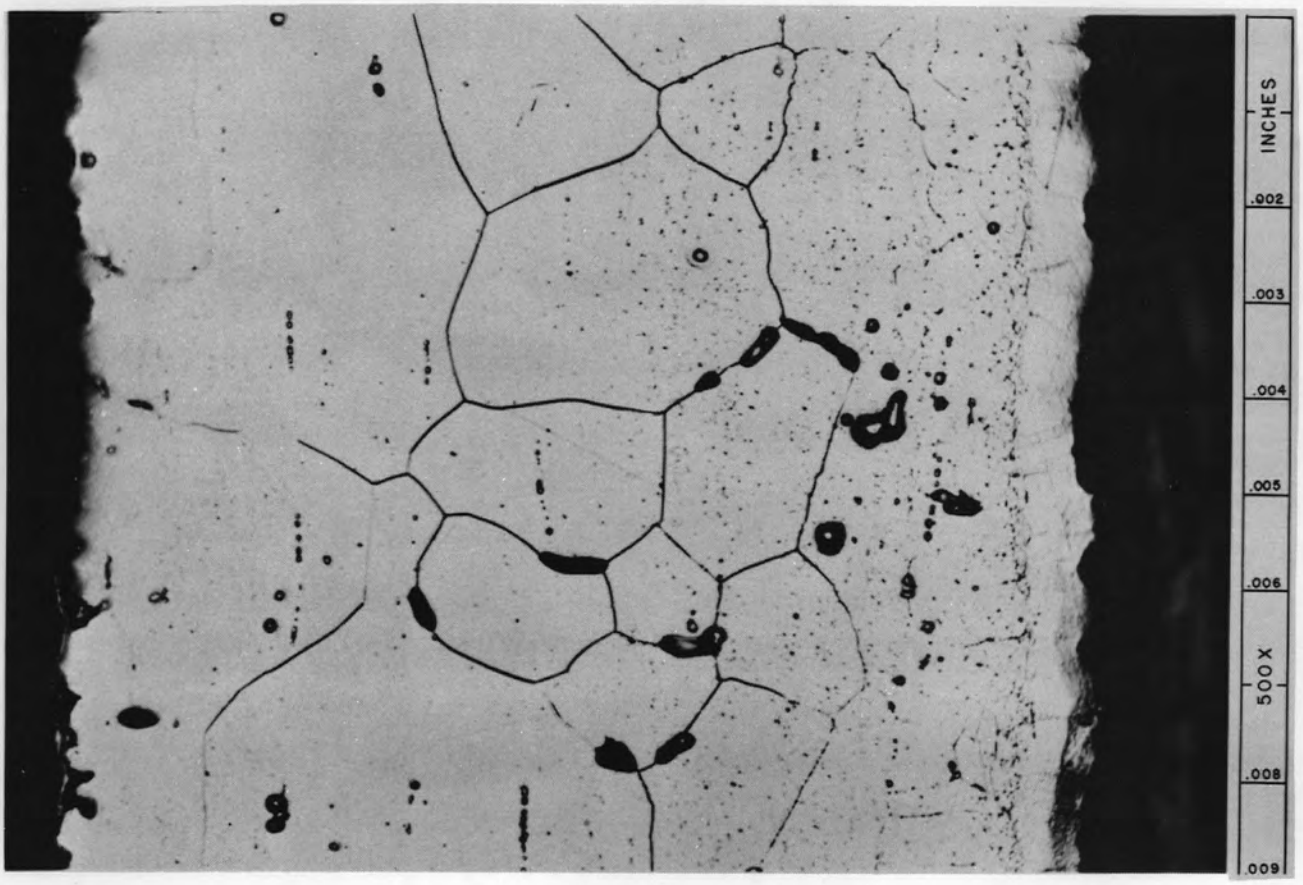

Fig. 18 (Y-12529) This Surface in Contact with the Fused Salts. Specimen was tested with fused salts inside the tube. Unclassified - [redacted] with caption.

[redacted]

[redacted]

HEAT EXCHANGER FABRICATION

P. Patriarca
G. M. Slaughter
W. D. Manly

A major effort of the Welding Section of the Metallurgy Division at ORNL has been the development of joining methods and procedures for the fabrication of the compact and relatively complex radiators and heat exchangers being designed in conjunction with the circulating fuel reactor effort of the ANP Program.

Typical of the radiator designs being experimentally evaluated is the assembly shown in Figure 19 (Y-12-20696): an Inconel tube, type 304 stainless steel fin, Na-to-air radiator for service in the temperature range of 1300°F to 1600°F.

This radiator was approximately 4-in. x 10-in. x 12-in. overall and consisted of .185-in.-OD, .135-in.-ID Inconel tubing and .010-in.-thick fins. Holes to receive the tubing had been punched with a lip to provide a 15-fin-per-inch spacing.

It was quite apparent that the two major problems which existed were the achievement of a metallurgical bond between the fins and tubes to effect optimum heat transfer, and the achievement of numerous tube-to-header joints which would maintain their integrity under the rather severe environmental conditions imposed.

Since dry-hydrogen furnace brazing appeared to be a relatively simple method of providing several thousand tube-to-fin joints in one generation, a brazing-alloy-evaluation program was undertaken to determine the oxidation resistance of brazed joints at 1500°F. The experimental procedure consisted of the fabrication of Inconel "T" specimens of the type shown in Figure 20 (Y-6512) with each of a number of commercially available and experimentally developed elevated-temperature brazing

[redacted]

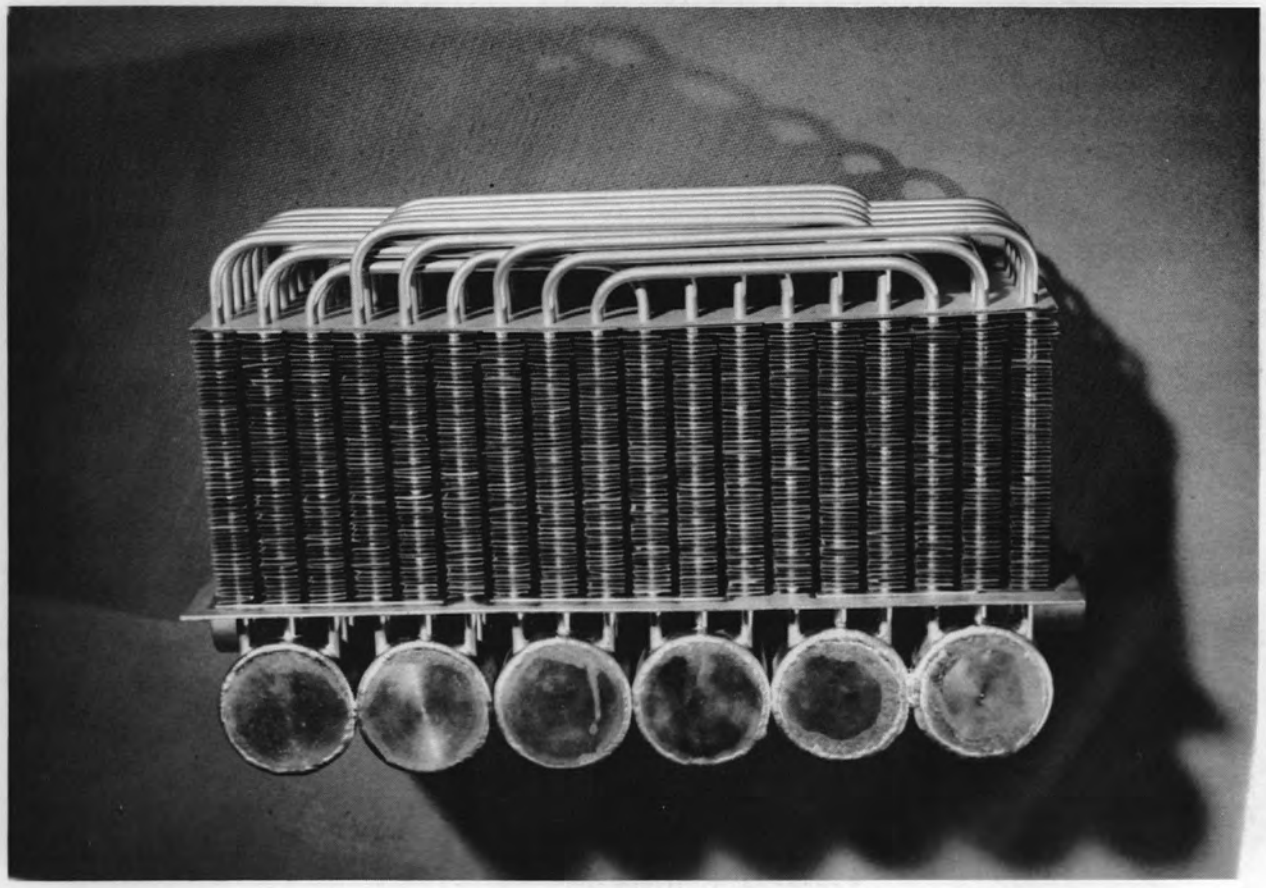

Fig. 19 (Y-12-20696) Typical Na-to-Air Radiator. 0.185-in.-OD, 0.135-in.-ID Inconel tubes, 0.010-in.-thick type 304 stainless steel fins spaced 15 fins per inch. Unclassified.

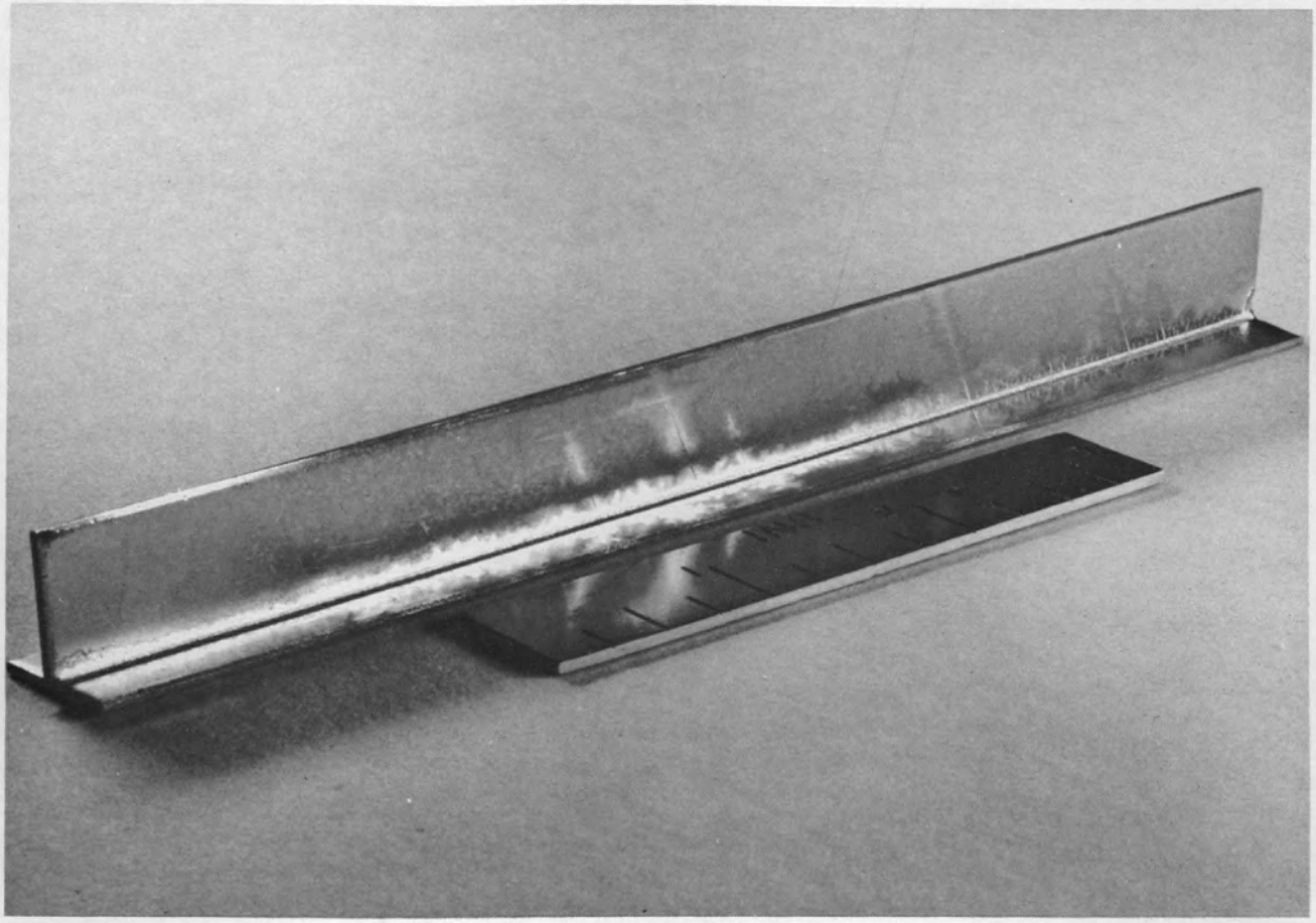

Fig. 20 (Y-7512) Typical Inverted "T" Test Specimen for Brazing Alloys. Unclassified.

alloys. Two 1/16-in. x 1/2-in. x 6-in. strips were assembled into an inverted "T" by tack welding. A small amount of brazing alloy was placed on one end and then allowed to flow the full length in a dry-hydrogen-atmosphere (-70°F dewpoint) furnace maintained at the proper flow temperature. The specimens were then sectioned into 1/2-in. increments and exposed to static air at 1500°F for varying periods of time. The results of metallographic examination after 200-hr and 500-hr exposures are summarized in tabular form in Fig. 21 (Y-13568). It may be seen that the majority of the brazing alloys tested exhibited excellent oxidation resistance within the limits of the investigation. Figure 22 (Y-13307) is a photomicrograph of a section of an Inconel "T" joint brazed with Coast Metals 52 alloy and then heated for 500 hr at 1500°F in static air. Only slight attack is in evidence in the fillet. The extent of this attack is typical of that observed for the majority of the alloys tested. Typical of a joint exhibiting extremely poor resistance to oxidation is that shown in Fig. 23 (Y-13423). This Inconel "T" specimen was assembled with a 60 Mn-40 Ni braze alloy and, as can be seen, has been severely oxidized in 500 hr of exposure at 1500°F.

In order to evaluate the possibility of all brazed construction for Na-to-air radiators, a number of the alloys listed in the table of Fig. 20 were tested in static Na at 1500°F for a period of 100 hr. The results of these tests indicated that the Ni-base and Ni-Cr-base alloys were favorably resistant to attack and, as was expected, the precious-metal-base alloys were severely corroded. Typical of specimens which exhibited excellent resistance to Na corrosion is that shown in Fig. 24 (Y-13066) (an Inconel "T" specimen assembled with the General Electric 62 alloy and exposed to static Na at 1500°F for 100 hr).

Experience acquired during the fabrication of several all-brazed radiators indicated that a one-cycle brazing operation was extremely difficult to achieve.

Parent Metal - Inconel
Average Fillet Throat - 0.015 inch

Air Temperature - 1500°F
Exposure Time - 200 Hours and 500 Hours

Alloy	Composition (Weight Per Cent)	Brazing Temp. °F	Extent of Attack* 200 Hours	500 Hours
Commercial:				
Nicrobraz	70 Ni-14 Cr-6 Fe-5 B-4 Si-1 C	2150	Slight	Slight
Low Melting Nicrooraz	80 Ni-5 Cr-6 Fe-3 B-5 Si-1 C	1950	Slight	Slight
Coast Metals #50	93 Ni-3.5 Si-2.5 B- 1 Fe	2050	Slight	Slight
Coast Metals #51	92 Ni-4.5 Si-3 B-0.5 Fe	2050	Slight	Slight
Coast Metals #52	89 Ni-5 Si-4 B-2 Fe	1840	Slight	Slight
Coast Metals #53	81 Ni-4 Si-4 B-8 Cr-3 Fe	1950	Slight	Slight
Coast Metals #NP	50 Ni-12 Si-28 Fe-4 Mo-4.5 P-1 Mn-0.5 Cr	2050	Slight	Slight
Mond Nickel Company Alloy	64 Ag-33 Pd-3 Mn	2150	Severe	Severe
Copper	100 Cu	2050	Complete	- -
Experimental: Nickel Base				
General Electric #62	69 Ni-20 Cr-11 Si	2150	Slight	Slight
General Electric #81	66 Ni-19 Cr-10 Si-4 Fe-1 Mn	2150	Slight	Slight
Ni-Cr-Si	73.5 Ni-16.5 Cr-10 Si	2150	Slight	Slight
Ni-Si	88 Ni-12 Si	2200	Slight	Slight
Ni-Ge	75 Ni-25 Ge	2150	Slight	Slight
Ni-Ge-Cr	65 Ni-25 Ge-10 Cr	2140	Slight	Slight
Electroless Ni-P	88 Ni-12 P	1740	Slight	Slight
Ni-P-Cr	80 Ni-10 P-10 Cr	1830	Slight	Slight
Ni-Mo-Ge	50 Ni-25 Mo-25 Ge	2150	Slight	Slight
Ni-Sn	68 Ni-32 Sn	2150	Slight	Moderate
Ni-Mn	40 Ni-60 Mn	1950	Complete	- -
Ni-Mn-Cr	35 Ni-55 Mn-10 Cr	2050	Severe	Severe
Experimental: Precious Metal Base				
Pd-Ni	60 Pd-40 Ni	2300	Very slight	Very slight
Pd-Ni-Si	60 Pd-37 Ni-3 Si	2150	Very slight	Very slight
Pd-Al	92 Pd-8 Al	2020	Very slight	Very slight
Pd-Ge	90 Pd-10 Ge	2050	Very slight	Slight
Au-Ni	82 Au-18 Ni	1830	Very slight	Very slight
Au-Co	92 Au-10 Co	1830	Very slight	Slight
Au-Cu	80 Au-20 Cu	1740	Moderate	Complete

* Very slight - 0 - 0.001 inch penetration
Slight - 0.001 inch - 0.002 inch penetration
Moderate - 0.002 inch - 0.005 inch penetration
Severe - >0.005 inch penetration

Fig. 21 (Y-13568) Oxidation Resistance of Dry Hydrogen Brazed "T" Joints. Unclassified.

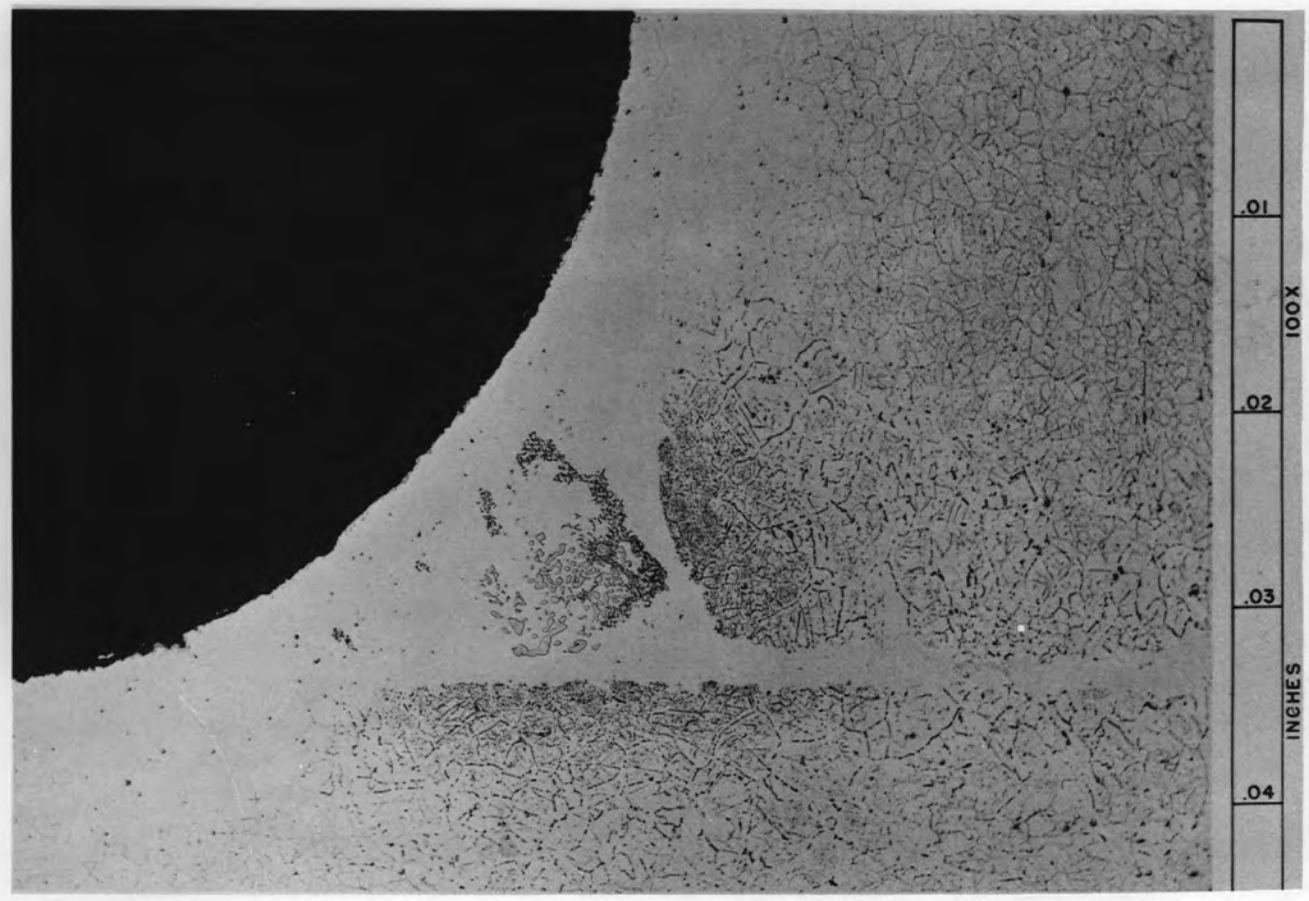

Fig. 22 (Y-13307) Section of an Inconel "T" Joint Assembled with the Coast Metals 52 Alloy after Exposure to 500 Hr at 1500°F in Static Air. Excellent oxidation resistance is exhibited. 100X Unclassified.

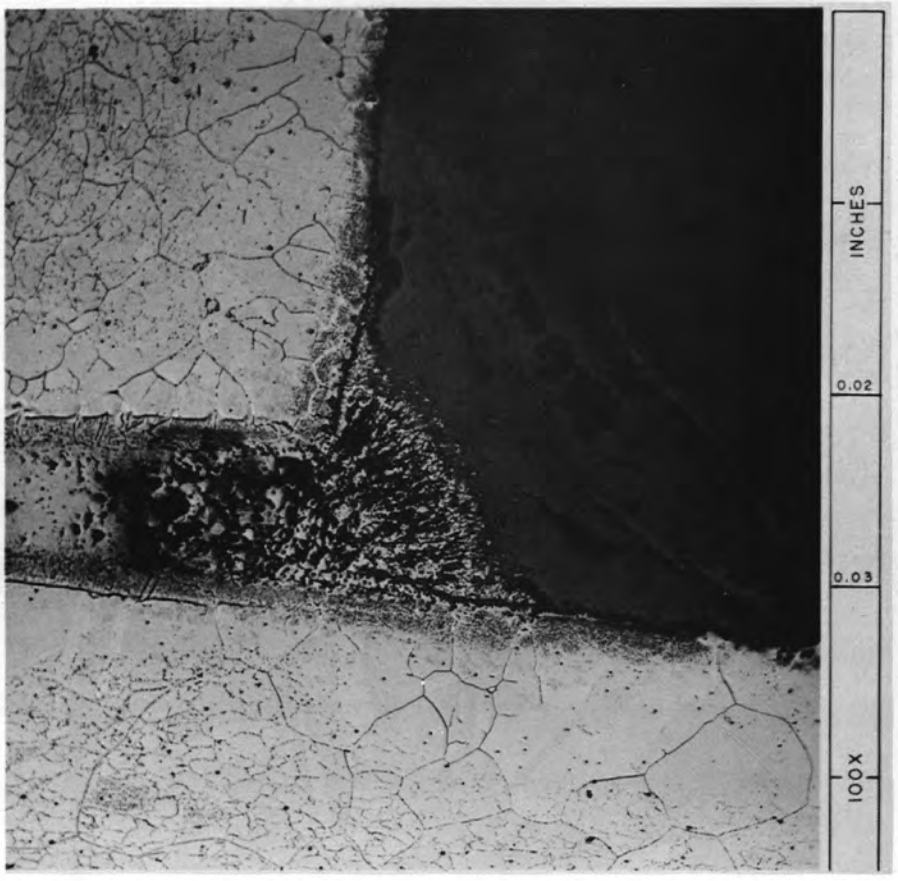

Fig. 23 (Y-13423) Section of an Inconel "T" Joint Assembled with a 60 Mn-40 Ni Alloy after Exposure to 500 Hr at 1500°F in Static Air. Severe oxidation is evident. 100X. Unclassified.

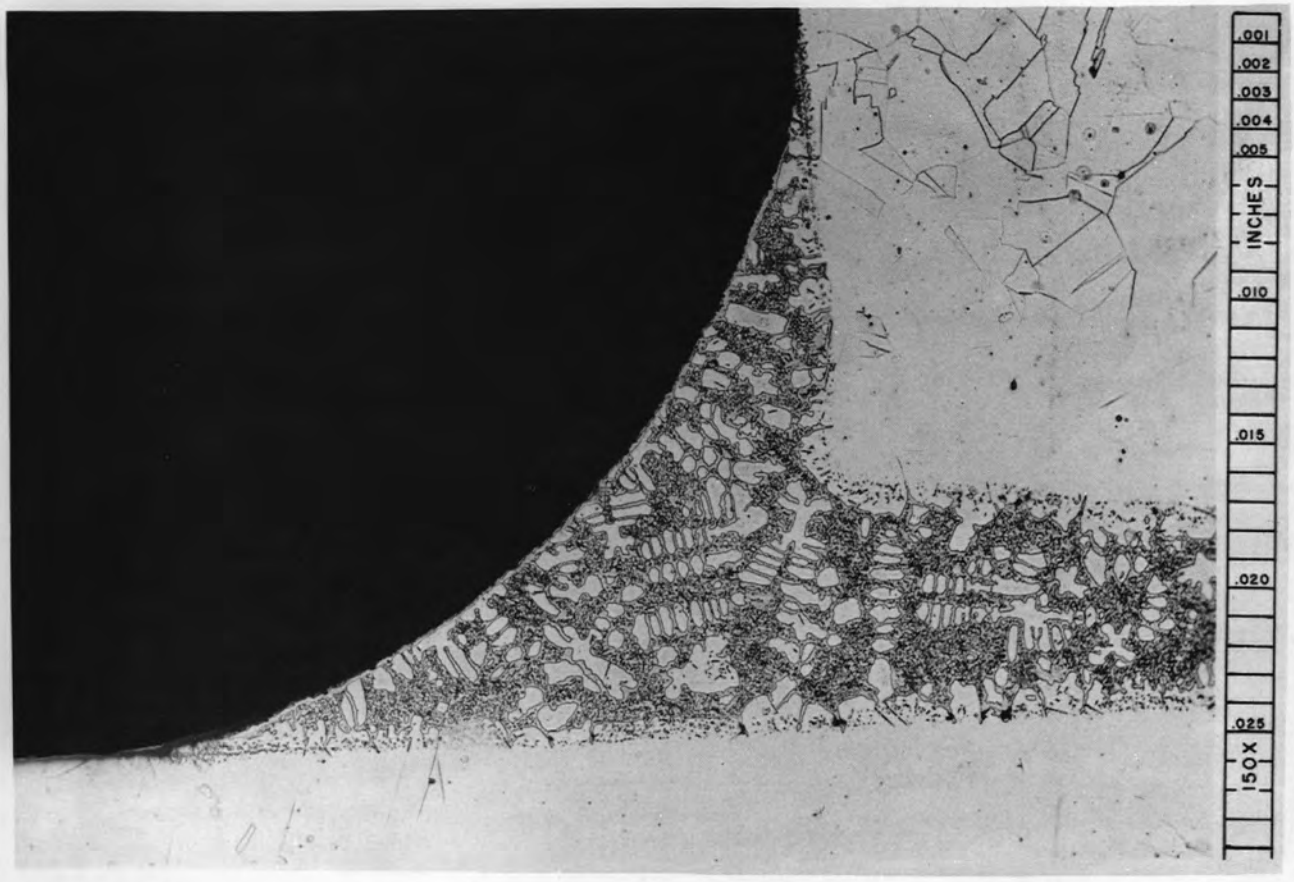

Fig. 24 (Y-13066) Inconel "T" Specimen Assembled with General Electric 62 Braze Alloy and Exposed to Static Na for 100 Hr. 150X. Unclassified.

One or more additional rebrazing operations were generally required before a completely leak-tight system was realized. Accordingly, a combination of welded tube-to-header joints supplemented by a back-brazing operation was attempted and found to be quite successful. The radiator shown in Fig. 19 was fabricated in this manner and has operated successfully in the range of 1300°F to 1500°F for a period of 2000 hr. The General Electric 62 brazing alloy was used on tube-to-fin joints and to back braze the tube-to-header welds.

A typical tube-to-fin test specimen, after exposure to 1500°F static air for a period of 1300 hr, is shown in Fig. 25 (Y-10423). Sections of two type 304 stainless steel fins are shown brazed to an Inconel tube (to the right of the photomicrograph) with the General Electric 62 alloy. The excellent oxidation resistance of the joint is evident.

Typical of the 180 tube-to-header joints used in this heat exchanger is that shown in Fig. 26 (Y-10984) (a photomicrograph of an Inconel tube-to-header inert-arc weld back-brazed with the General Electric 62 alloy). As may be seen, the brazing operation provides a supplement to the weld and the additional advantage of eliminating the notch, which is an objectionable characteristic of tube-to-header welds.

The development of the high-conductivity fin to improve the heat transfer characteristics of Na-to-air radiators posed several additional fabrication problems. The most popular fin materials have been the roll-clad copper fins using either Inconel, 400 series stainless steel, or 300 series stainless steels as cladding for protection against oxidation. A limited number of brazing alloys could be considered in view of the 1980°F melting point of copper. One of these was the Ni-P alloy, also attractive because of the possibility of preplacement by the "electroless" plating

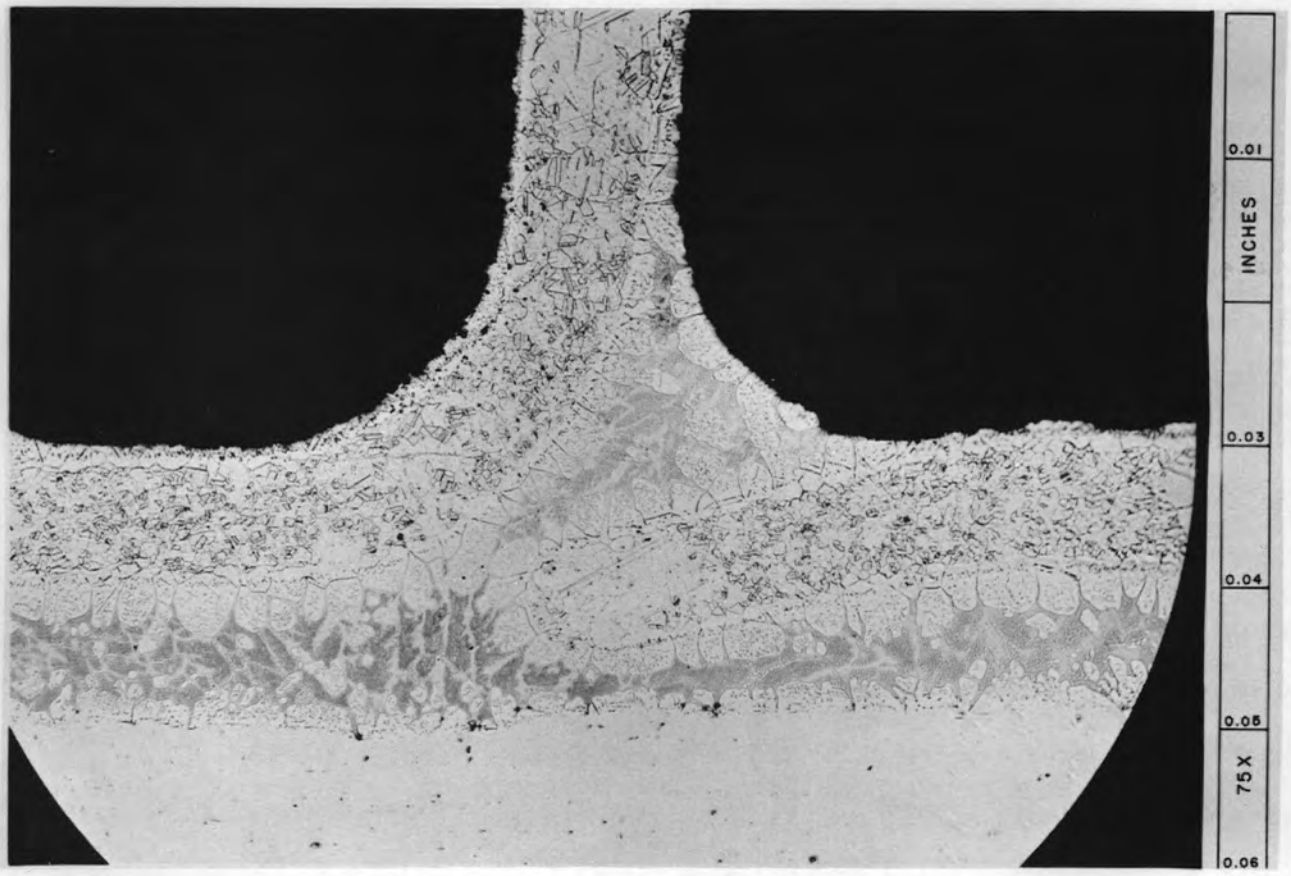

Fig. 25 (Y-10423) Type 304 Stainless Steel Fins Brazed to Inconel Tube (at right) with General Electric 62 Alloy after Exposure to 1500°F Static Air for 300 Hr. 75X. Unclassified.

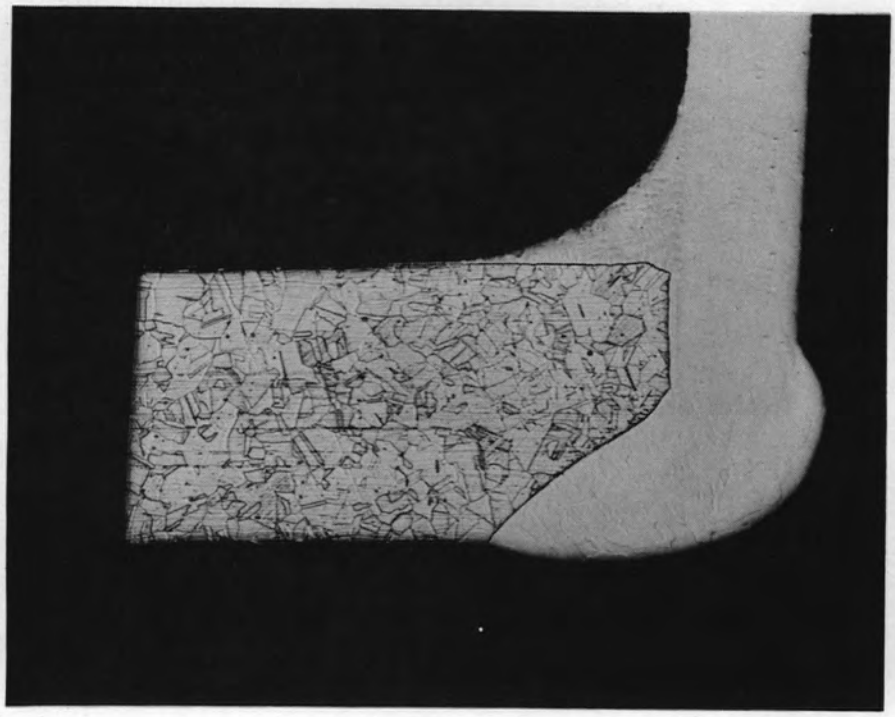

Fig. 26 (Y-10984) Inconel Tube-to-Header Inert-Arc Weld Back Brazed with General Electric 62 Alloy. 50X. Unclassified.

method. A microsection is shown in Fig. 27 (Y-12604) of an Inconel-clad copper fin (2 mils of Inconel on each side of 6 mils of copper) joined to Inconel tubing with the 88 Ni-12 P alloy and then exposed to static air at 1500°F for 600 hr. Solution of the tube wall during brazing was negligible but rather severe solution of the fin lip occurred. It is evident that the oxidation resistance of the joint was not affected. The effects of diffusion, however, were in evidence after test. Color changes in the copper core, along with formation of voids, indicated formation of a copper-nickel alloy and reduction of heat transfer efficiency of the fin.

A joint of 430 stainless steel-clad copper brazed to Inconel tubing with the 88 Ni-12 P alloy is shown in Fig. 28 (Y-12602). It may be seen that intergranular penetration of the brazing alloy into the tube wall has occurred. This penetration is believed due to the solution of iron from the clad during the brazing cycle.

The tube-to-fin joints shown in Fig. 29 (Y-12605) are type 430 stainless steel-clad copper fins brazed to Inconel with the Coast Metals 52 alloy and exposed to static air for 400 hr at 1500°F. A negligible amount of dilution and a relatively minor amount of boron diffusion into the Inconel has occurred. The excellent oxidation resistance of the joint is evident.

In order to translate laboratory-scale experience to practice, a high-conductivity fin core was assembled from a stock of available Inconel-clad copper. The assembly shown in Fig. 30 (Y-13505) was fabricated by a combination of heliarc welding and brazing with the Coast Metals 52 alloy. All of the 180 tube-to-header joints were semiautomatically inert-arc welded with a commercially available torch mechanically rotated around the tube periphery by a variable-speed motor-driven mechanism.

An Inconel sodium-to-air radiator with type 430 stainless steel-clad copper fins was fabricated for service test using the combination heliarc welding and brazing procedures previously described. The tube-to-fin section was assembled and

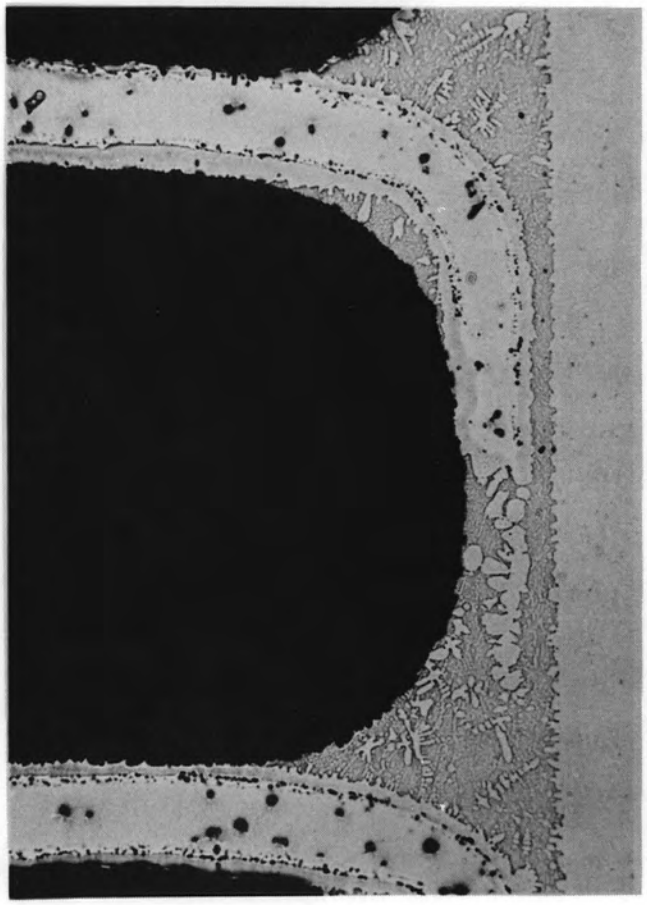

Fig. 27 (Y-12604) Inconel-Clad Copper Fins Brazed to Inconel Tubing with 88 Ni-12 P Alloy and Exposed to Static Air at 1500°F for 600 Hr. 50X. Unclassified.

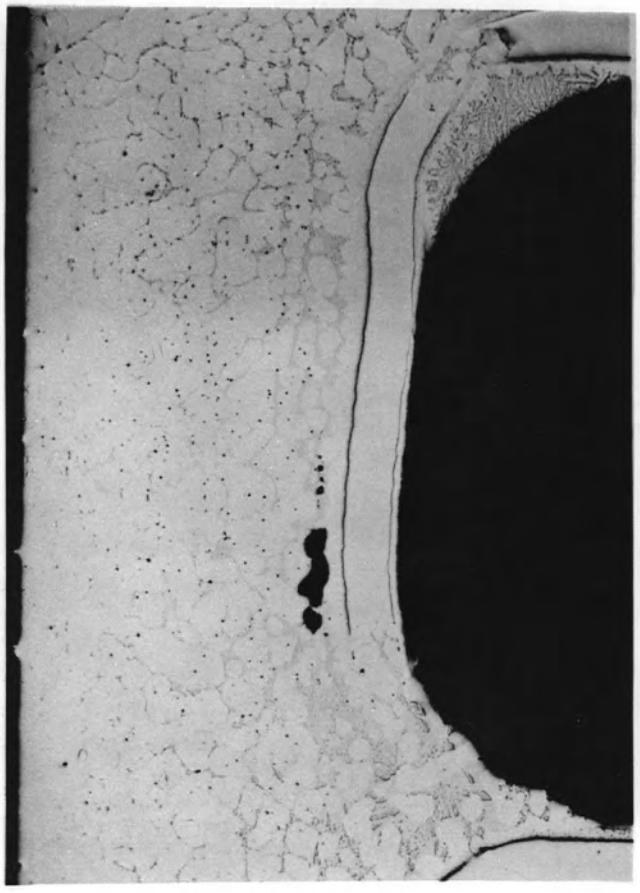

Fig. 28 (Y-12602) Type 430 Stainless Steel-Clad Copper Fins Brazed to Inconel Tubing with 88 Ni-12 P Alloy. 50X. Unclassified.

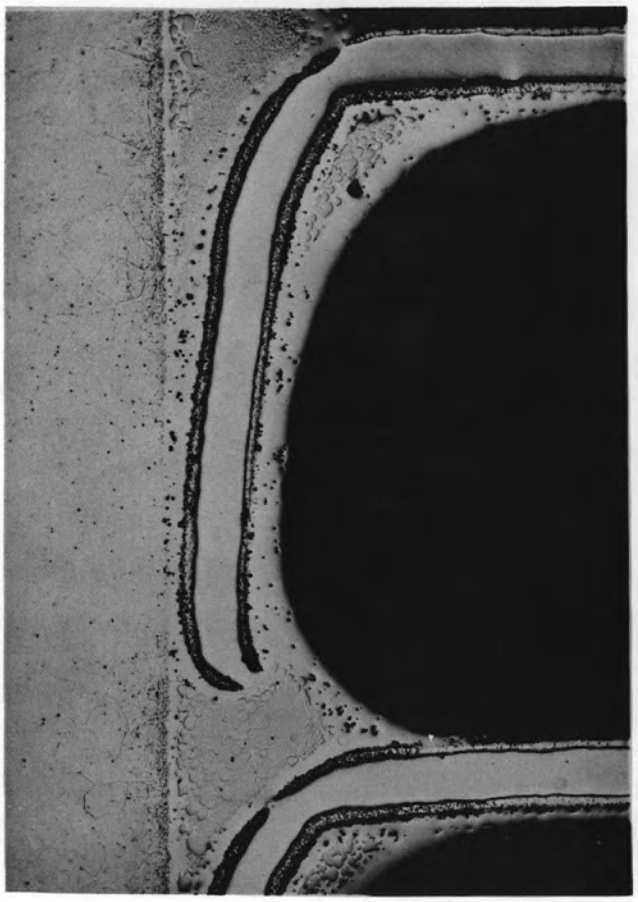

Fig. 29 (Y-12605) Type 430 Stainless Steel-Clad Copper Brazed with Coast Metals 52 and Exposed to Static Air at 1500°F for 400 Hr. 50X. Unclassified.

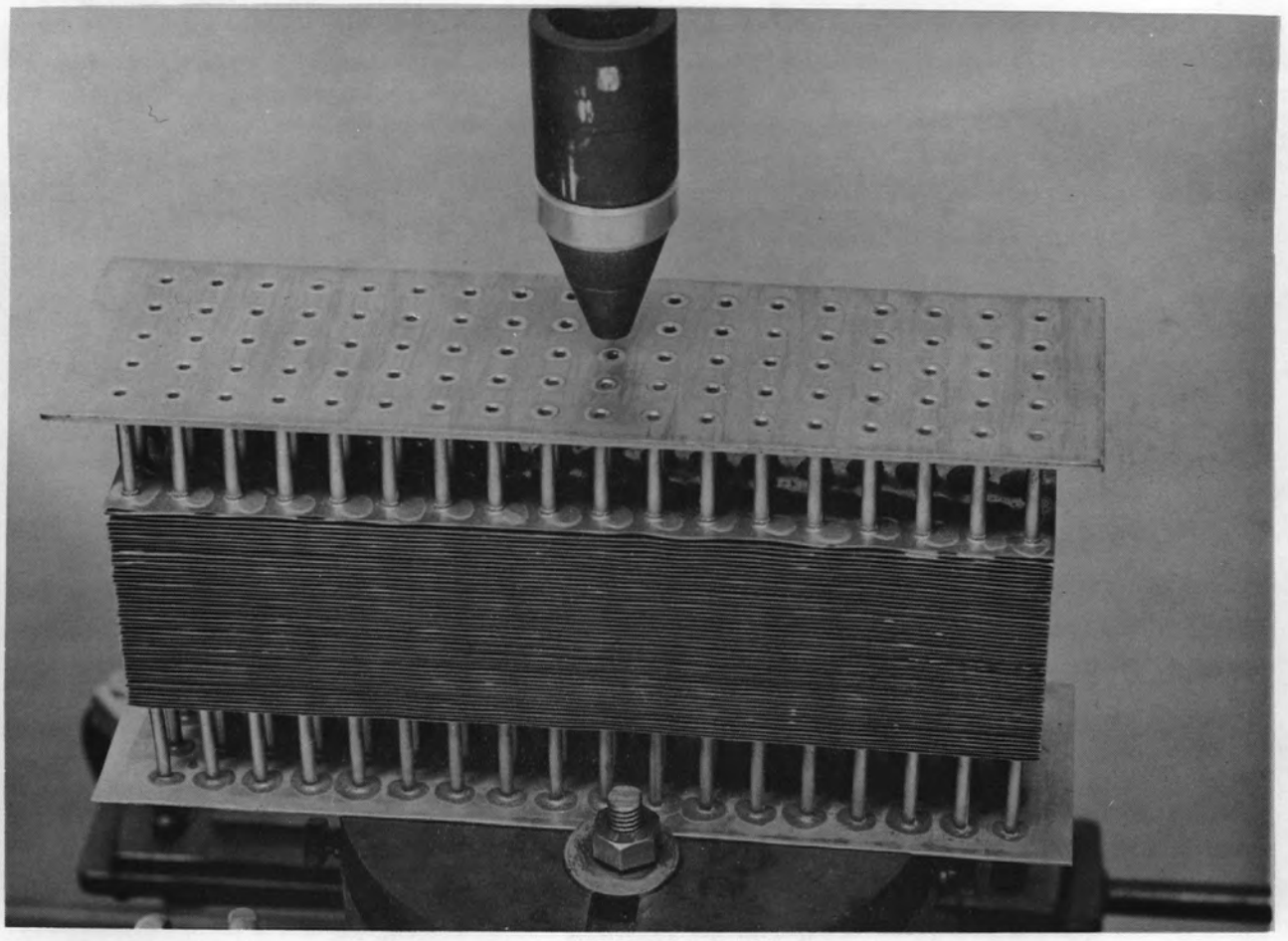

Fig. 30 (Y-13505) Inconel-Clad Copper High-Conductivity Fin Radiator Core. Unclassified.

brazed at 1850°F with Coast Metals 52. The split headers were then assembled and heliarc welded using automatic equipment to effect the tube-to-header welds and manual welding procedures to complete the manifolding. The completed structure following a rebrazing operation to back braze the tube-to-header joints is shown in Fig. 31 (Y-13019). To date, this radiator has been in service in the temperature ranges of 1300°F to 1500°F for a period of approximately 400 hr without failure. This is strong evidence of the reliability of combination welding and brazing procedures for this type of fabrication.

Another very important bi-corrodant system, consisting of Na and fused flouride salts, is under consideration for use in the type of heat exchangers required for the Circulating Fuel Reactor Experiment.

A typical test assembly is illustrated in Fig. 32 (Y-9060), which shows three completed tube bundles welded into a half section which constituted the cylindrical vessel of a six-tube-bundle heat exchanger when welded to its mate. One tube bundle consisted of 35 Inconel tubes (.148-in. OD, .025-in. wall) manually inert-arc welded into a .125-in.-thick dished header, as illustrated in Fig. 33 (Y-8894). Since the tube bundles contained a free span of approximately 40 inches, grid-type spacers were provided at 8-in. intervals. A cone-arc wire-to-header plug welding technique was developed and applied to the fabrication.

This heat exchanger was operated for a period of approximately 2000 hr in the temperature range of 1200 to 1400°F and was subjected to a series of thermal shocks which are believed to have been responsible for its failure in a number of tube-to-header welds.

Figure 34 (Y-13230) illustrates the propagation of fissures in the tube-to-header welds. Examination of numerous as-welded specimens revealed the presence

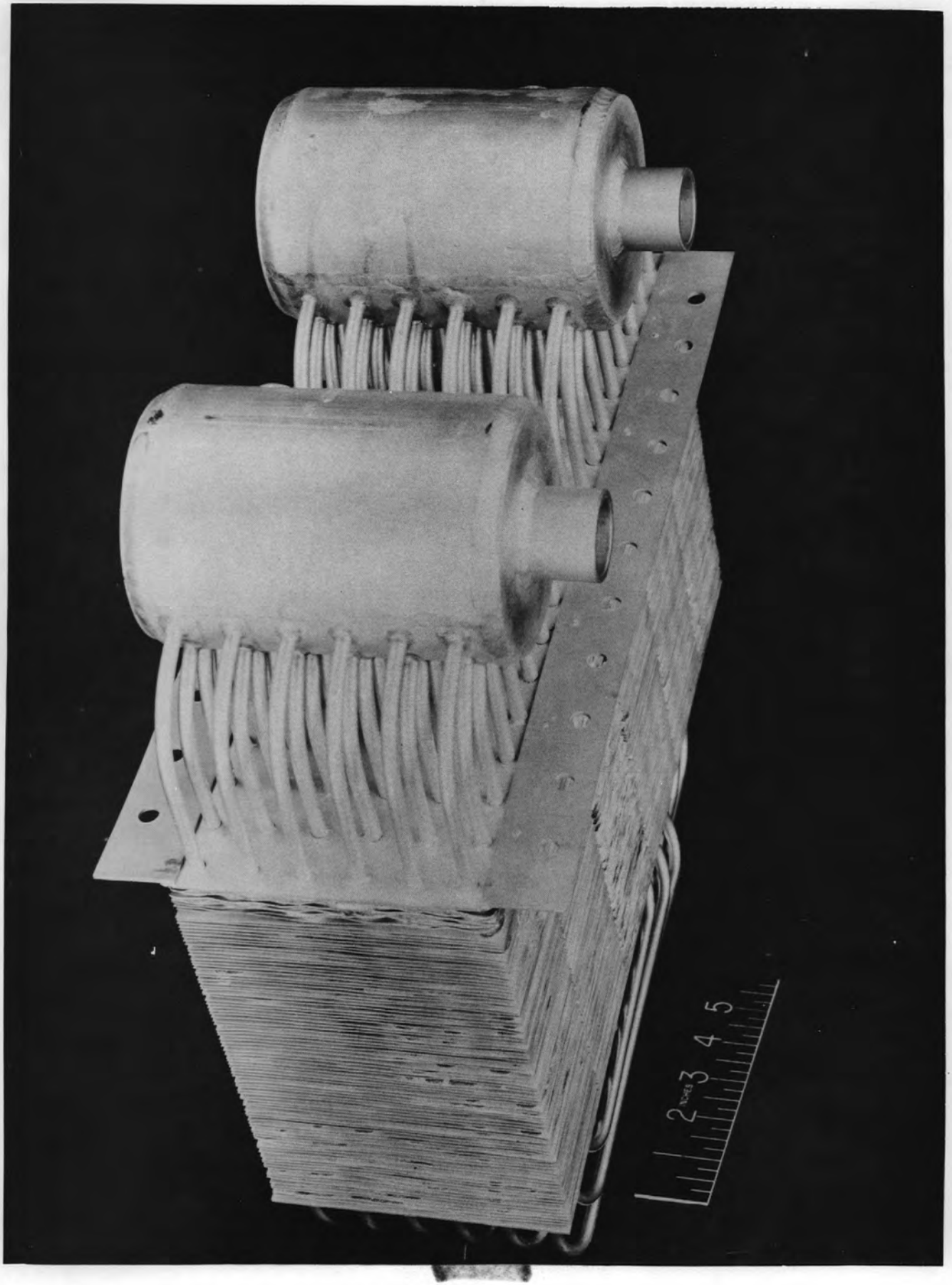

Fig. 31 (Y-13019) Inconel Sodium-to-Air Radiator, Type 430 Stainless Steel-Clad Copper Fins, Coast Metals 52 Brazing Alloy. Unclassified.

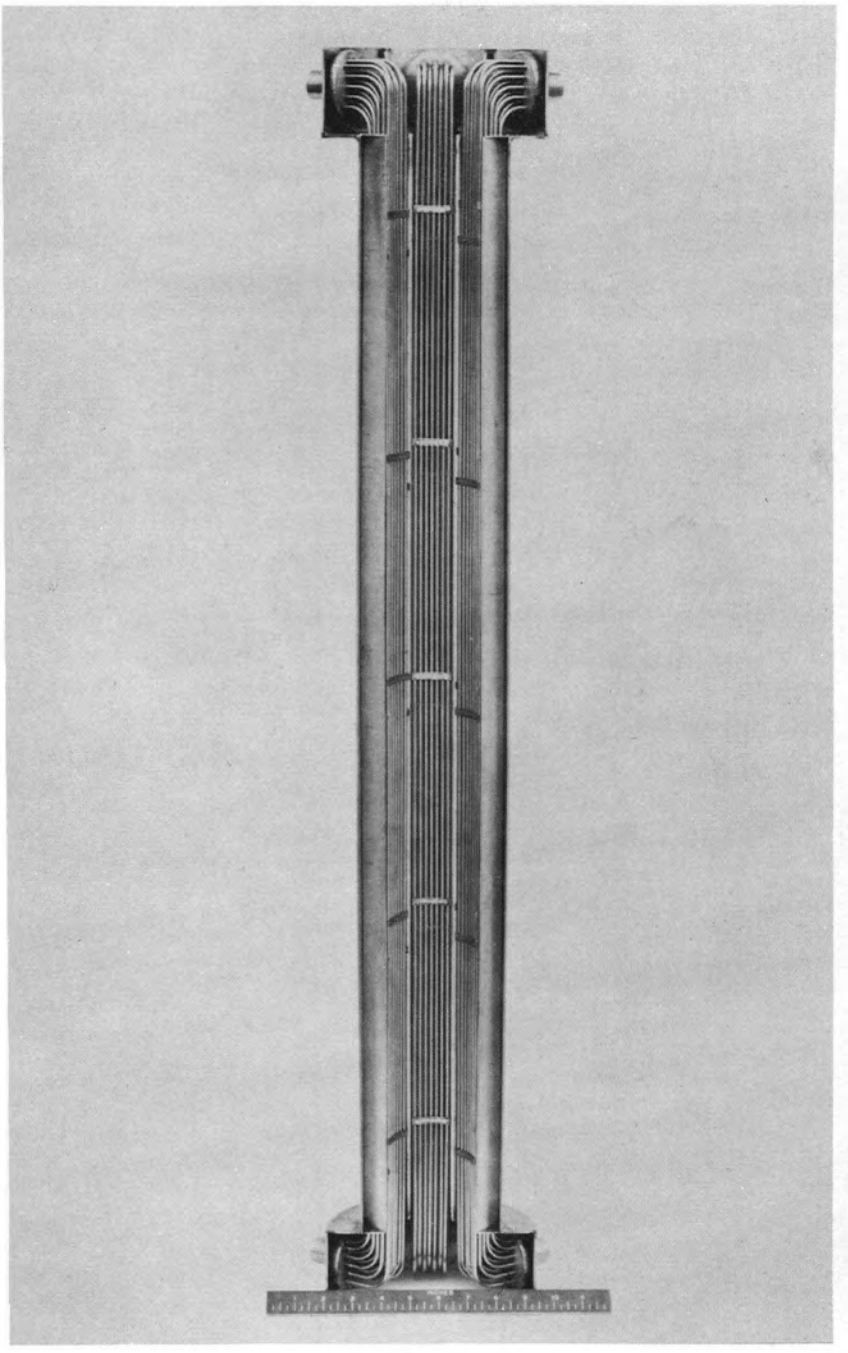

Fig. 32 (Y-9060) Half-Section of Six-Tube Bundle Na-to-Fused Salt Heat Exchanger. [redacted] with caption.

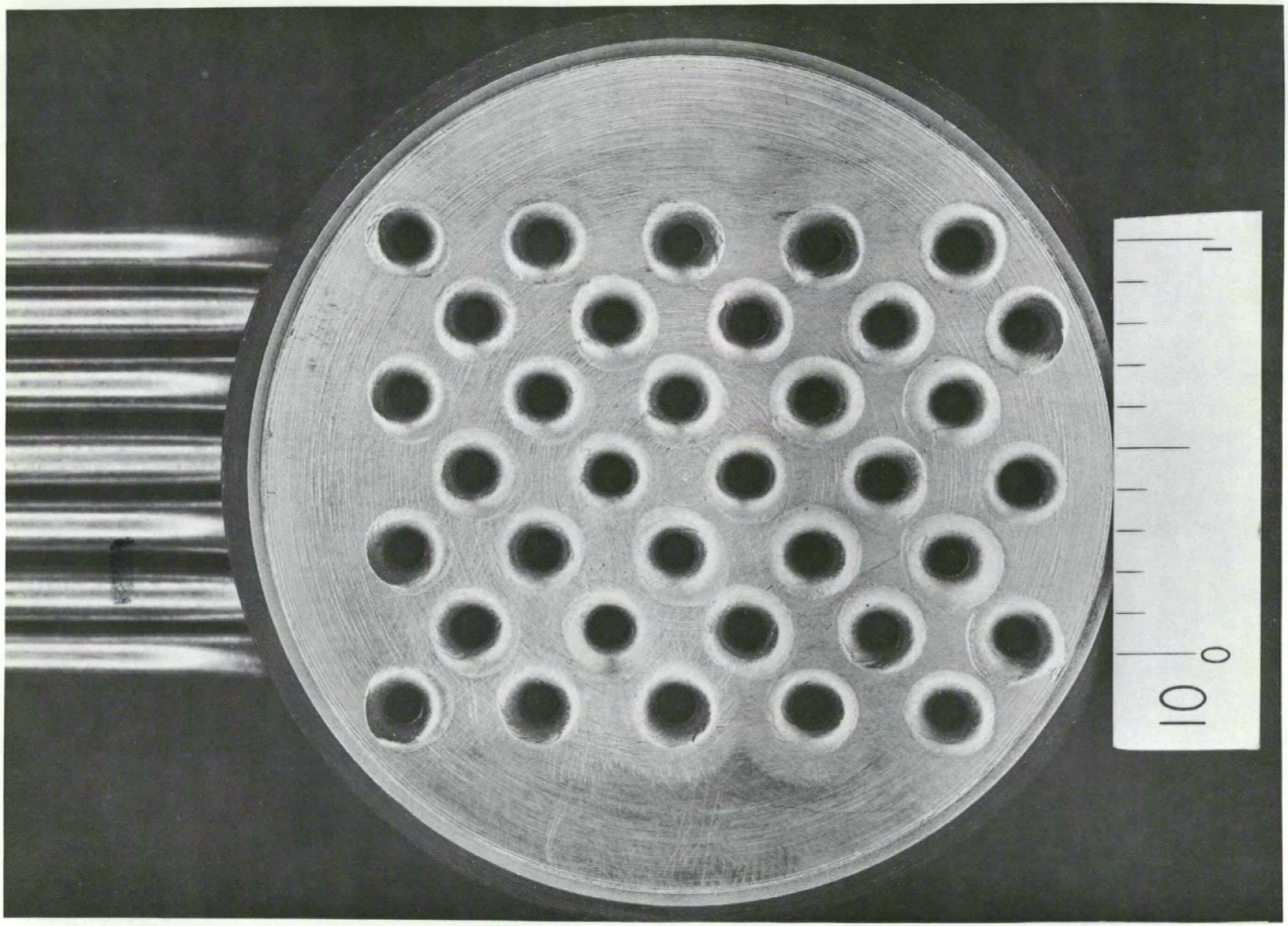

Fig. 33 (Y-8894) Manual Inert-Arc Tube-to-Header Welds in One Header of the Heat Exchanger of Fig. 31. Unclassified.

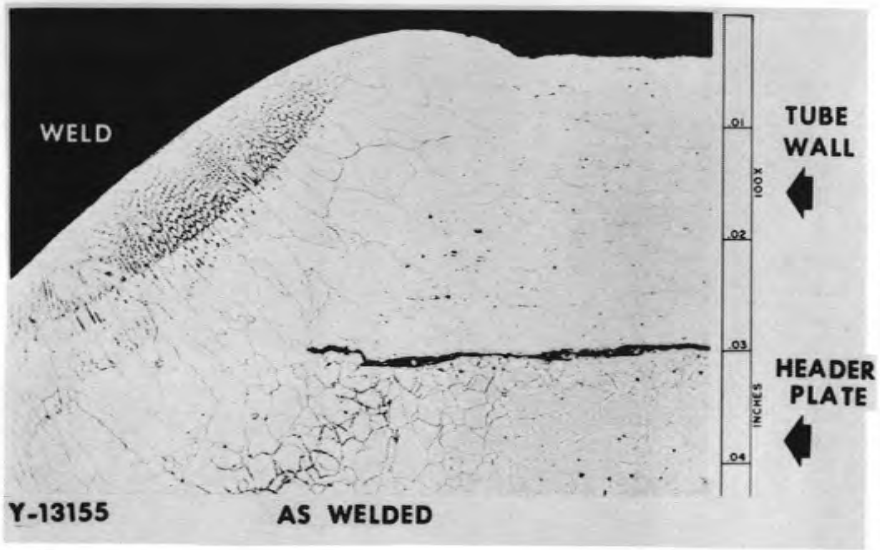

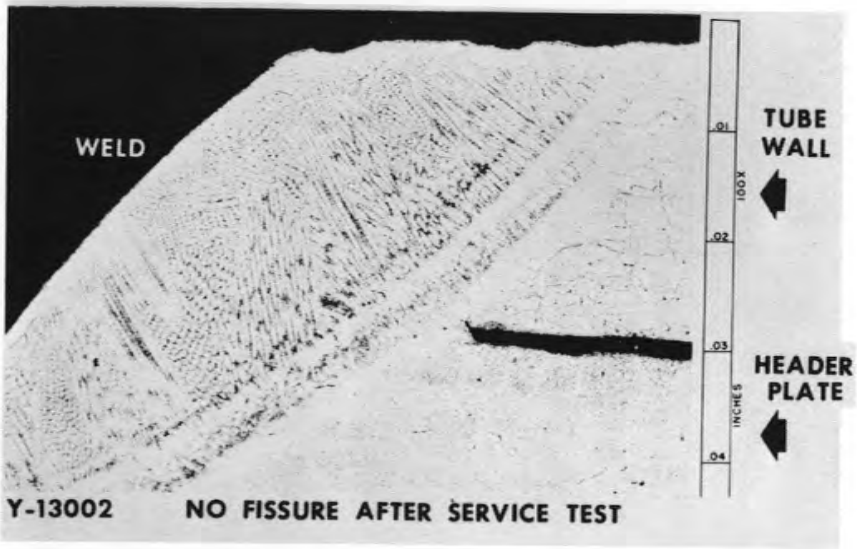

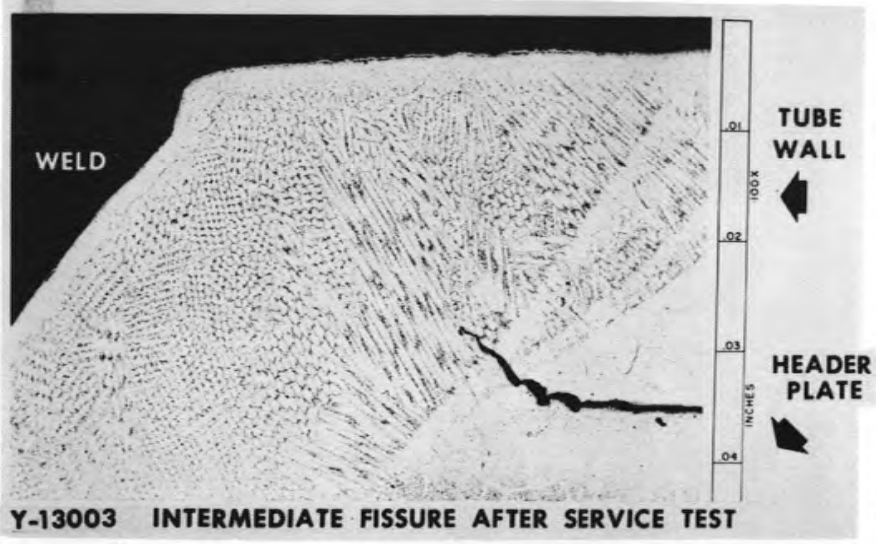

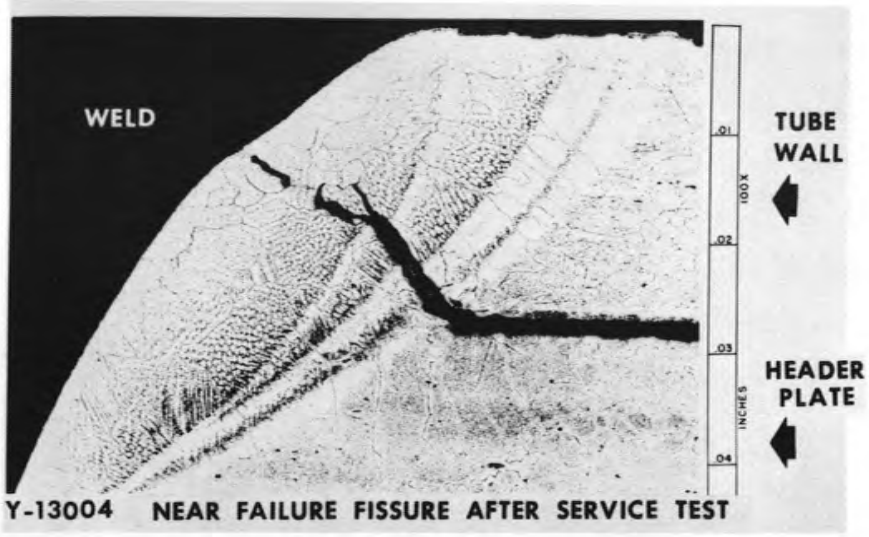

Fig. 34 (Y-13230) Propagation of Fissures in Tube-to-Header Welds of the Heat Exchanger of Fig. 31.

of microfissures in approximately 10% of the welds. The frequency of the failures, however, indicated that the unwelded root, characteristic of tube-to-header welds, may have been largely responsible for the initiation and subsequent propagation of cracks. It was quite apparent that a back braze was required to relieve this objectionable condition.

Research is in progress to evaluate a number of brazing alloys with respect to static and dynamic-corrosion resistance and to investigate the effects of the presence of Ni- and Ni-Cr-base brazing alloys on mass-transfer corrosion in heat transfer systems.

[redacted]

CONTROL ROD AND SHIELDING MATERIALS

J. H. Coobs

This report is given as a review of work done on control rod and shielding materials by the Aircraft Nuclear Propulsion Group at the Oak Ridge National Laboratory, using boron in the form of B_4C as the absorber material and utilizing several fabrication techniques to obtain suitable properties in the finished elements.

These control and shield elements may be divided into two general types: 1) small components fabricated directly into final form with close dimensional control, and, 2) larger elements requiring intermediate working (rolling or swaging) to obtain the desired properties and final size. We shall first consider several types of small components fabricated directly into useful parts by hot pressing.

The regulating rod elements designed for the Aircraft Reactor Experiment required very low boron concentrations of about 4 to 16 mg/cm^3 suspended in an inert carrier. A compatibility test in which Al_2O_3 plus 10% B_4C were hot pressed at 1800°C in a graphite die showed that these two materials were compatible.

A technique was next developed for fabrication of these control-rod slugs, which were required in the form of a hollow cylinder about 2-in. OD by 1-1/4-in. ID by 2-in. long. Mixtures of Norton 38-500 alumina and -325 mesh B_4C were prepared and hot pressed in the graphite die shown in Fig. 35. During loading, the bottom punch and mandrel rod were first positioned in the die. The powder was then added and leveled around the core rod, the top punch put in place and pressure applied to seat the punches. The die was then loaded into a hot-pressing furnace shown in Fig. 36, in which it was insulated with bubble alumina and heated by the induction coil while pressure was applied to the punch extensions. The lower punch rested on a graphite block which was insulated from the base by two alumina bricks. Hot pressing was carried out at a pressure of 2500 psi for five minutes at a temperature of 1650°C, and measured optically by means of a sight hole and prism.

The core rod and die were allowed to "float" during pressing, but it was found necessary to push the core rod out of the finished compact at the maximum temperature to eliminate breakage of the compacts by shrinking around the core.

These slugs of Al_2O_3-B_4C were then assembled into a finished regulating rod,

[redacted]

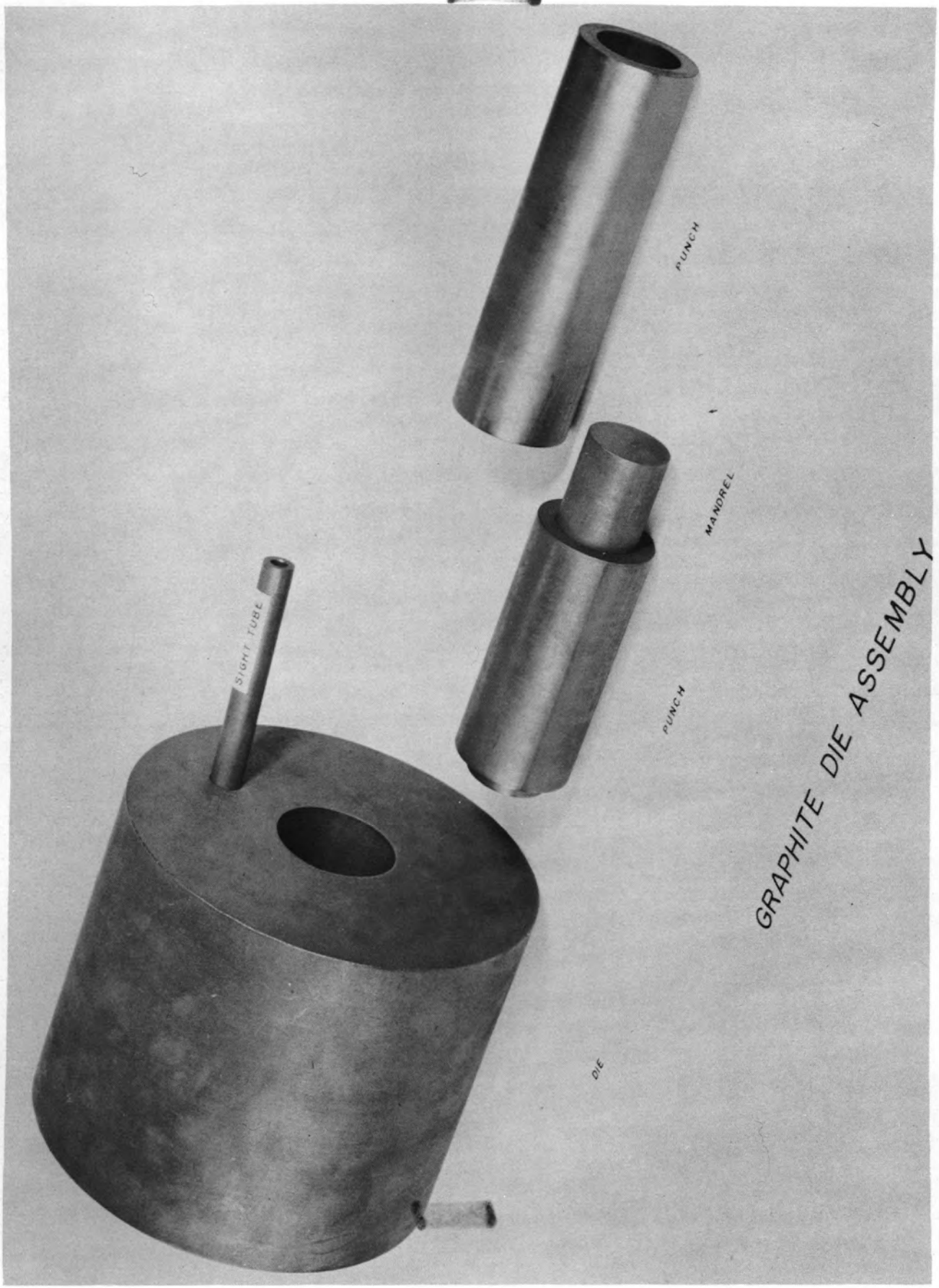

Fig. 35 (Y-7089) Graphite Die Assembly. Unclassified.

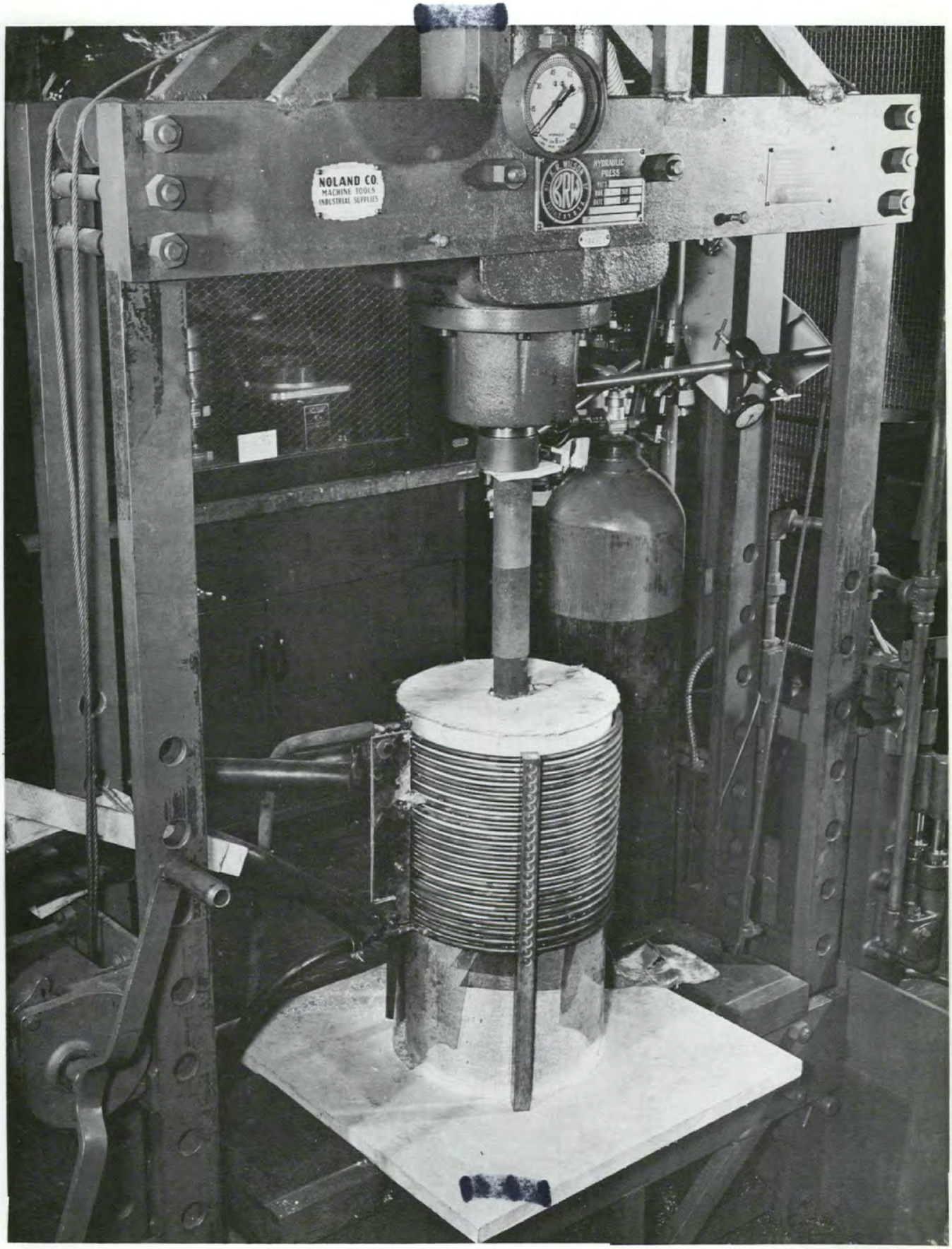

Fig. 36 (Y-7059) Hot Pressing Furnace. Unclassified.

[redacted]

as shown in Fig. 37. Fifteen of the components were assembled into the annular space between the inner and outer tubes, and the end caps were brazed in place using Nicrobraz.

The absorber slugs designed for use in the Aircraft Reactor Experiment's safety rods, or shim rods, were produced in much the same manner. Here, however, the prime objective was to incorporate as much B_4C as was feasible into a solid slug, which could then be canned in stainless steel and used in the flexible safety rods. Pure B_4C can be fabricated into highly dense and refractory bodies, but is prohibitively expensive. Therefore, some development work was done using metals such as copper, nickel, chromium, and iron to bond the B_4C powders. Of these, only iron was successful in producing sound bodies, and further work revealed that a mixture of 44% Fe and 56% B_4C by weight was quite strong and had an acceptable boron concentration. The two components react during the hot-pressing cycle to produce FeB and graphite, with the FeB acting as the cementing agent.

Sufficient cylinders were produced for the three safety rods, using essentially the same hot-pressing technique as described for the shim-rod components, except that the final pressing temperature was 1530°C. It was again necessary to push the core rod out of the slug at the maximum temperature to prevent breakage.

These slugs were quite uniform in size, were quite refractory, and would withstand thermal shock reasonably well. They were canned in stainless steel using Nicrobraz, as shown in Fig. 38.

A third type of absorber produced by the hot-pressing technique was several sets of shielding plugs for use in shielding instruments and equipment during "in-pile" experiments. This application requires a moderately high boron concentration in a solid body which, however, must be machinable, in order that holes may be cut as needed for passage of thermocouples, etc. The B_4C content was reduced to 30% by weight (40 volume %), and the B_4C was added as coarse particles of 44-105 micron size range to minimize reaction with the iron powder. By hot pressing at 1000°C with a pressure of 1750 psi, discs of this material up to 6-1/2-in. dia by 3/8-in. thick were prepared, containing about 0.52 g of boron per square centimeter of exposed area.

[redacted]

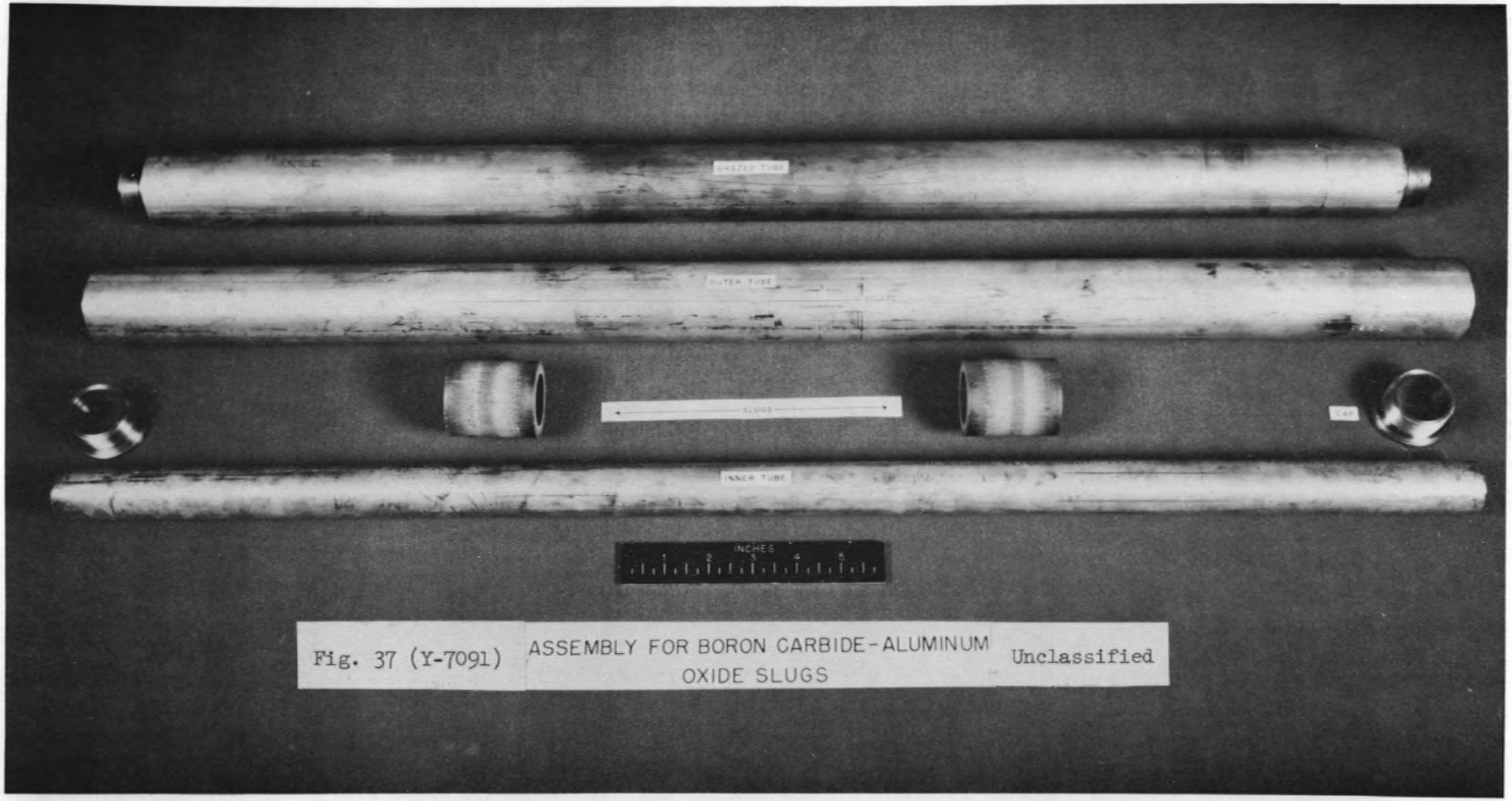

Fig. 37 (Y-7091) Assembly for Boron Carbide-Aluminum Oxide Slugs. Unclassified.

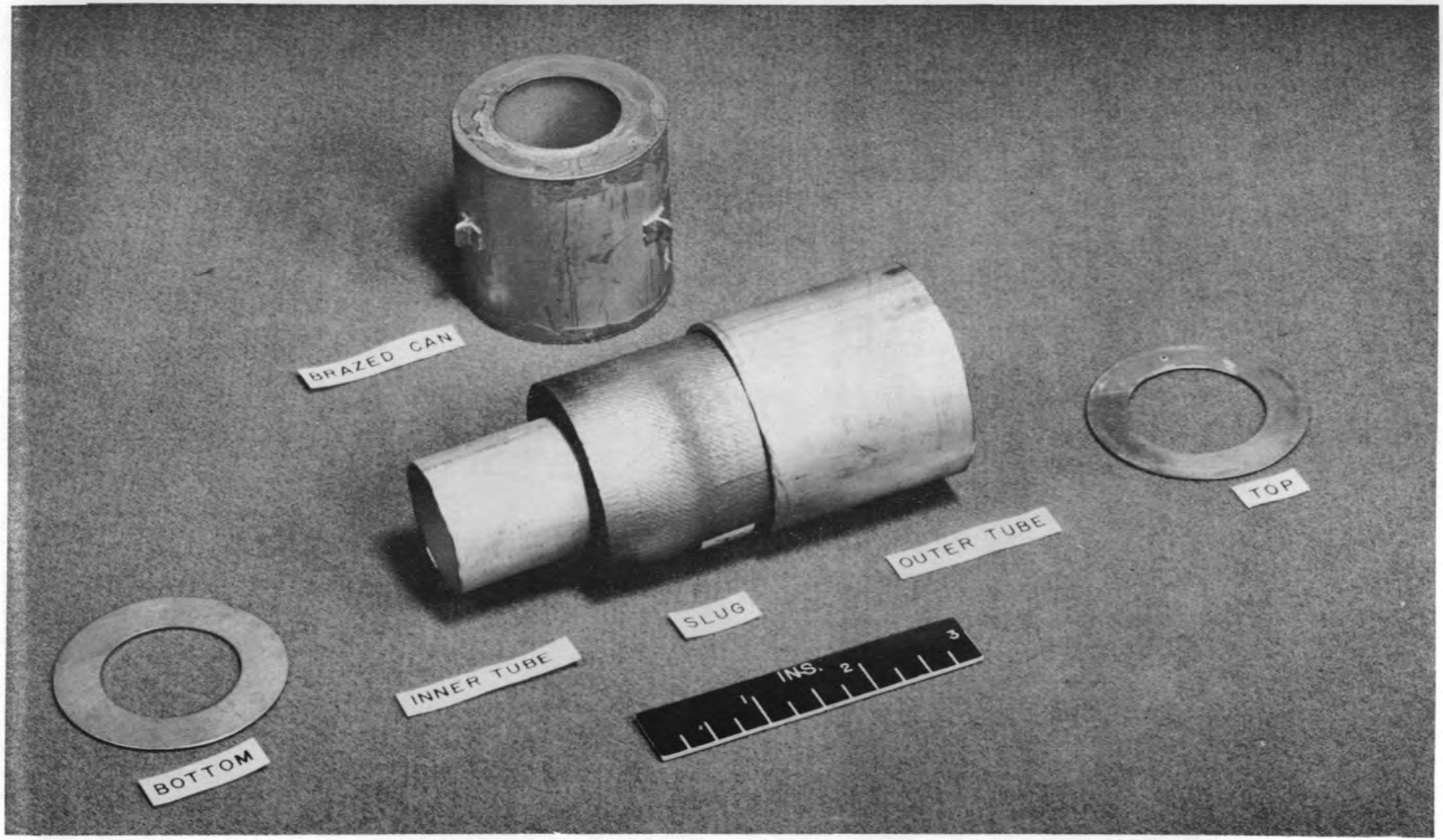

Fig. 38 (Y-7090) Assembly for Boron Carbide-Iron Slug. Unclassified.

[redacted]

The second general type of control element, which requires intermediate working to obtain final size and properties, is usually fabricated in the form of plate or rod 15 to 30 inches in length. Examples of these elements are those designed for the Homogeneous Reactor Experiment and Army Package Power Reactor, incorporating a core of Cu-B_4C clad with 0.030-in. of stainless, and the control rod of the General Electric-ANP design, 1/2-in. dia by 30-in. long with an Al-B_4C core and stainless cladding. These elements require a matrix of high thermal conductivity to dissipate the heat released by absorption of neutrons. A good bond between clad and core is desirable for the same reason.

Difficulties with the stainless clad Al-B_4C, or Boral, control plates originally specified for the Homogeneous Reactor Experiment led to development work using copper as a matrix material for the core of the plates.

The core composition of 16% by weight B_4C in copper (40% by volume) was prepared by powder-metallurgy techniques, using fine electrolytic copper and -325 mesh B_4C. Compacts were pressed, sintered at 900°C, and coined to a final density of 88% of theoretical. The plates were assembled using these core compacts, by the familiar picture-frame technique, as shown in Fig. 39. The compacts were pieced together to fill the frame, after which the assembly was sealed by edge welding, evacuated, and hot rolled at 1000°C.

Control plates for the Homogeneous Reactor Experiment and Army Package Power Reactor were prepared by this technique. They are superior to clad Boral plates in that a definite bond may be established between the cladding and core, thus promoting high thermal conductivity and eliminating voids which may lead to blister formation. The finished plates are ductile and may be bent on a modest radius without cracking in the core or at the interface.

A photomicrograph of the core-to-clad interface of a typical plate, containing 16 wt % B_4C in copper clad with 347 stainless steel is shown in Fig. 40. A partial bond is shown at the interface. A similar component is shown in Fig. 41, which is a photomicrograph of a plate containing 20 wt % B_4C in copper clad with Nichrome. In this plate a thin layer of copper was placed between the core and cladding to promote bonding, and the plate was cold rolled a total of 60% reduction with repeated anneals.

[redacted]

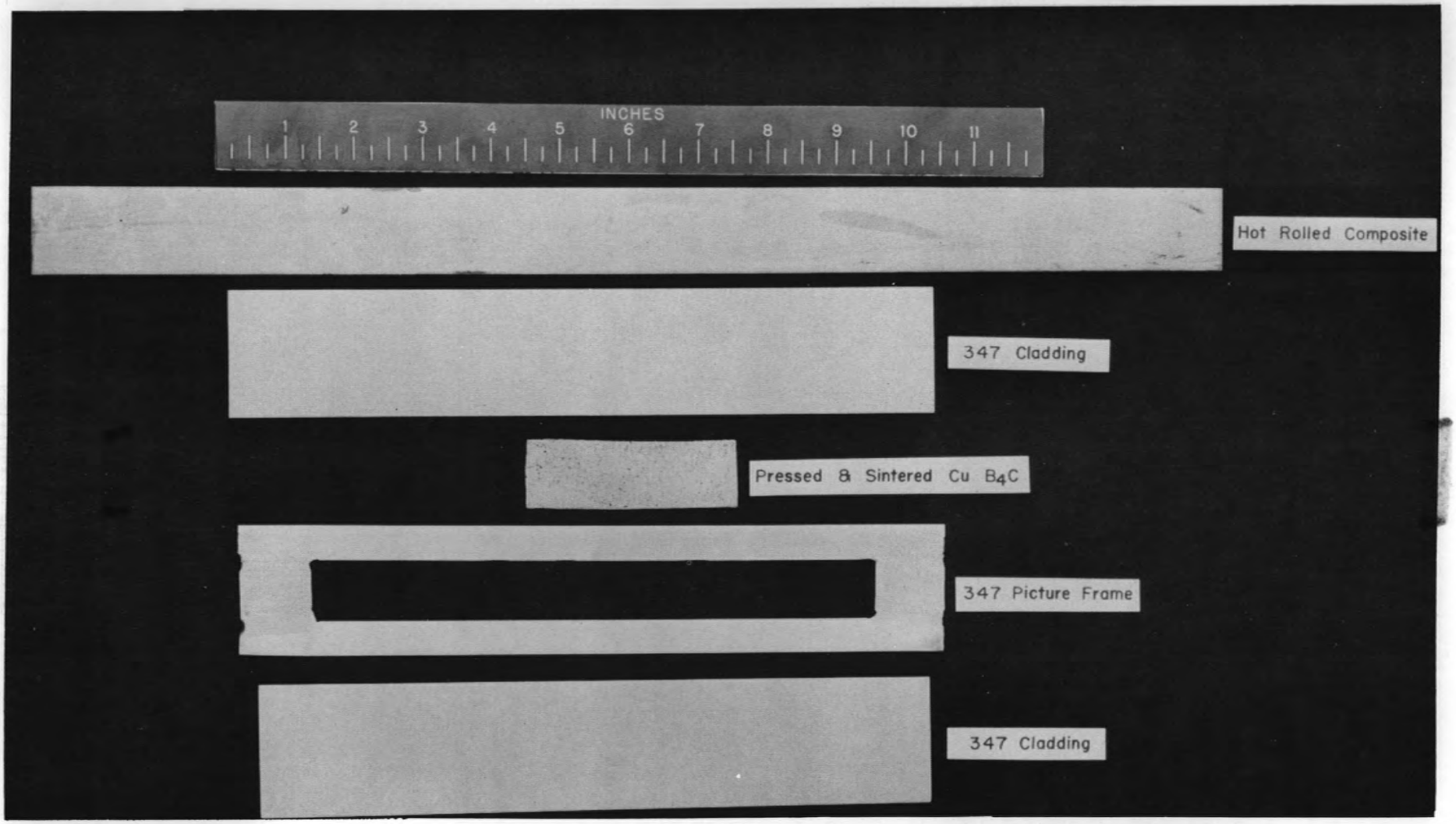

Fig. 39 (Y-7284) Components for HRE Control Plate. Unclassified.

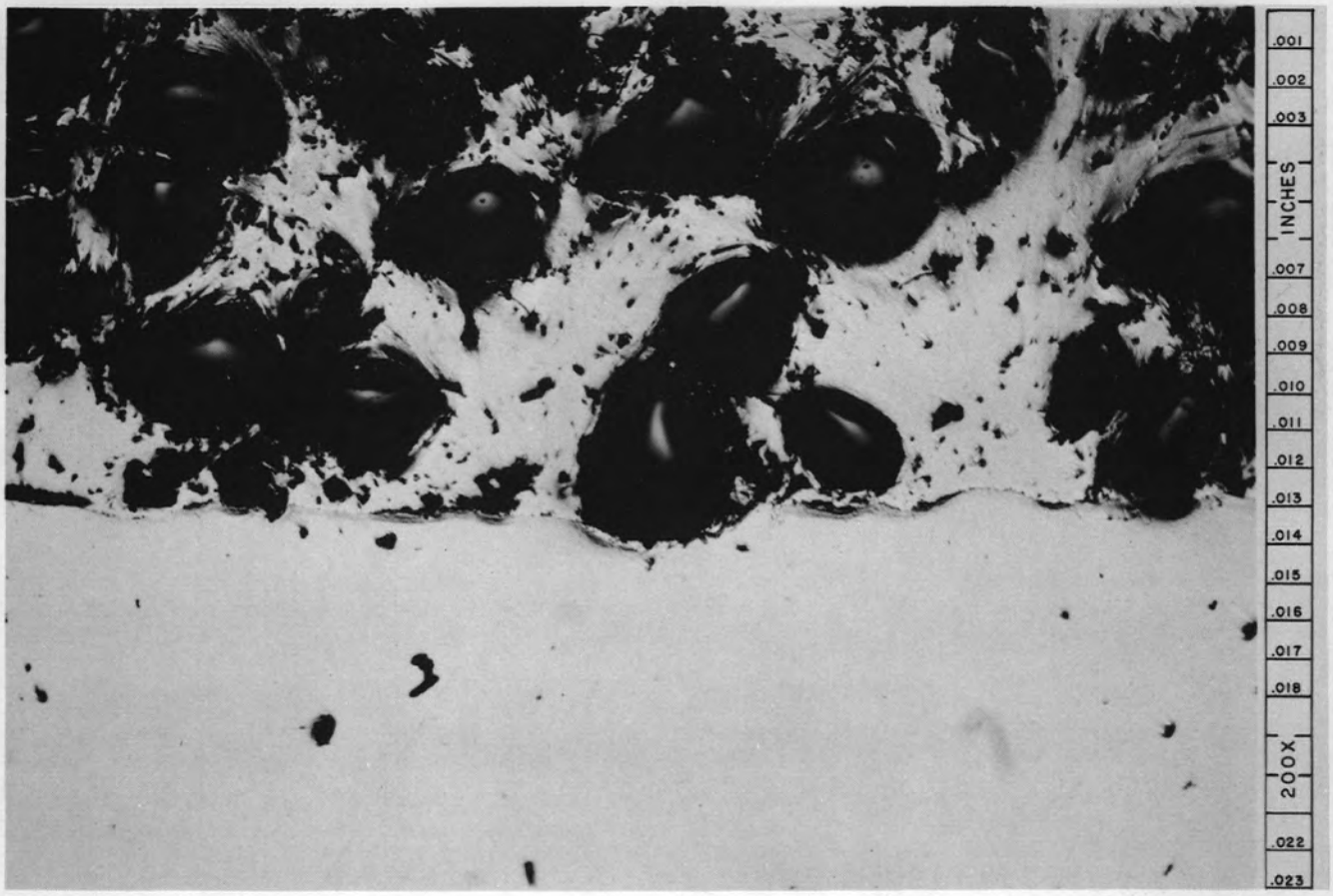

Fig. 40 (Y-6247) Interface of Stainless Steel Cladding with Boron Carbide-Copper Core. 200X. Unclassified.

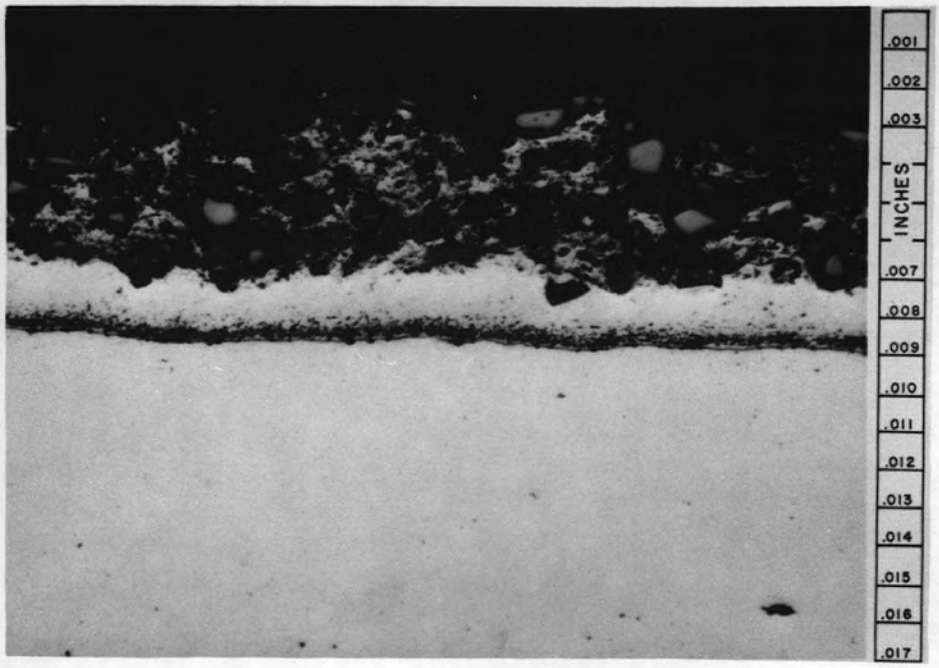

Fig. 41 (Y-13538) Interface of Nichrome Cladding with 20% Boron Carbide-Copper Layer. Note intermediate copper layer. 200X. Unclassified.

[redacted]

Control rods of the General Electric-ANP design are also of this general type, using a mixture of aluminum and B_4C powders which is packed into a tube and swaged to consolidate the mixture and form a solid rod. First attempts were to adapt the Fe-B_4C composition to this design. However, the inherent porosity and low thermal conductivity of this material, as well as failure of efforts to bond it to the tube wall by brazing, caused interest to turn to copper and aluminum for the matrix.

Mixtures of the powders were tamped into the tubes, evacuated and hot swaged to consolidate and establish a bond between tube wall and core. The finished rods had a boron density of about 1 g/cc, with good conductivity. For this application the additional weight of the copper was objectionable, and the Al-B_4C mixture has been used for fabrication of finished rods.

In recent work, the Al-B_4C mixture has been tamped tightly into the tube with a pneumatic hammer followed by cold swaging instead of hot swaging, with good results.

The final control element to be discussed is the proposed boron shield for the Circulating Fuel Reactor Experiment. This will be in the form of two spheres, on either side of the heat exchanger, and should have a high boron density of 1.4 - 1.5 g/cc with a thickness of only about 1/8-in. due to space limitations. Some experimental work has been done on this shield, using a composition of 53% B_4C in copper (60% by volume) and warm pressing at a temperature of 450°C at 40 tsi. By this means fairly strong bodies were obtained with a boron density of about 1.1 g/cc, or somewhat lower than the 1.4 g/cc specified. Further development work is being done on this problem using various non-metallic binders.

A summary of the various materials discussed is presented in Table III. The materials are tabulated according to the matrix material used, with the B_4C content tabulated both on a volume and weight basis. The boron concentration of the materials is also tabulated on a density basis and as a function of the exposed area. And finally, the proposed application for each element is listed.

[redacted]

TABLE III. CONTROL ROD AND SHIELDING MATERIALS

Matrix Material	B_4C Content % by Weight	% by Volume	Boron Concentration g/cc	g/sq.cm.	Application
Fe	56	64	1.15	0.75	ARE Safety Rods
Fe	30	41	0.74	0.52	Shielding Plugs
Cu	16	41	0.74	0.10	HRE Control Plates
Cu	16	41	0.74	0.20	APPR Control Rods
Cu	20	47	0.85	0.015	Nichrome Clad
Cu	25	54	0.97	0.105	G. E.-ANP Control Rods
Cu	53	60.5	1.09	0.43	CFRE Shield
Al	53	50	0.90	0.098	G. E.-ANP Control Rods
Al_2O_3	0.02	0.03	0.016	0.014	ARE Control Rods

PRESENT STATUS OF LITHIUM, SODIUM AND RUBIDIUM

E. E. Hoffman
M. J. Whitman
W. D. Manly

The majority of the work carried on by the General Corrosion Group of the Oak Ridge National Laboratory Metallurgy Division in the liquid metal field recently has centered on lithium, sodium and rubidium. The loading and handling technique is similar for all materials tested by the General Corrosion Group and will be discussed briefly, since testing methods are extremely important, especially in the testing of the very active alkali metals.

The lithium, sodium, and rubidium metal used in the tests to be discussed is handled in a purified inert-gas atmosphere at all times during the loading operation. All installations working with active materials of the nature being discussed in this paper have need of a dry box in their work, and Fig. 42 (Y-10944) shows the type currently being used by our group. This vacuum dry box is evacuated to one micron or less prior to introducing helium gas, which is purified by passing it through a copper coil packed with activated charcoal and immersed in a stainless steel dewar flask containing liquid nitrogen. This box employs a large plexiglass dome which may easily be removed. Figure 43 (Y-10945) shows a top view of the box, with the plexiglass dome removed. Melting, casting, loading, and heliarc-welding operations can be carried out with little if any contamination of the materials being tested.

The following is a brief summary of the present status of the lithium, sodium, and rubidium corrosion work, in that order.

Lithium

As is quite well known to those associated with the lithium-corrosion picture, a large amount of work was done three or four years ago at the Oak Ridge National

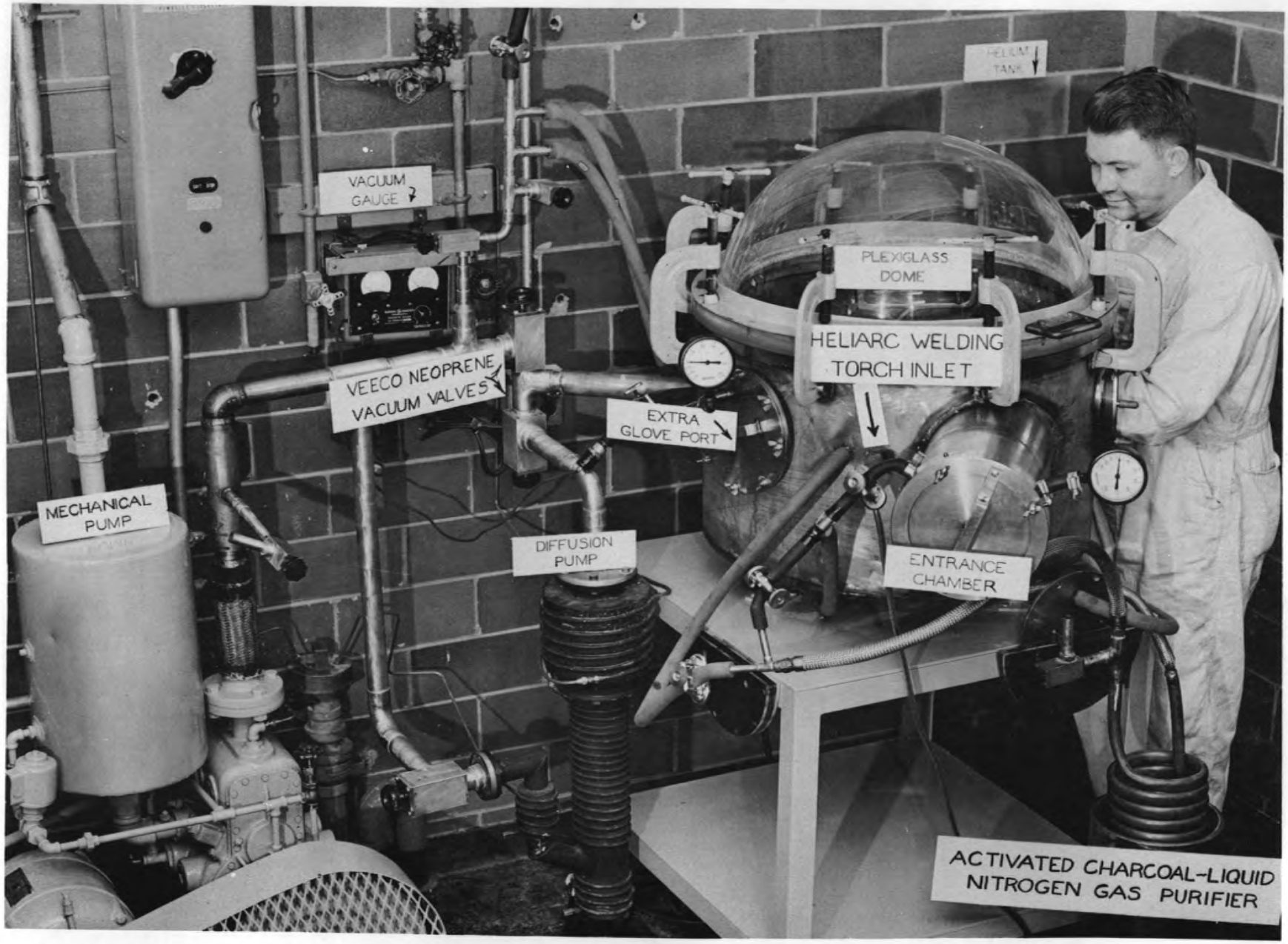

Fig. 42 (Y-10944) Vacuum-Atmosphere Dry Box. Unclassified.

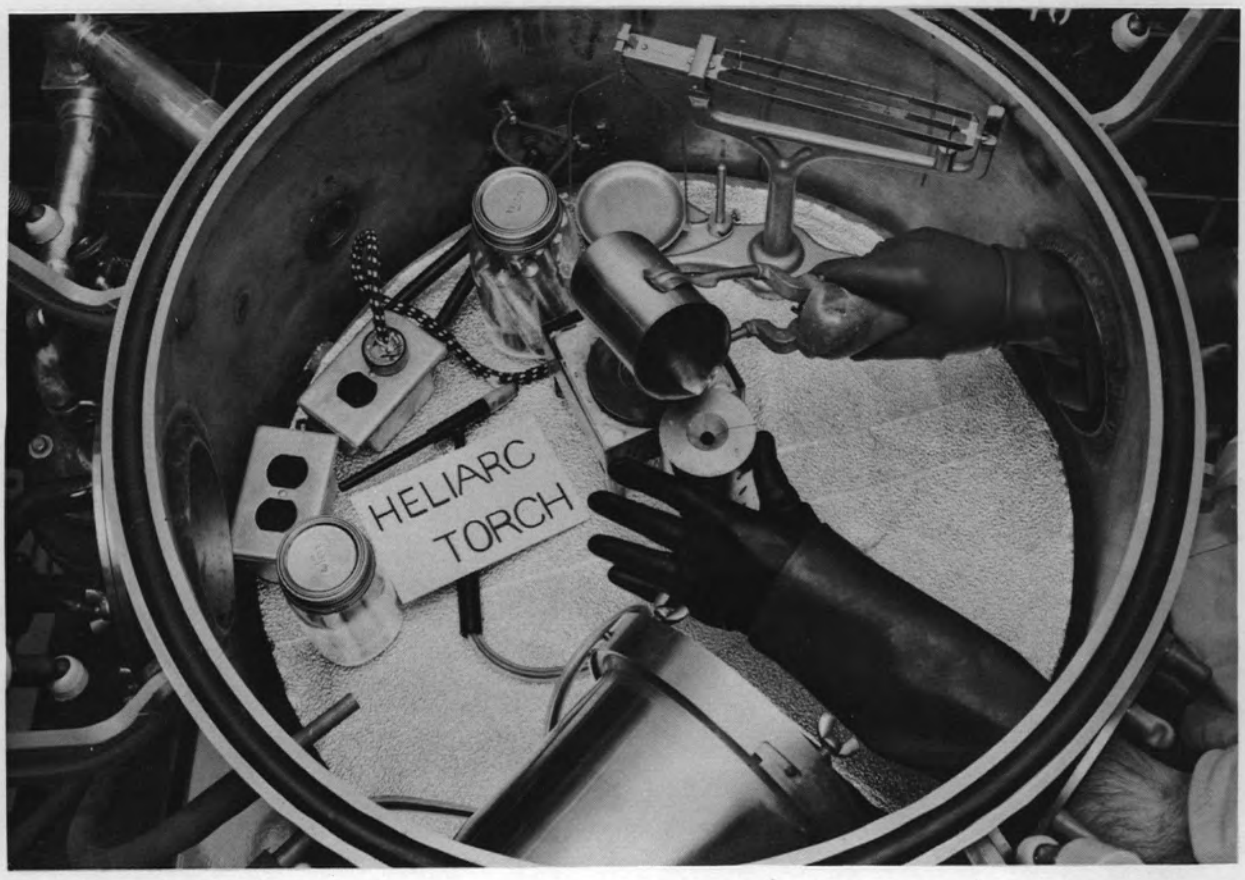

Fig. 43 (Y-10945) Top View of Vacuum-Atmosphere Dry Box with Plexiglass Dome Removed. Unclassified.

Laboratory, and elsewhere, in an effort to find materials with satisfactory corrosion resistance to attack by high-temperature lithium. A large amount of the early work was done in so-called three-component tests. Tests of this nature employ a capsule of a relatively inert material to contain a specimen of the material being tested and the bath metal. Obviously, many reactions, such as dissimilar-metal mass transfer, occur under these conditions, which obscure the actual corrosion resistance of the material being tested. In spite of this, the early tests conducted at 1500°F and 1830°F showed that pure metals, such as iron, niobium, tantalum, molybdenum, and tungsten, possess good resistance, but that potential materials of construction, such as the nickel-base alloys, cobalt-base alloys, and the austenitic stainless steels were severely damaged. The mode of attack on the austenitic stainless steels was generally intergranular in nature, the attacked regions being transformed from austenite to ferrite due to preferential leaching of nickel. The ferritic grades of stainless steel were found to be unsatisfactory in this temperature range, although they were superior to the austenitic grades. As a result of these early corrosion tests, the use of lithium was deemed unattractive in spite of the many other desirable properties of lithium-7 as a reactor heat transfer medium.

Quite a few two-component tests have been conducted on lithium during the past year or so. The principal purpose of these tests is to find a potential engineering metal or alloy, which will withstand the corrosiveness of molten lithium both under static and dynamic conditions at a maximum temperature in the range from 1000°F to 1800°F. This research is far from complete but tests to date tend to indicate that in two-component tests the corrosion and mass transfer are not as serious as was indicated by the earlier three-component tests.

Although the present tests have been conducted on a variety of materials and alloys, only the results on 316 stainless steel will be reported. Figure 44 (Y-2681) shows the extent of the attack (15 to 20 mils) in an early three-component test on this

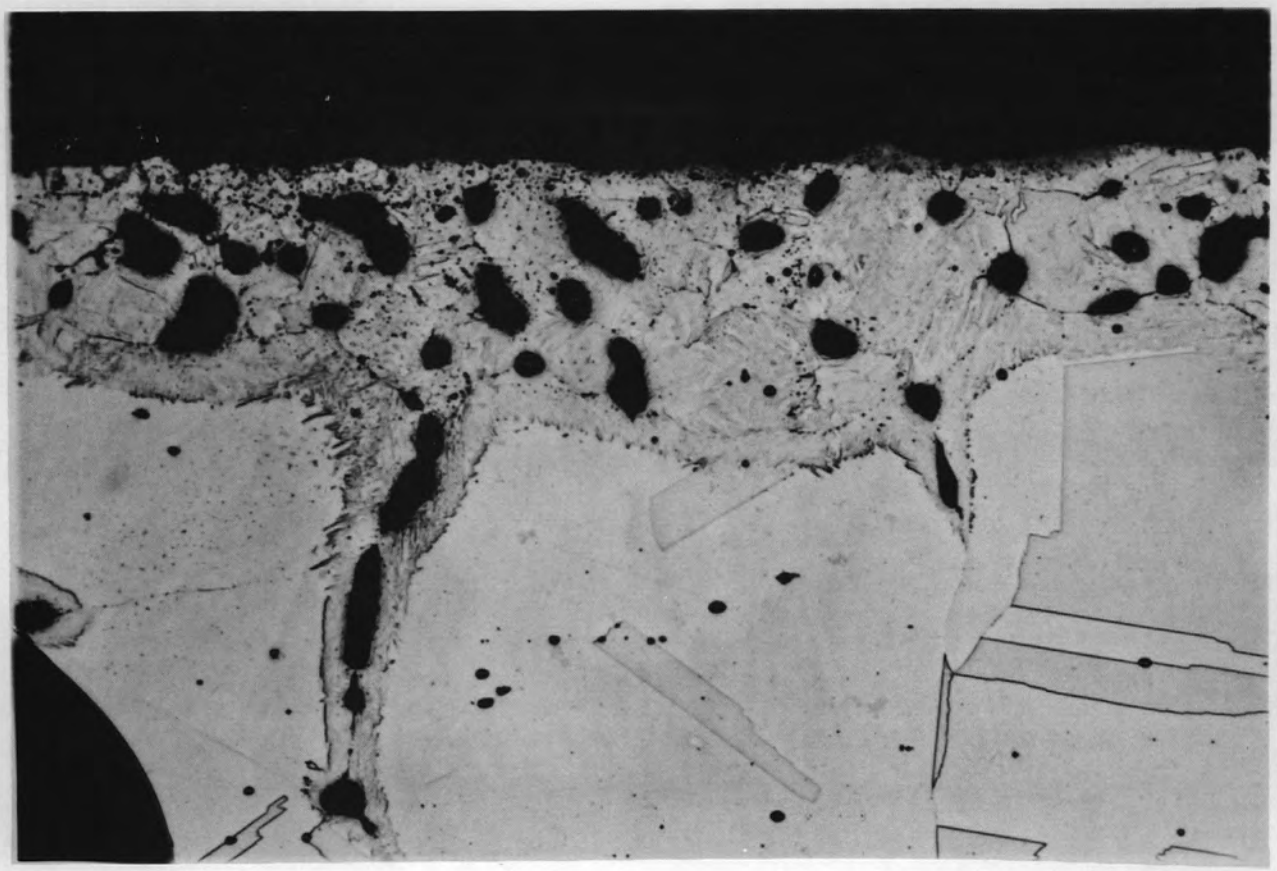

Fig. 44 (Y-2681) Type 316 Stainless Steel Specimen Following 400-Hr Exposure to Static Lithium at 1000°C (1830°F) in Armco-Iron Container. 250X. Etched with Aqua Regia. Unclassified.

austenitic alloy during a 400-hr exposure to lithium at 1830°F. The test container in this case was Armco iron. The magnification of this photomicrograph is to 250X, while that of Fig. 45 (Y-8636) is 1000X. This specimen was tested at the same temperature and time as the preceding specimen. This was a two-component test, both specimen and the tube being 316 stainless steel, and the attack was reduced from approximately 20 mils to 2 mils. This improvement in performance may be attributed both to the elimination of the third component, the Armco-iron capsule, and increased purity of the lithium bath metal. The results tend to indicate that the attack on the steel itself, and consequent failure, may not be the real problem since attack to depths of this magnitude would not prohibit the metal's use in such a system. However, mass transfer is thought to be a major problem in lithium-stainless steel systems and small amounts would be very serious in a system where small tubing might be plugged by crystal deposition. Two types of dynamic tests have been employed in determining the extent of mass transfer. The first is a seesaw furnace (Fig. 46, Y-9782), which rocks up and down, allowing the bath, which is sealed in a tube inside the furnace, to flow from one end of the tube to the other. Any desired temperature differential may be obtained by adjusting the temperatures of the hot and cold zones. Figure 47 (Y-10174) shows the hot-and cold-zone surfaces of a 316 stainless steel tube in which lithium has been circulated for 500 hr at the indicated temperatures.

Appreciable mass transfer occurred and is visible on the cold-zone surface. This test was conducted at a hot-zone temperature of 1600°F. A similar test in which the hot-zone temperature was 1400°F had only microscopically visible amounts of crystal deposition on the cold-zone surface.

Three 316 stainless steel thermal-convection loop tests have been completed recently and the results of these have been encouraging. Figure 48 (Y-12638) shows one of these loops which has been split longitudinally following test. This loop

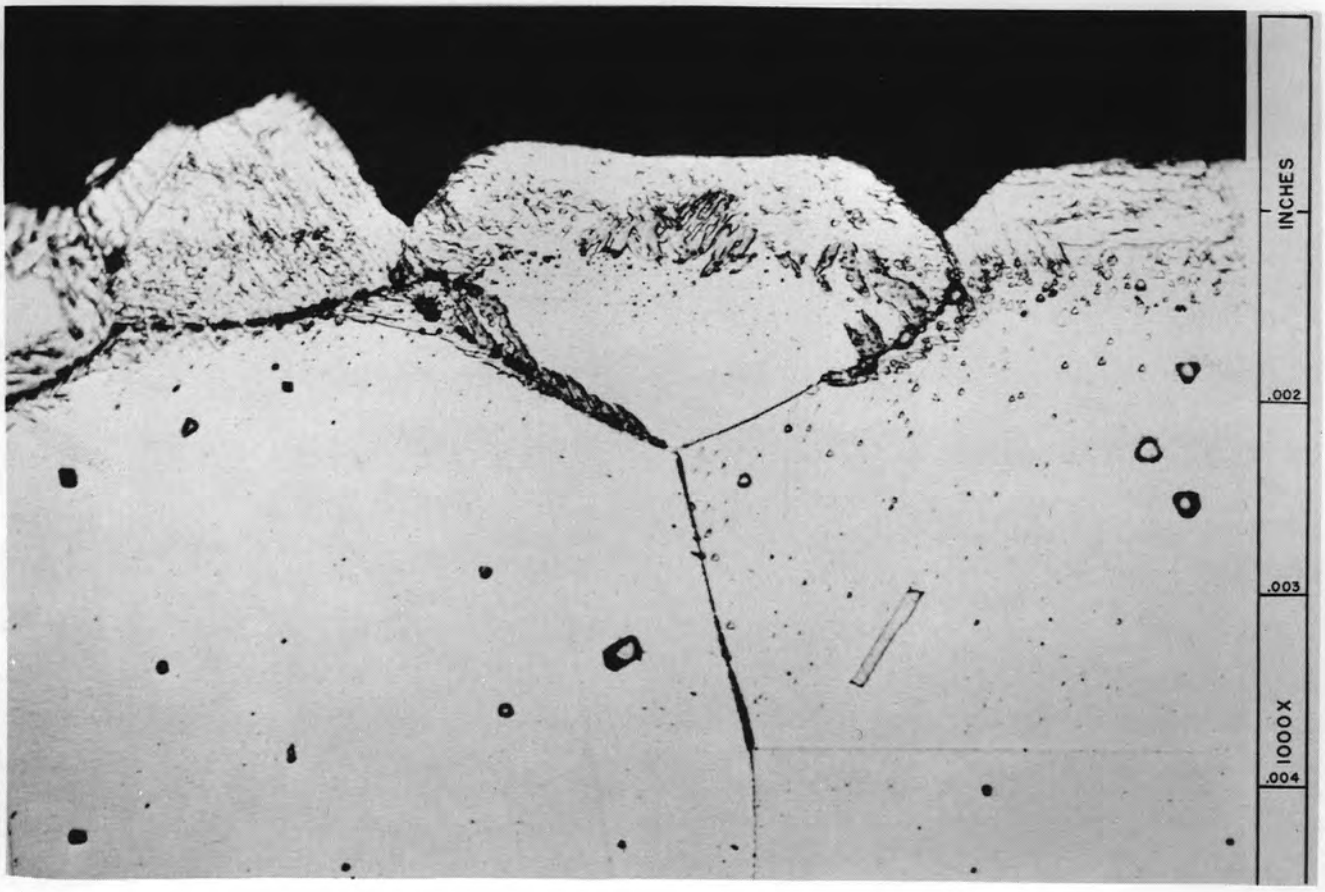

Fig. 45 (Y-8636) Type 316 Stainless Steel Specimen Following 400-Hr Exposure to Static Lithium at 1000°C (1830°F) in Type 316 Stainless Steel Container. 1000X. Etched with Glyceria Regia. Unclassified.

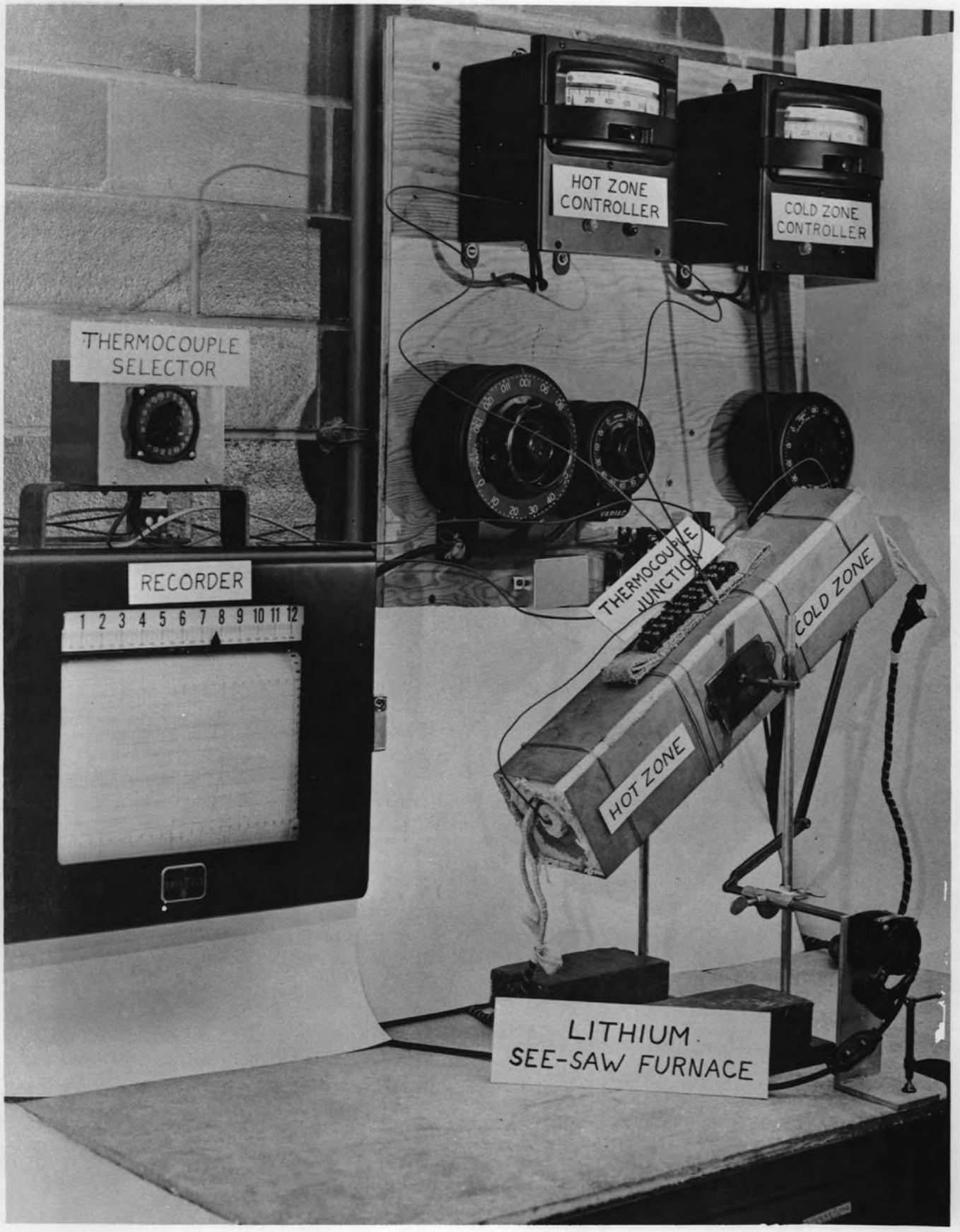

Fig. 46 (Y-9782) Lithium See-Saw Furnace. Unclassified.

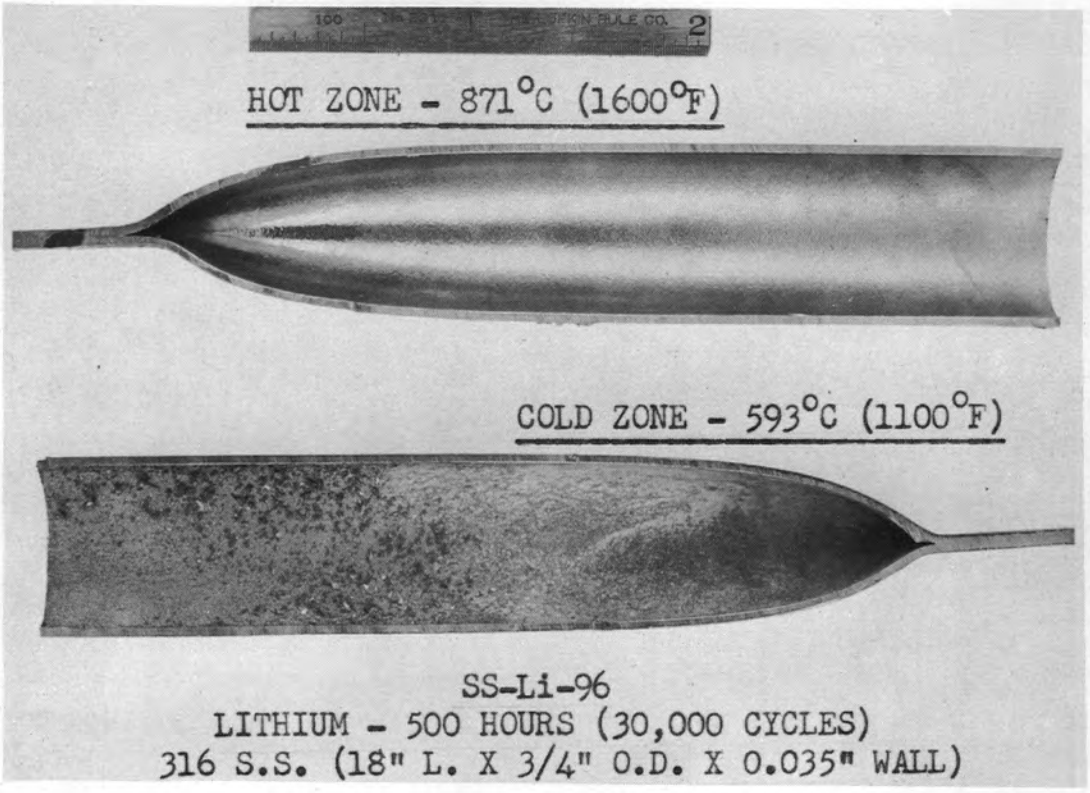

Fig. 47 (Y-10174) Hot- and Cold-Zone Sections of Type 316 Stainless Steel Tube Following Lithium See-Saw Test. Note crystals on cold-zone surface. Unclassified.

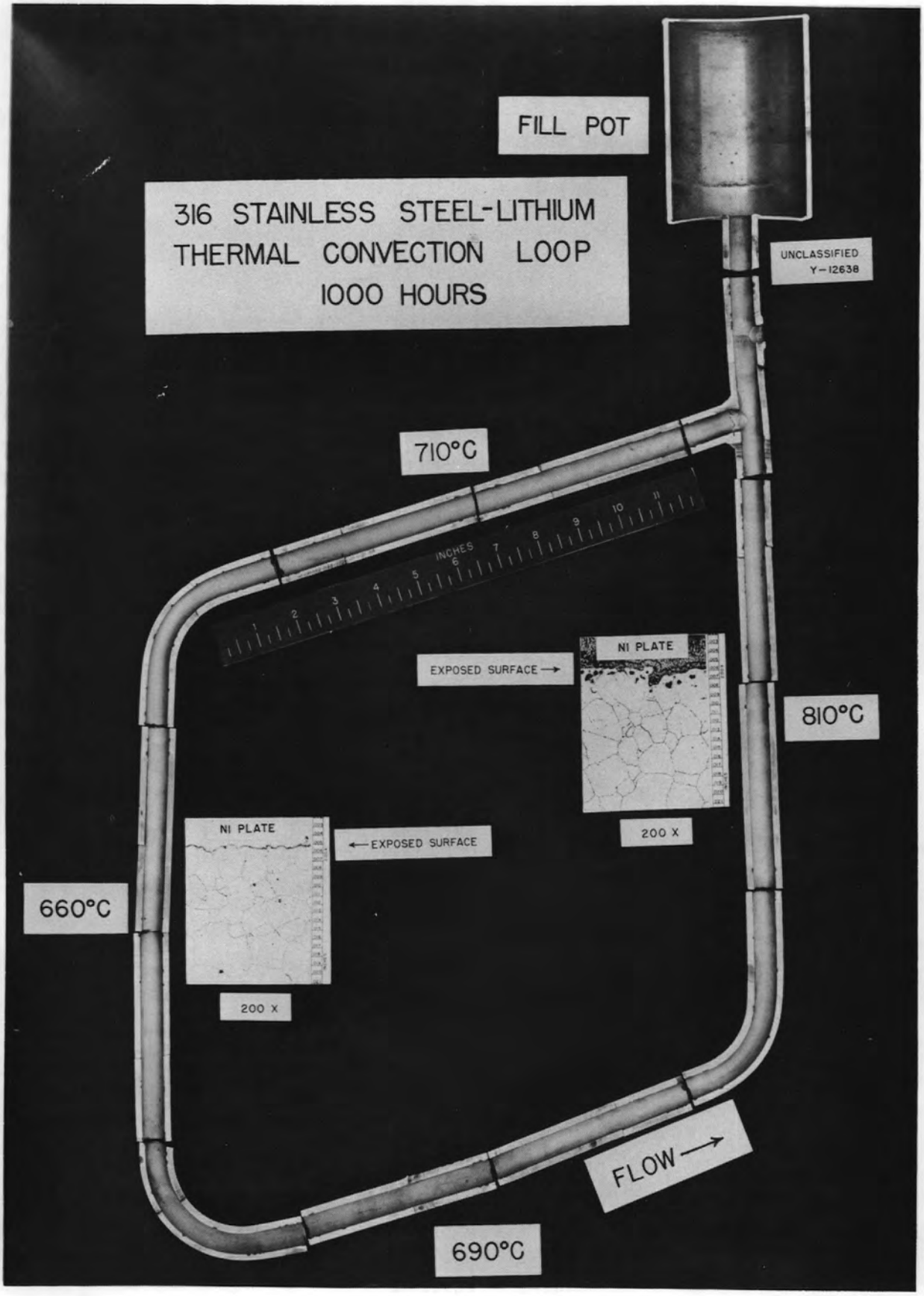

Fig. 48 (Y-12638) Insets Show Extent of Attack on Hot and Cold Zones of Pipe. Specimens nickel plated following test to preserve edge during metallographic polishing. Unclassified.

operated at a hot-zone temperature of 1490°F for 1000 hr and gave no thermal evidence of plugging during test. There was no crystal deposition on the surface of the loop except for a small amount which occurred at the liquid-gas interface just below the fill pot. Metallographic examination revealed less than one mil of attack on the cold zone and a two-mil attack on the hot zone (Fig. 49, Y-12573). Specimens examined metallographically are nickel plated following test to preserve the edge of the specimen during polishing. Two similar tests at hot-zone temperatures of 1450 and 1300°F, respectively, did not plug during the 1000-hr test period, although the latter test at the lower temperature did have macroscopically visible crystal deposition in the cold zone. The reason for these differences in amount of crystal deposition are not understood at present.

It should be mentioned, before concluding on lithium, that a slight amount of contamination of the lithium metal with lithium nitride has a serious effect on the corrosiveness of the lithium bath. Figure 50 (Y-10604) shows the wall of a 316 stainless steel tube following a 100-hr static test at 1600°F in lithium to which 0.1% Li_3N had been added. This tube was attacked throughout its entire 35-mil wall thickness, the top edge being exposed to the bath, while a similar standard test with no addition was attacked to a depth of less than 2 mils.

Mass transfer crystals in tests on iron-base alloys have been found to be chiefly iron, while those in tests on nickel-base alloys are chiefly nickel. Although iron has very good resistance to static lithium, it is guilty of mass transfer in dynamic systems constructed of iron-base alloys.

Sodium Corrosion

Most of the work done on sodium recently at our installation has been directed at determining the compatibility of a beryllium-sodium-Inconel system and this special topic is being covered in one of the other papers.

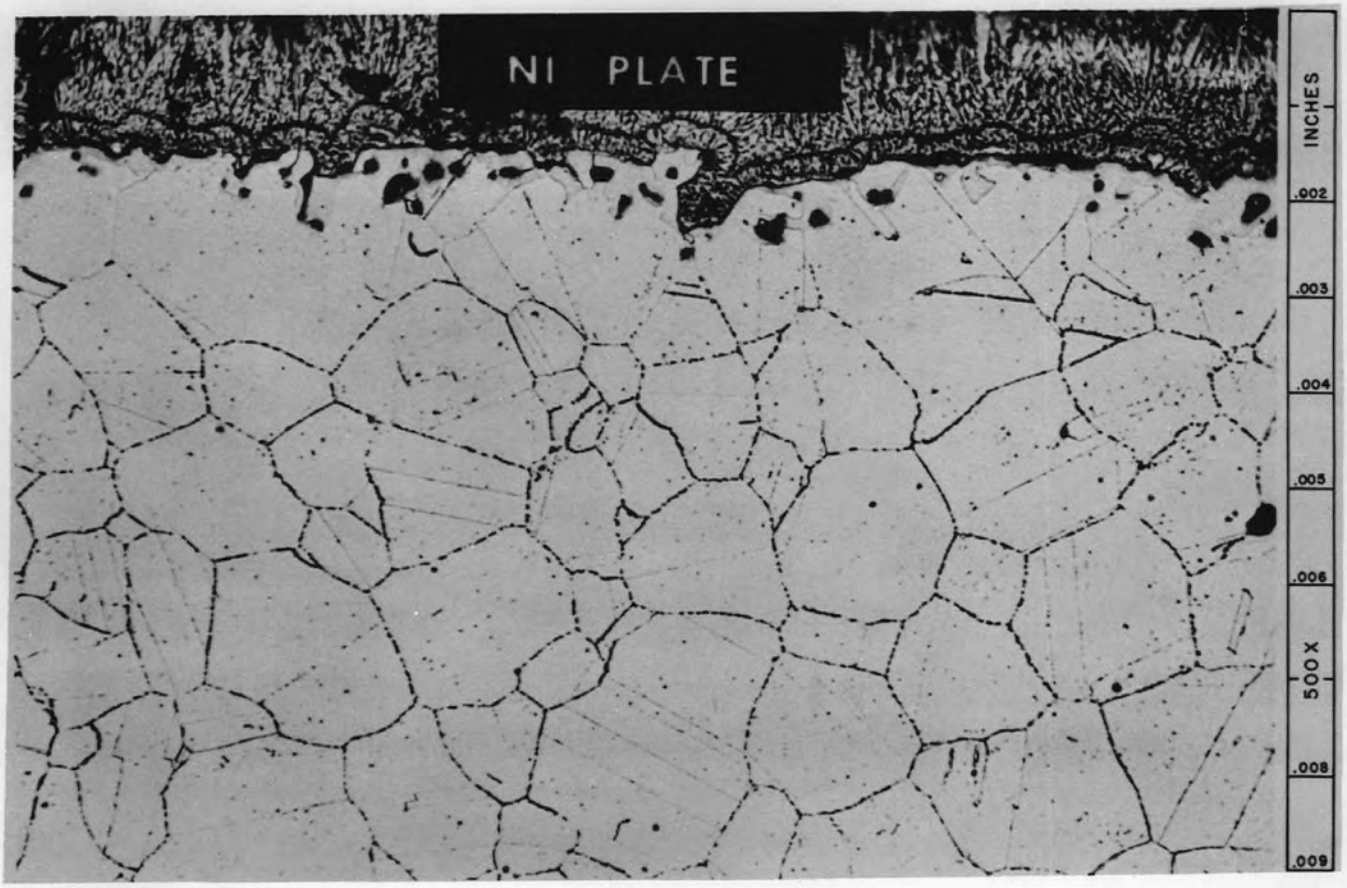

Fig. 49 (Y-12573) Hot-Zone Surface of Type 316 Stainless Steel Thermal-Convection Loop Shown in Fig. 48. Etched with Glyceria Regia. 500X. Unclassified.

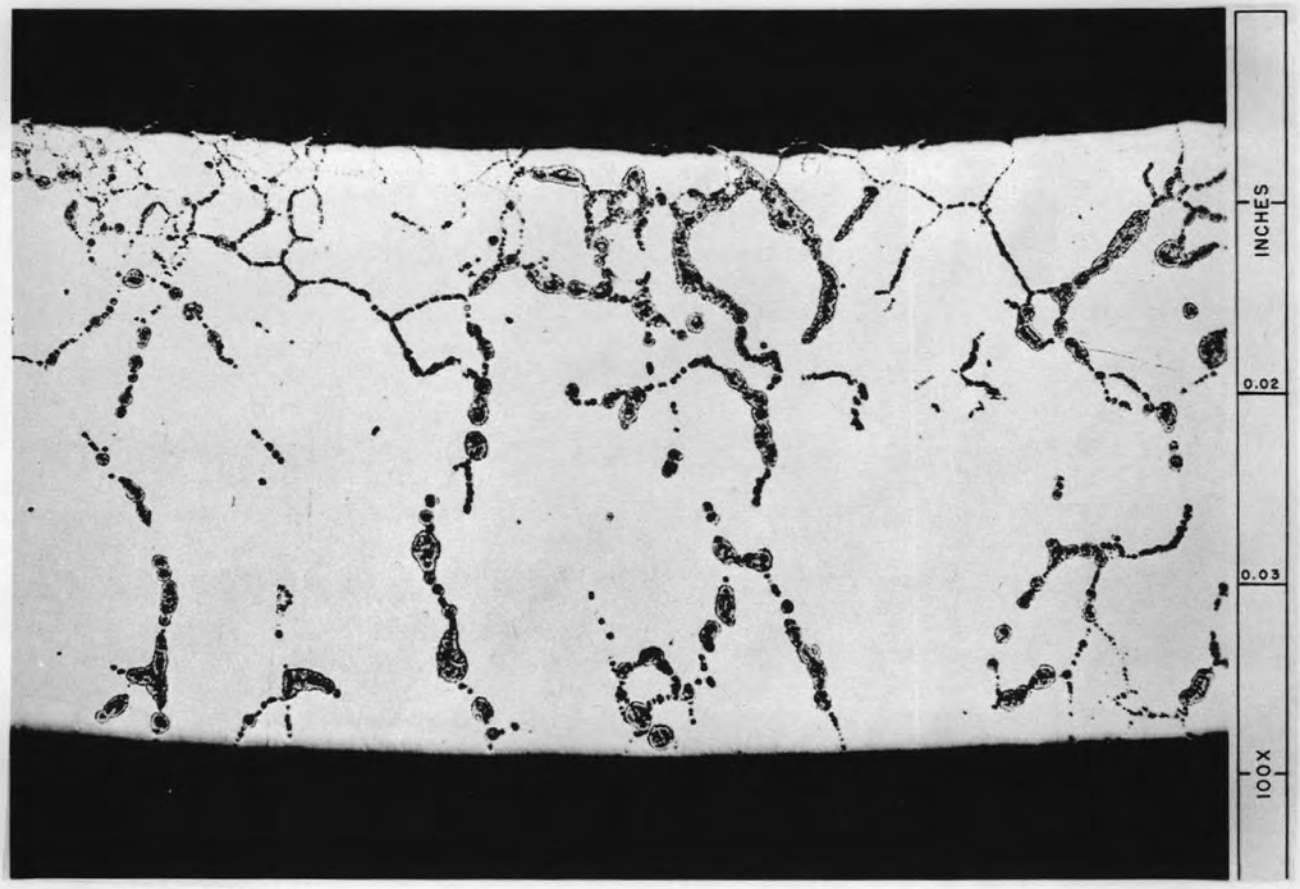

Fig. 50 (Y-10604) Type 316 Stainless Steel Tube Following 100-Hr Exposure to Lithium (Plus 0.1% Li_3N) at 1600°F. Tube attached intergranularly throughout 35-mil wall thickness. Exposed surface at top. Unetched. 100X. Unclassified.

Since there is hope of using an alloy of the Hastelloy-B type in the Circulating Fuel Reactor Experiment, thermal-convection-loop tests have been conducted to determine the resistance of this material to sodium in a dynamic system. Two tests conducted at 1500°F for 1000 hr have recently been completed. One loop showed a slight amount of metal deposition while the other loop plugged completely, shortly before the test was scheduled to be terminated. The metallic plug was 1-1/2-in. in length and was magnetic. It was analyzed and found to contain nickel with a small amount of molybdenum. This mass transfer is attributed to solution in the hot zone of the loop during the test. However, tests will also be conducted on similar alloys with chromium additions to study their effect on the mass transfer of nickel-molybdenum alloys in sodium systems.

Rubidium

Recent tests have been conducted on rubidium metal in cooperation with an Oak Ridge School of Reactor Technology Summer Project Group. Rubidium, having a low melting point of 102°F and a boiling point of 1270°F, coupled with good nuclear properties, would make an excellent reactor coolant. The rubidium metal, used in the experiments which will be discussed, was prepared by calcium reduction of the rubidium fluoride salt by the Stable Isotopes Division of the Oak Ridge National Laboratory.

Static tests at 1500 and 1650°F on rubidium in Inconel containers showed an attack of 1 to 2 mils in 100 hr. The attack, which is both intergranular and in the form of subsurface voids, may be seen in Fig. 51 (Y-12923).

Since these tests indicated that under static isothermal conditions corrosion of Inconel by rubidium was not a serious problem, a dynamic test was conducted. The resistance of Inconel to corrosion by flowing liquid and vapor rubidium in a closed system incorporating a temperature gradient was determined by means of a dynamic loop apparatus, somewhat similar in appearance to the conventional thermal-convection loops. The sectioned loop following test may be seen in Fig. 52 (Y-13038). The hot legs of the loop

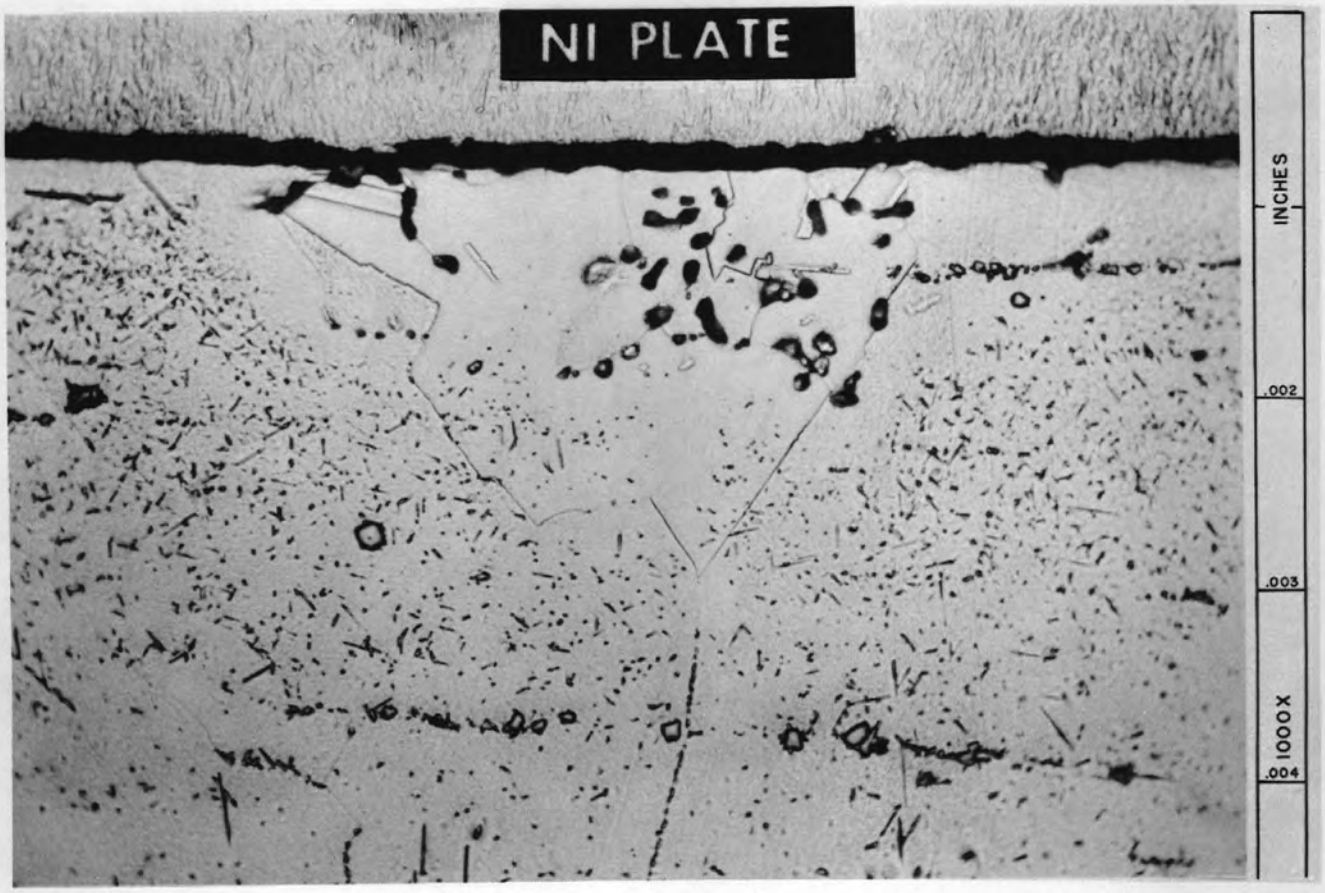

Fig. 51 (Y-12923) Inconel Exposed to Static Rubidium for 100 Hr at 1650°F. Specimen nickel plated after test to protect edge. Etched with Glyceria Regia. 1000X. Unclassified - [redacted] with caption.

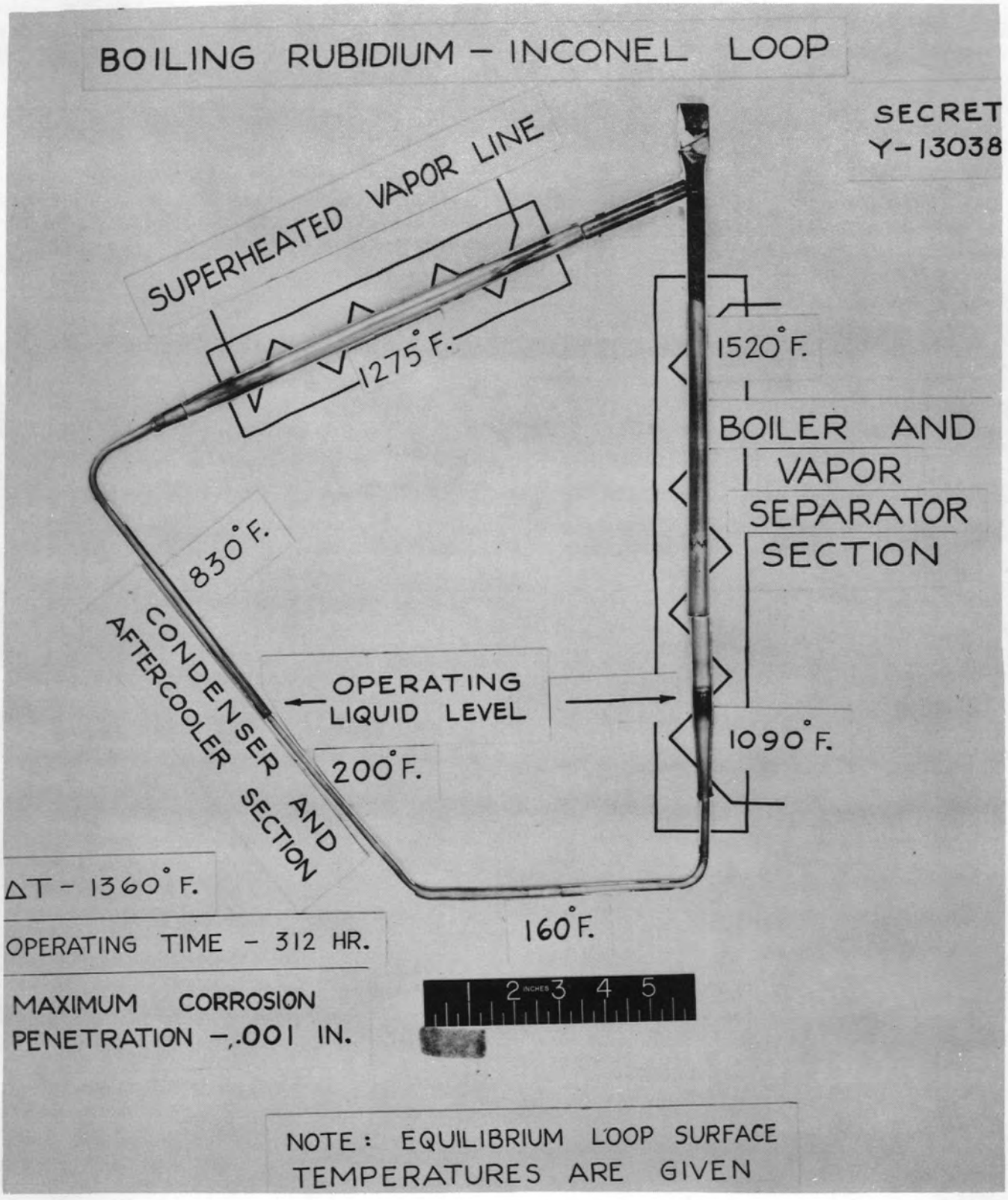

Fig. 52 (Y-13038) Inconel - Rubidium Boiling Loop.
Classification [redacted]

were constructed of 1/2-in.-OD, 49-mil-wall tubing while the condenser section was of 1/4-in, 35-mil-wall tubing. The loop was loaded with 8 cc (12 g) of vacuum-distilled rubidium, which filled it to the level indicated in Fig. 52. This test was conducted at a hot-zone temperature of 1500°F for 312 hr. Specimens from various sections of the loop were examined metallographically. The maximum attack in the loop was to a depth of one mil and occurred in the hot leg of the loop (see Fig. 53, Y-13041). The attack is intergranular in nature and one grain appears to be ready to fall from the wall.

Figure 54 (Y-13597) shows a schematic diagram of the present apparatus used to distill rubidium. The large Pyrex boiler on the right is loaded with impure rubidium in an inert-atmosphere dry box. Three pounds of rubidium have been purified in this manner.

In conclusion, it may be stated that insofar as lithium corrosion is concerned, increasing the purity of the lithium shows a promising trend and, therefore, studies on it will continue with the hope of using it as a reactor coolant at some time in the future.

Future work on sodium will involve further testing on the compatibility of sodium-beryllium-Inconel systems. Tests will also be conducted with high-purity distilled sodium in contact with certain materials. Dissimilar-metal mass transfer and the effect of chromium on the mass transfer observed in nickel-molybdenum alloys when in contact with sodium will be investigated.

More rubidium boiling loops will be run to check further on possible mass transfer with loop materials other than Inconel. Also, since 8% sodium reduces the melting point of rubidium to approximately 20°F, tentative plans call for the investigation of the corrosion properties of the sodium-rubidium eutectic.

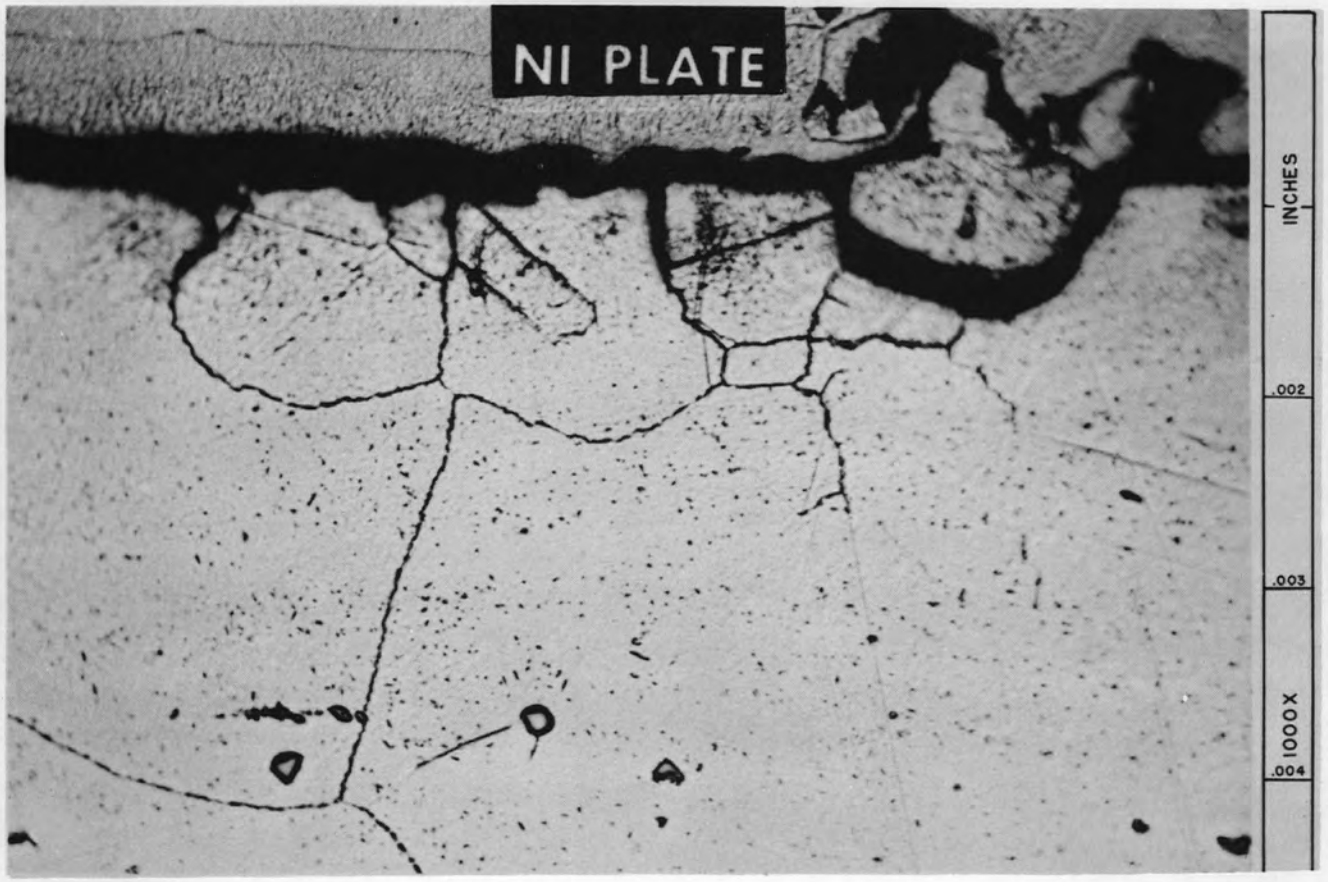

Fig. 53 (Y-13041) Inconel Exposed to Rubidium in Hot Leg Just Below Bath Level (See Fig. 52) for 316 Hr at Temperature of ~ 1090°F. Specimen nickel plated after test to protect edge. 1000X.
Unclassified - [redacted] with caption.

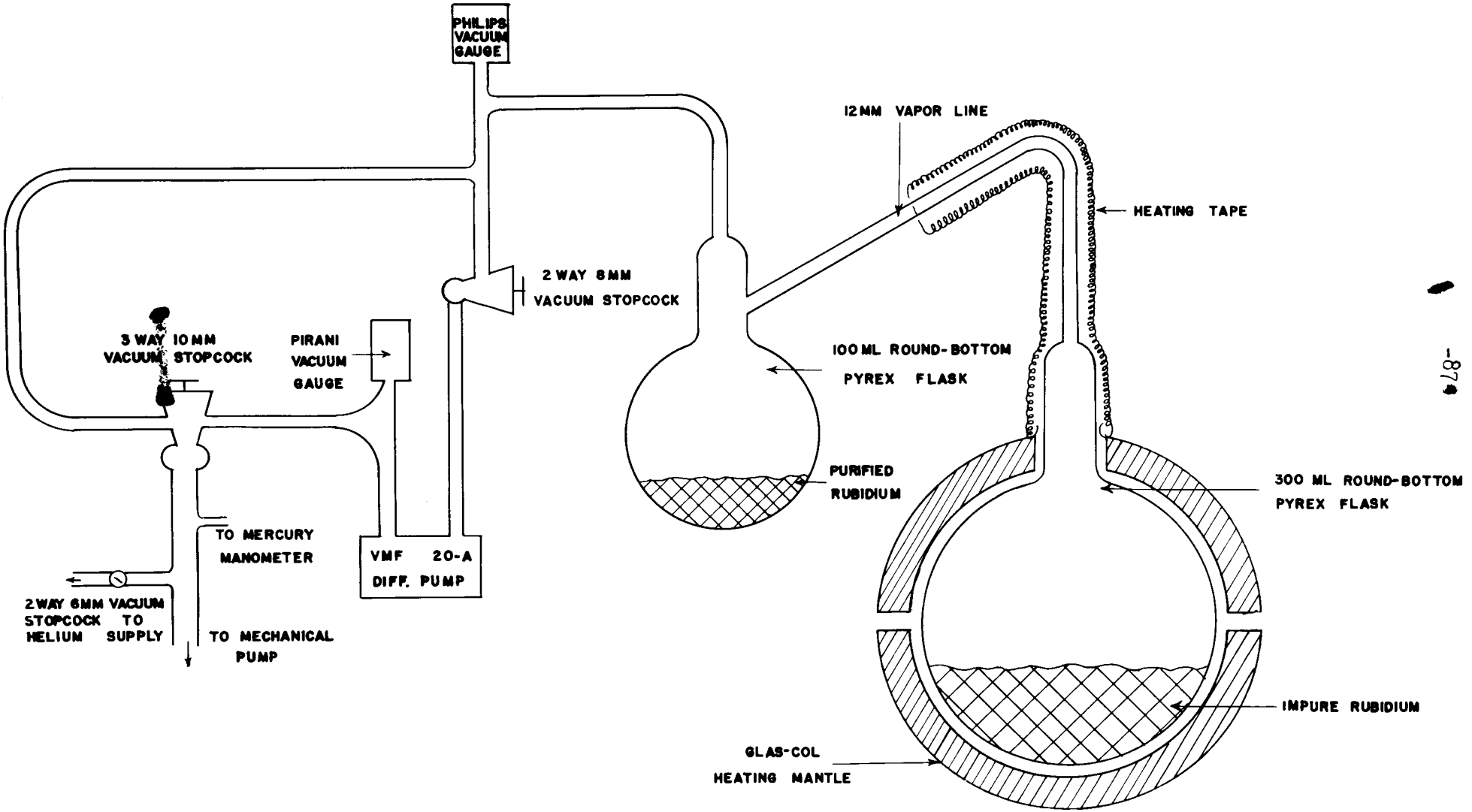

Fig. 54 (Y-13597) Apparatus for Distilling Rubidium [redacted]

COMPATIBILITY OF BERYLLIUM, SODIUM, INCONEL SYSTEM

G. M. Adamson
E. E. Hoffman
C. R. Brooks

The research discussed in this paper concerns the corrosion studies being carried out at ORNL as part of the Aircraft Reactor Program. A section of a typical reactor core has been shown in previous papers.[2,3] Both the island moderator and the reflector shell are to be fabricated from beryllium metal and both regions are to be cooled with sodium. The question requiring an answer was: Do the walls of the small-diameter cooling holes have to be clad? This is undesirable since it would be a difficult operation and would cause a considerable increase in critical mass.

Because of the urgency of the program, it was necessary to carry out all phases of this research simultaneously. These phases consisted of static corrosion tests on small pieces of beryllium, inserting beryllium samples into two sizes of thermal-convection loops, and inserting beryllium samples into Inconel toroid test loops and large pump loops. No data will be presented in this paper on the static tests.

The toroid tests are adapted from similar tests developed by NACA for hydroxide studies.[4] A short beryllium tubular piece protected by an Inconel sleeve is welded into an Inconel toroid in which sodium is circulated. The clearance between the outside of the beryllium and the Inconel sleeve is 0.005 in. A group of isothermal tests were carried out for 300 hr at 100-degree intervals between 1100° and 1400°F. The results of these tests

---

(2) A. J. Miller, "ORNL and P and WA Program," ANP Materials Conference, November, 1954, CF-55-1-87 (January, 1955).

(3) W. D. Manly, Container Materials for Circulating Fuel Reactors, (p 108, this report).

(4) R. A. Lad and Sidney Simon, "Corrosion and Mass Transfer of Ni by Molten Sodium Hydroxide," Corrosion 10, 435 (December, 1954).

are tabulated below. With the exception of the sleeve, no visible layers were found on any portion of the Inconel toroid. In these isothermal tests, evidence of corrosive attack was found on the inside of the insert only in the 1400°F test. Attack was noted on the outside of the insert at all temperatures, but an increase in amount of attack was noted in the 1200° and 1300°F tests.

Toroid Test Results

Test No.	Temp. °F	Beryllium Attack - Mils Inside	Outside	Thickness Layer Mils
37	1100	0	1	0
36	1200	0	1	0.4
39	1300	0	5	1
38	1400	1	3	3

Figure 55 is a photomicrograph showing the outside of the beryllium insert from Test 38, while Fig. 56 shows the layer on the sleeve from the same test. This layer has been identified by x-ray diffraction as being composed of the two compounds BeNi and $Be_{21}Ni_5$. While definite proof is not available, it is thought that the mechanism of void formation is similar to that found in the Inconel-fused salt systems.[5] Thermal loops of two different sizes were utilized.

Figure 57 is a drawing showing the shape of the beryllium insert and how it was held in the larger loops. The beryllium insert was placed in the top of the hot leg with sodium present on both sides. On the outside of the insert the sodium was nearly stagnant,

(5) G. M. Adamson, R. S. Crouse, and W. D. Manly, Interim Report on High-Temperature Corrosion with Fluoride Mixtures, ORNL-2337. [redacted] (to be published)

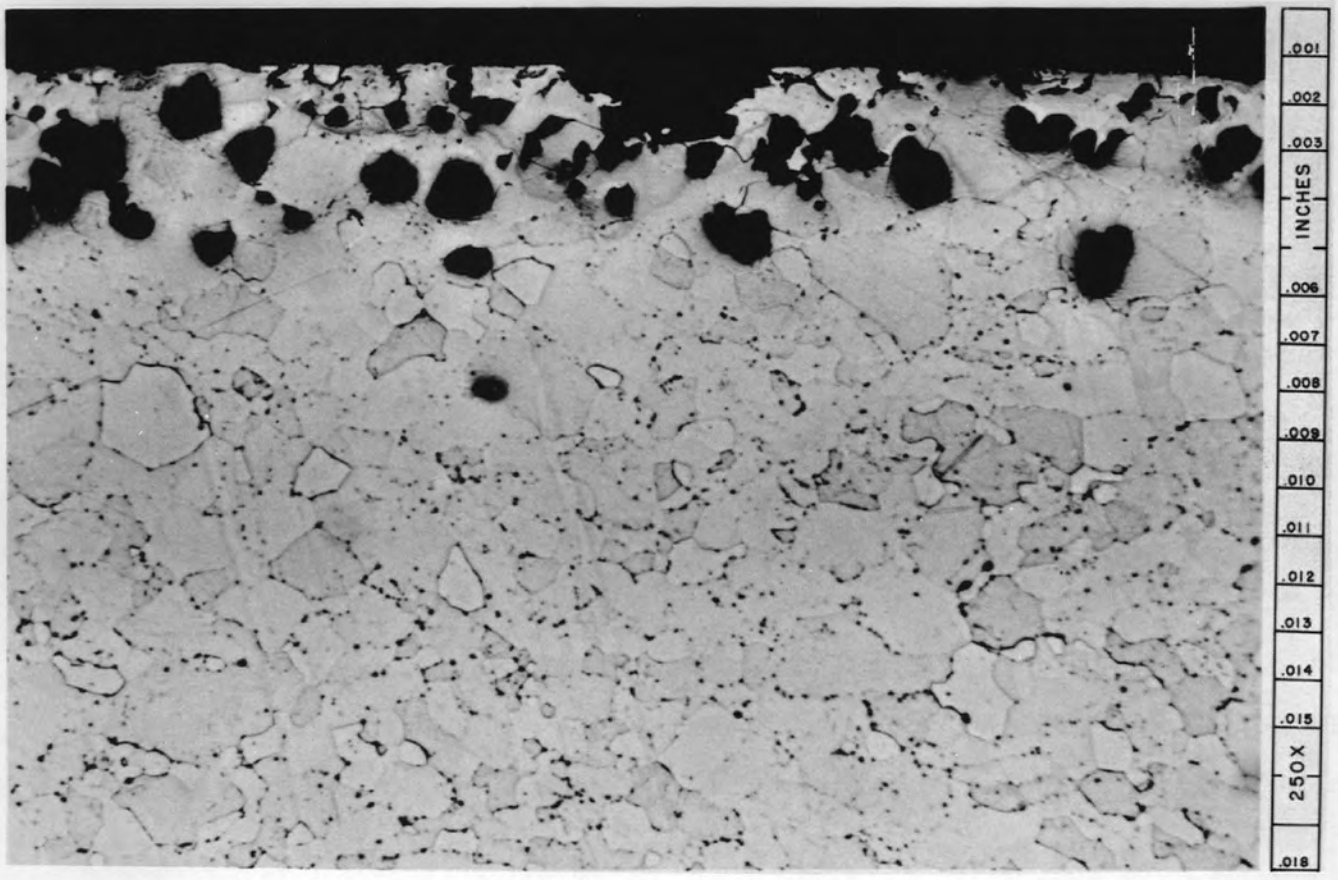

Fig. 55 (Y-13490) Attack on Outside of Beryllium Insert in Inconel Toroid After Exposure to Circulating Sodium for 300 Hr at 1400°F. 250X. Unclassified.

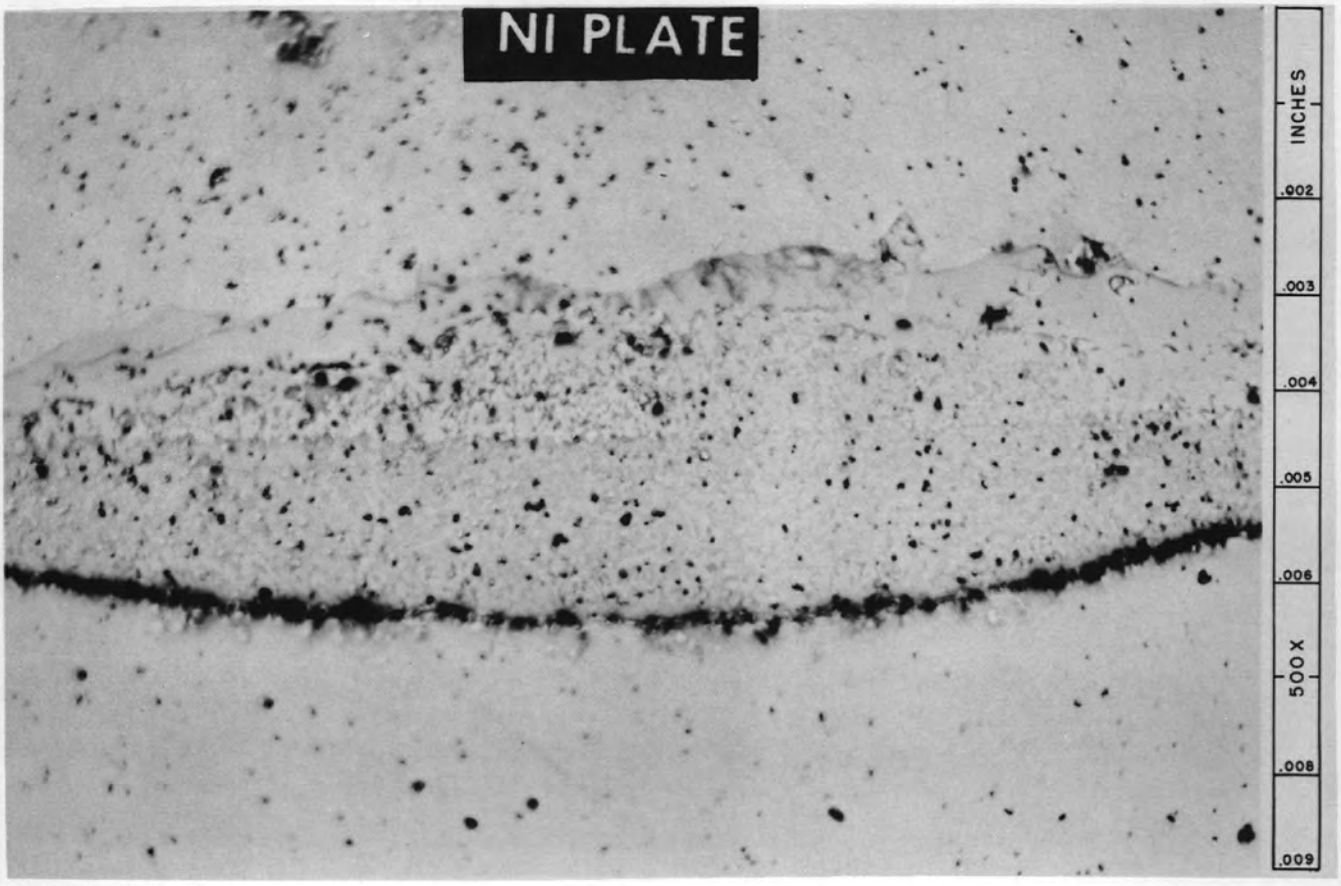

Fig. 56 (Y-13547) Layer on Protective Sleeve of Inconel Toroid after Exposure to Circulating Sodium for 300 Hr at 1400°F. Sleeve was nickel plated following the test to preserve the layer which formed during the test. Unclassified.

SUPPORT FOR INSERT

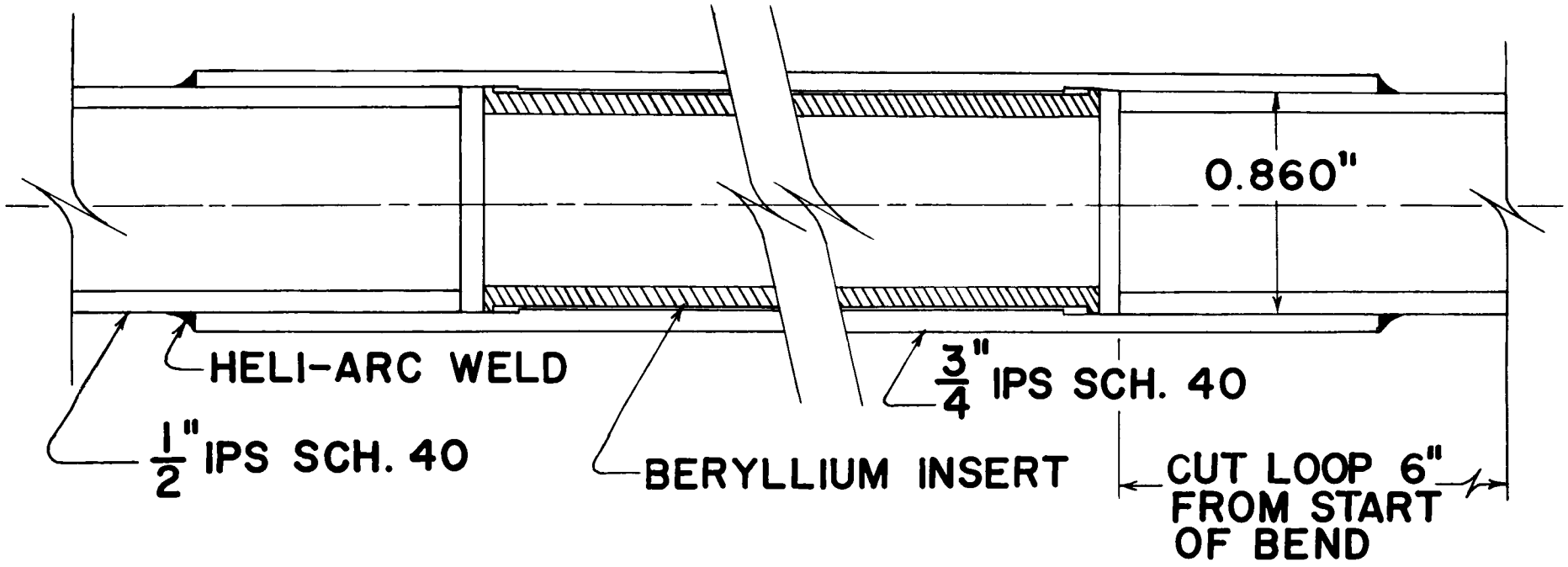

Fig. 57 (T-6631) Shape and Method of Support of Beryllium Insert in Hot Leg of a Thermal-Convection Loop. Unclassified.

while on the inside it was moving at about the usual loop velocity. The sodium was of high purity, containing only about 0.02% oxygen. The results from a series of loops operated at various temperatures for 500 hr are shown on the panel in Fig. 58. No attack was visible on the outside of the insert after exposure at 1100°F and very little after exposure at 1300°F, while the inner surface of the insert and the Inconel appeared unaltered in both cases. The 1500°F test revealed very little evidence of attack on the inside of the beryllium, but on the outside large voids to a maximum depth of 14 mils were found. The layer on the Inconel opposite this insert is shown in Fig. 58. It was also identified as BeNi and $Be_{21}Ni_5$. It must be pointed out that in the 1500°F loop the clearance was 0.035 in. while in the other two it was 0.050 in.

In the small loops the beryllium was inserted in about the same manner except it was of uniform wall thickness and the clearance was only 0.006 in. Results are available from two of these loops, both of which were tested for 1000 hr. The first loop was heated at temperatures between 1000° and 1150°F. The outside of the beryllium insert showed the usual void type of attack to 2 mils, while the inside was somewhat rough with what appears to be a nonmetallic material, probably BeO, trapped in the irregularities. A layer 0.0005 in. thick was found on the Inconel opposite the sleeve but none was visible in any other portion of the loop. The second loop was operated with temperatures between 1150° and 1300°F. The outer surface of the insert showed the usual voids to a depth of 4 mils. The inside beryllium surface was again rough with entrapped nonmetallics. No visible layer was found on any Inconel surface other than the sleeve. The cold-leg surface (Fig. 59) does not have a corrosion layer and is typical of the cold regions of all these tests. The area where the end of the beryllium was in actual contact with the spacer was examined and an altered layer 20 mils thick was found as shown in Fig. 60. This layer is the result of interdiffusion of the two metals.

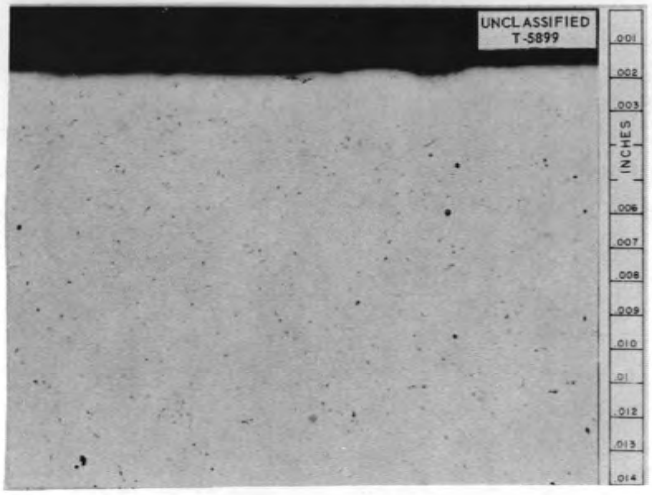

500 hr AT 1100°F

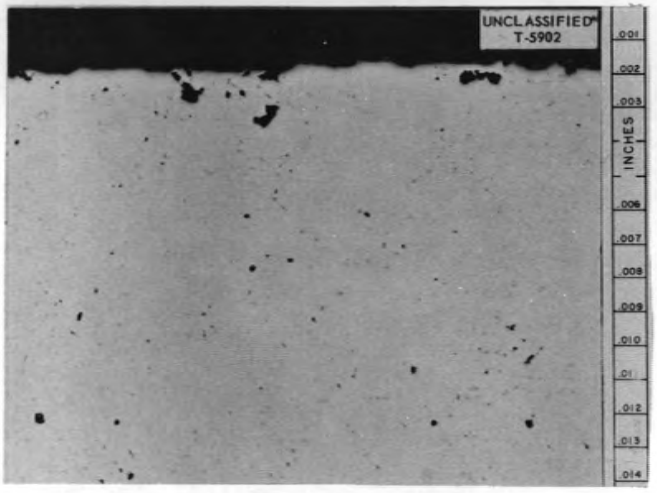

500 hr AT 1300°F

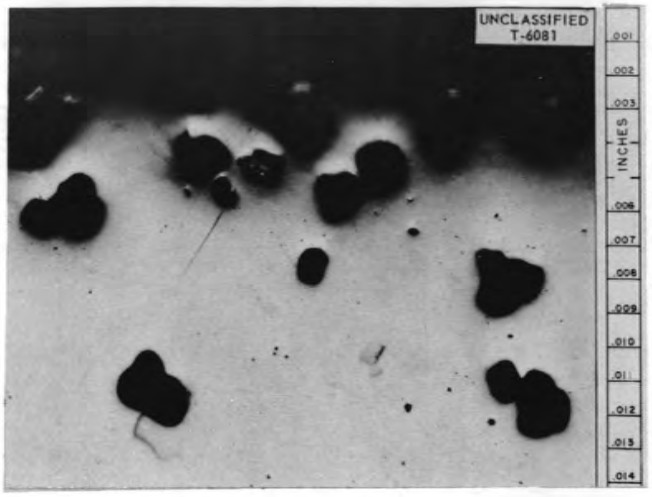

500 hr AT 1500°F

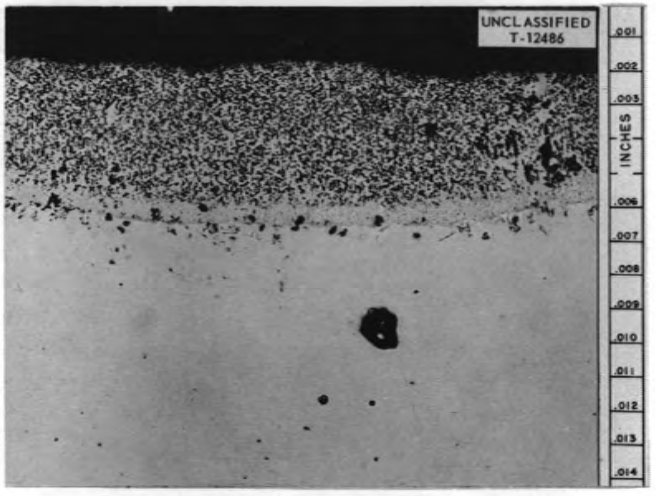

Be-INCONEL INTERFACE AT 1500°F

Fig. 58 Variation in Depth of Attack with Hot Leg Temperature, in Beryllium Inserts from Inconel Thermal Convection Loops. (Mag. 250X)

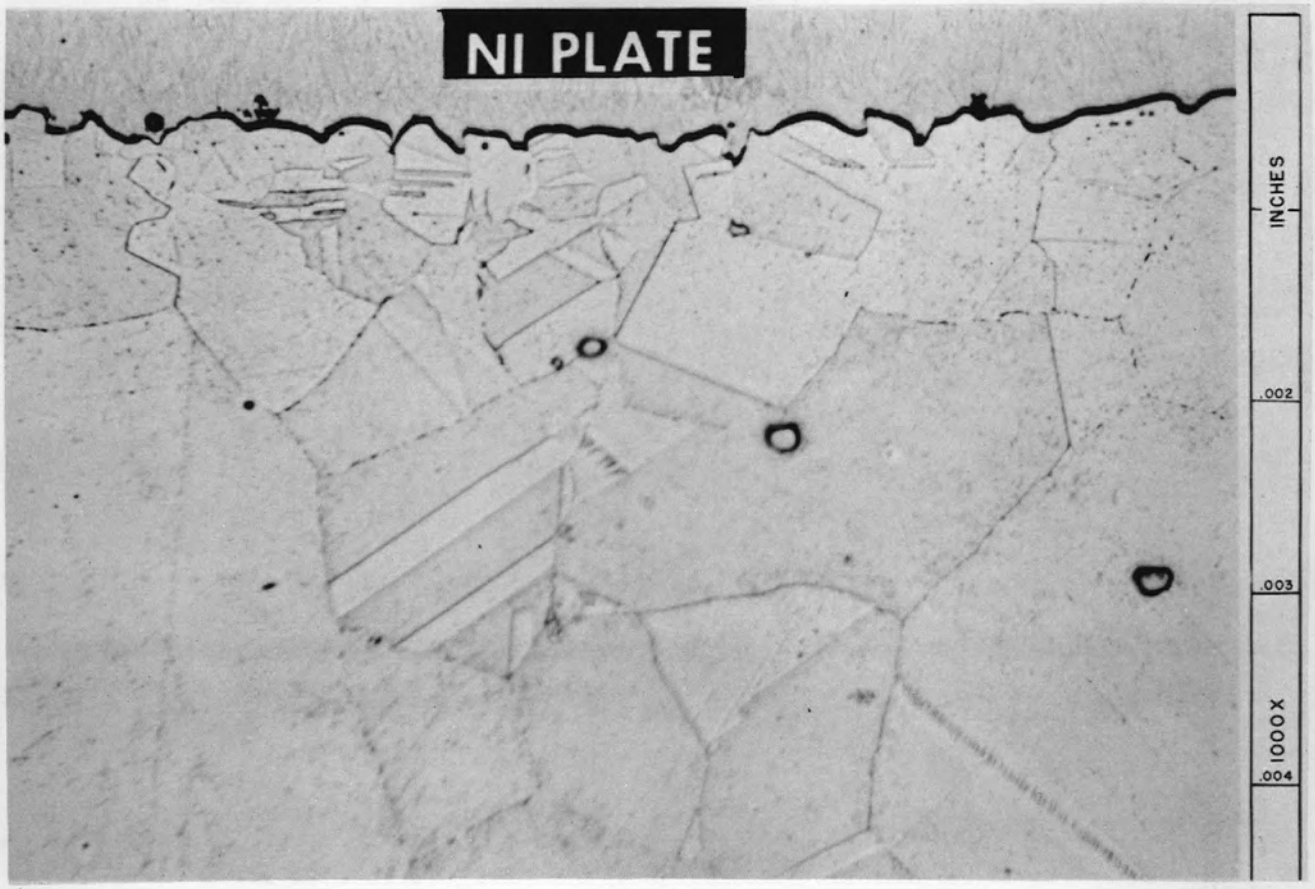

Fig. 59 (Y-13556) Unchanged Surface from Cold Leg of an Inconel-Beryllium Thermal Convection Loop. 1000X. Unclassified.

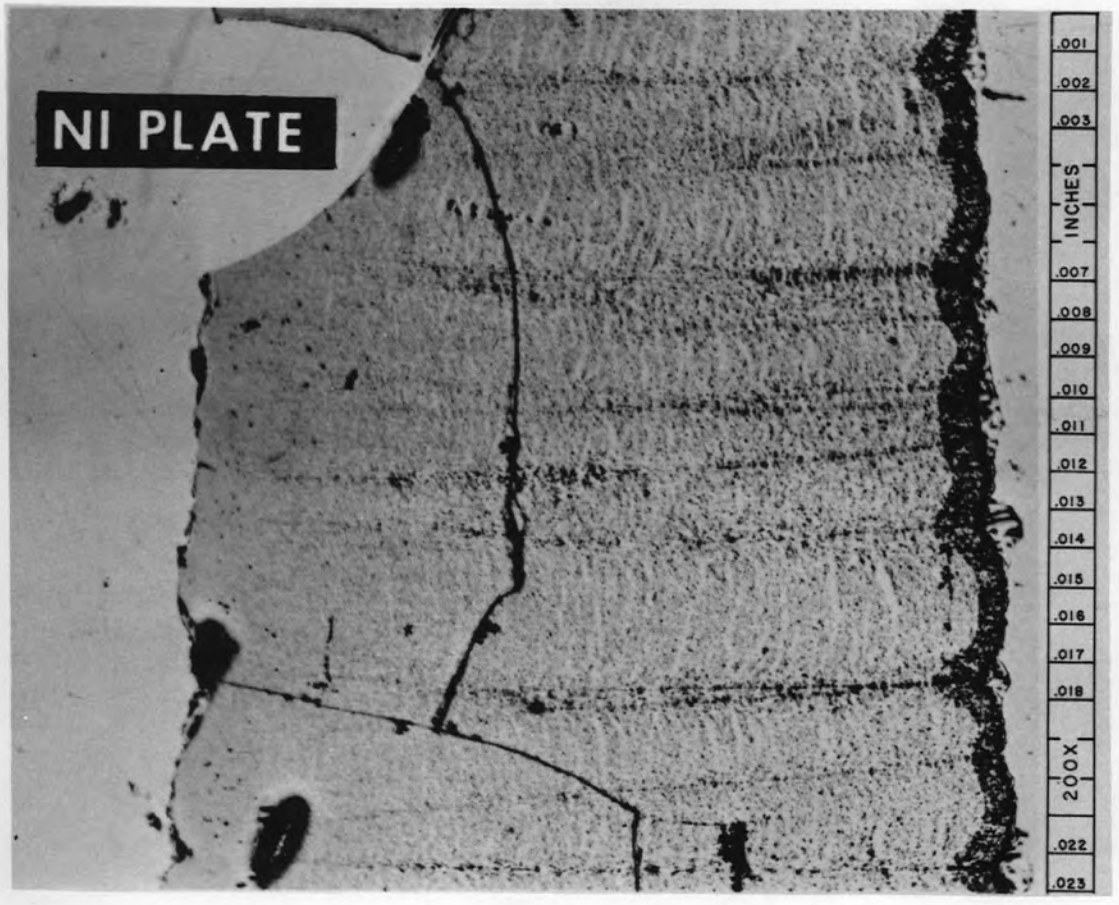

Fig. 60 (Y-13552) Layer in Contact Area between Beryllium Insert and Inconel Spacer from the Hot Leg of 1300°F Thermal Convection Loop. 200X. Unclassified.

Three pump loops were operated by the Experimental Engineering Section in the final phase of this program. The first loop was constructed as shown in Fig. 61 and operated for 270 hr at 1300°F with a Reynolds number of 395,000 in the insert, a fluid velocity of >45 fps, and a temperature gradient of 300°F. A small Venturi shaped insert of beryllium was held closely in an Inconel sleeve. Operation of the loop was terminated due to a leak, which was not caused by corrosion, but resulted from an attempt to restart this loop after a power failure. When examined, some attack was found to have occurred on the inside of the beryllium. In the throat of the Venturi, scattered voids to a depth of 0.004 in. and some surface roughening were noted. The heaviest attack was found on the outside of the insert with void penetration as deep as 0.007 in. and some surface roughening, as shown in Fig. 62. The corrosion layer on the Inconel surrounding the beryllium was a complete envelope up to 0.008 in. thick. No visible corrosion layer was found elsewhere in the loop.

The second loop was similar to the first except that the insert and tubing were smaller. This loop operated for 1000 hr with a maximum temperature of 1200°F and a Reynolds number of 95,000. Small scattered voids to a depth of 0.003 in. were found on the inside of the insert and considerable surface roughening was found (Fig. 63). On the outside of the insert the voids extended to 0.005 in. and were much more numerous (Fig. 64). An 0.001-in. layer was present on the Inconel, as can be seen at the top of the same figure.

Although the third loop was operated primarily as a thermal stress test, valid corrosion data was obtained. This loop operated for 1000 hr with a maximum temperature of 1200°F and a temperature gradient of 130°F. The maximum temperature was measured on the surface of the beryllium rather than in the surrounding sodium as in the other loops. The total temperature gradient in the sodium was 60°F with a maximum temperature of 1100°F. Once every 24 hr the maximum beryllium temperature was cycled

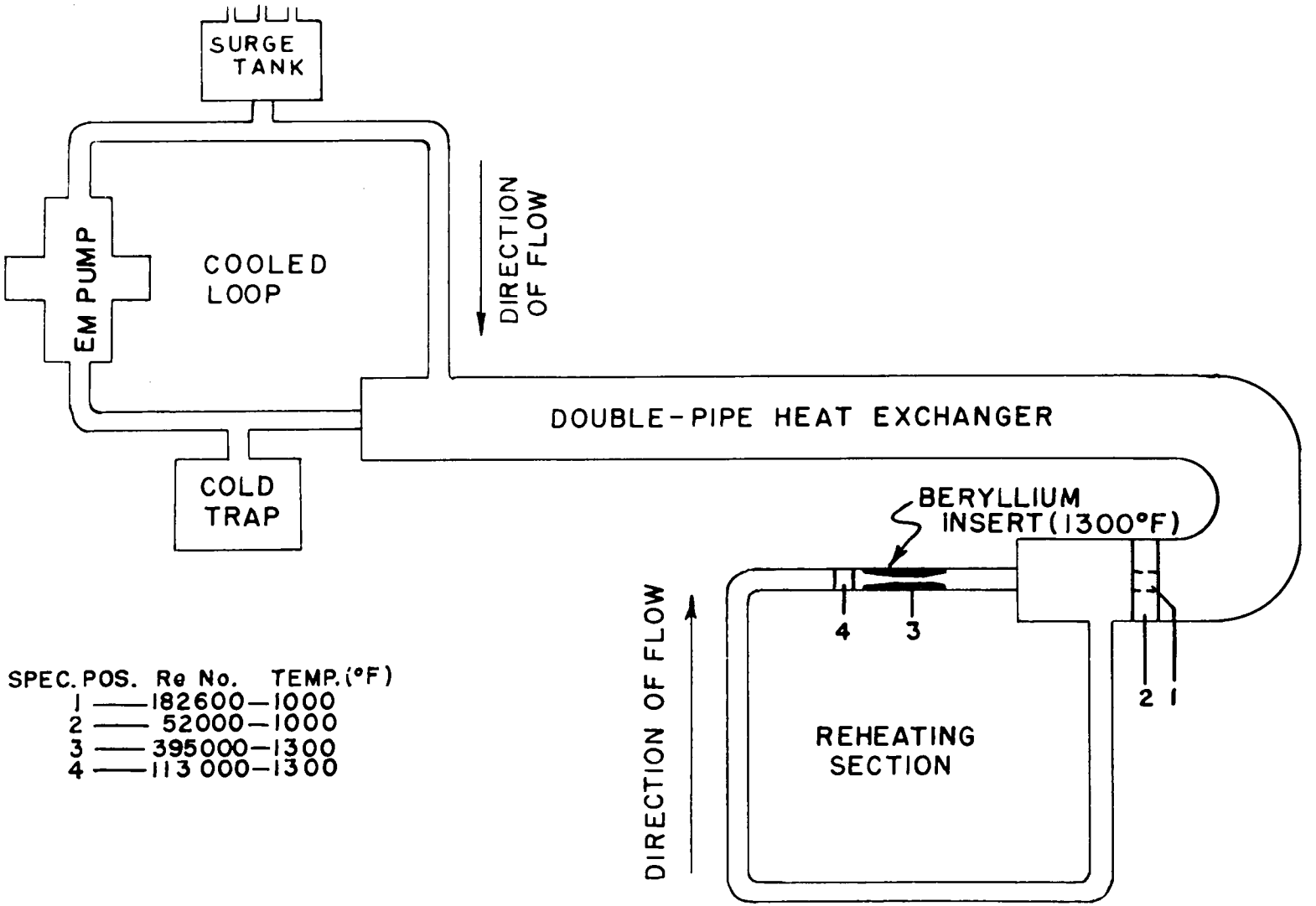

Na-Be-INCONEL HIGH ΔTV LOOP No.2 TEST UNIT ASSEMBLY

Fig. 61 (T-6551) Configuration of Large Pump Loops.
Unclassified.

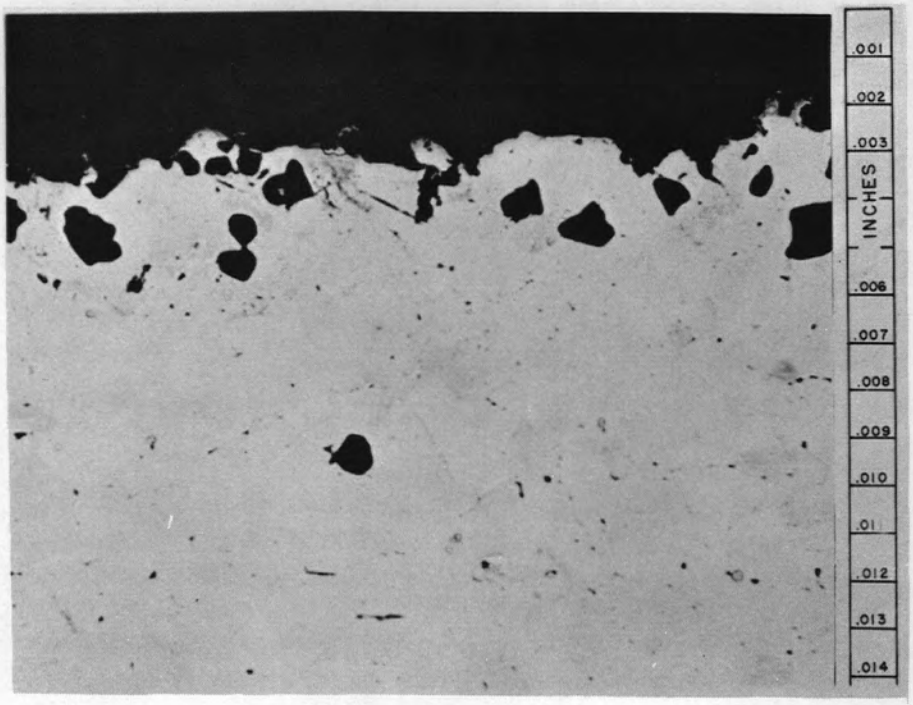

Fig. 62 (T-6347) Outside Surface of Beryllium Insert from 1300°F Inconel Pump Loop No. 1. 250X. Unclassified.

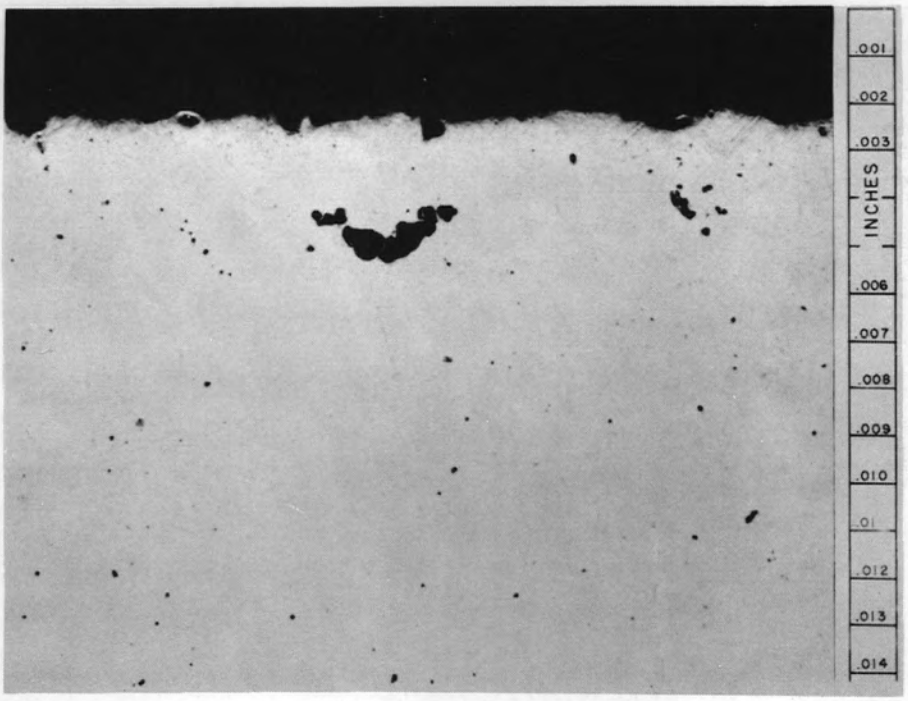

Fig. 63 (T-6133) Inside Surface of Beryllium Venturi Insert from 1200°F Inconel Pump Loop No. 2. 250X. Unclassified.

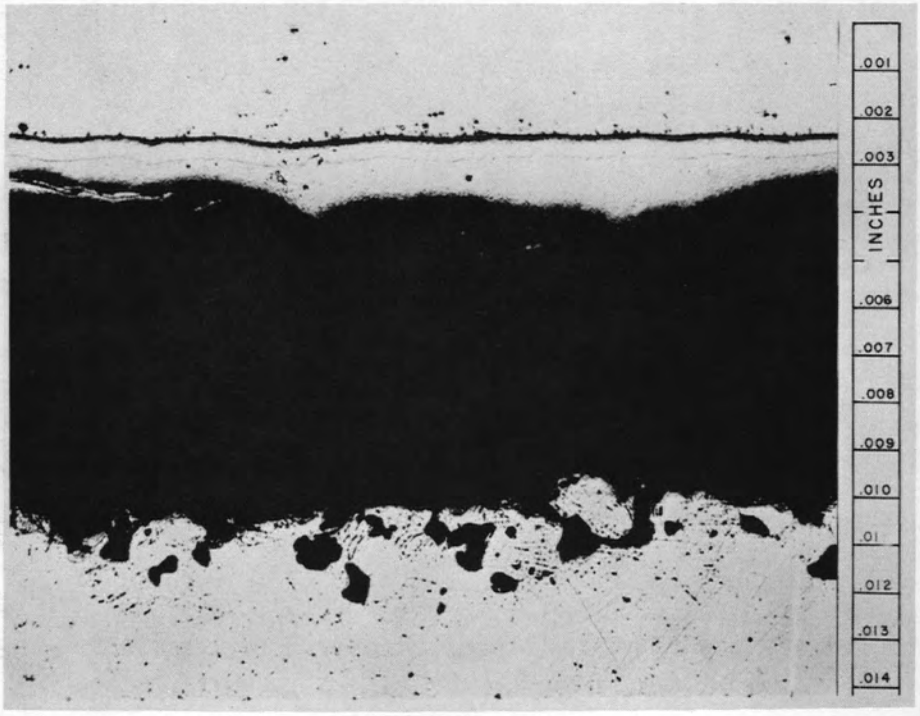

Fig. 64 (T-6056) Outside Surface of Beryllium Venturi Insert from 1200°F Inconel Pump Loop No. 2. 250X. Unclassified.

90°F. Figure 65 shows the configuration of the heated portion of this loop. All heating during operation was accomplished by passing a very large current lengthwise through the box in the center of the assembly. Most of this current was carried through a thin layer of sodium and passed through the beryllium block. The power generation in the beryllium was 41.5 watts/cc at the high power level and 14.9 at the low level. The sodium entered the heating section through the small tubes from the lower header, passed through the beryllium,and left through the small tubes to the upper header. The beryllium block and the can, after completion of the test, are shown in Fig. 66. The sodium flowed through the small holes shown in the face of the block. With the entire block being heated and cold sodium passing through the holes, large thermal stresses were set up. These stresses were increased further by the periodic temperature cycling. It is evident from Fig. 66 that the beryllium was still intact and no large scale cracking or disintegration due to the excessive thermal stresses was found.

On the surface of the block are longitudinal grooves and others are located around the edges of some of the holes. These grooves lie either directly opposite the spacers shown on the can, or opposite welds in which an excessive weld bead was found. A typical surface of the small cooling holes in the block is shown in Fig. 67. No corrosive attack or cracking occurred. Figure 68 presents a panel of photomicrographs from various areas on the surface of the block. The first two photomicrographs are from the area under the spacer and show the maximum attack of 0.008 in. including the groove and voids. In areas where the Inconel and beryllium were not as closely spaced, the maximum void penetration was 0.006 in. with no groove. In the third picture the small amount of attack found on the surface between the inserts is seen to consist of widely scattered voids no deeper than 0.002 in. The last photomicrograph is of the corrosion layer found on the spacers.

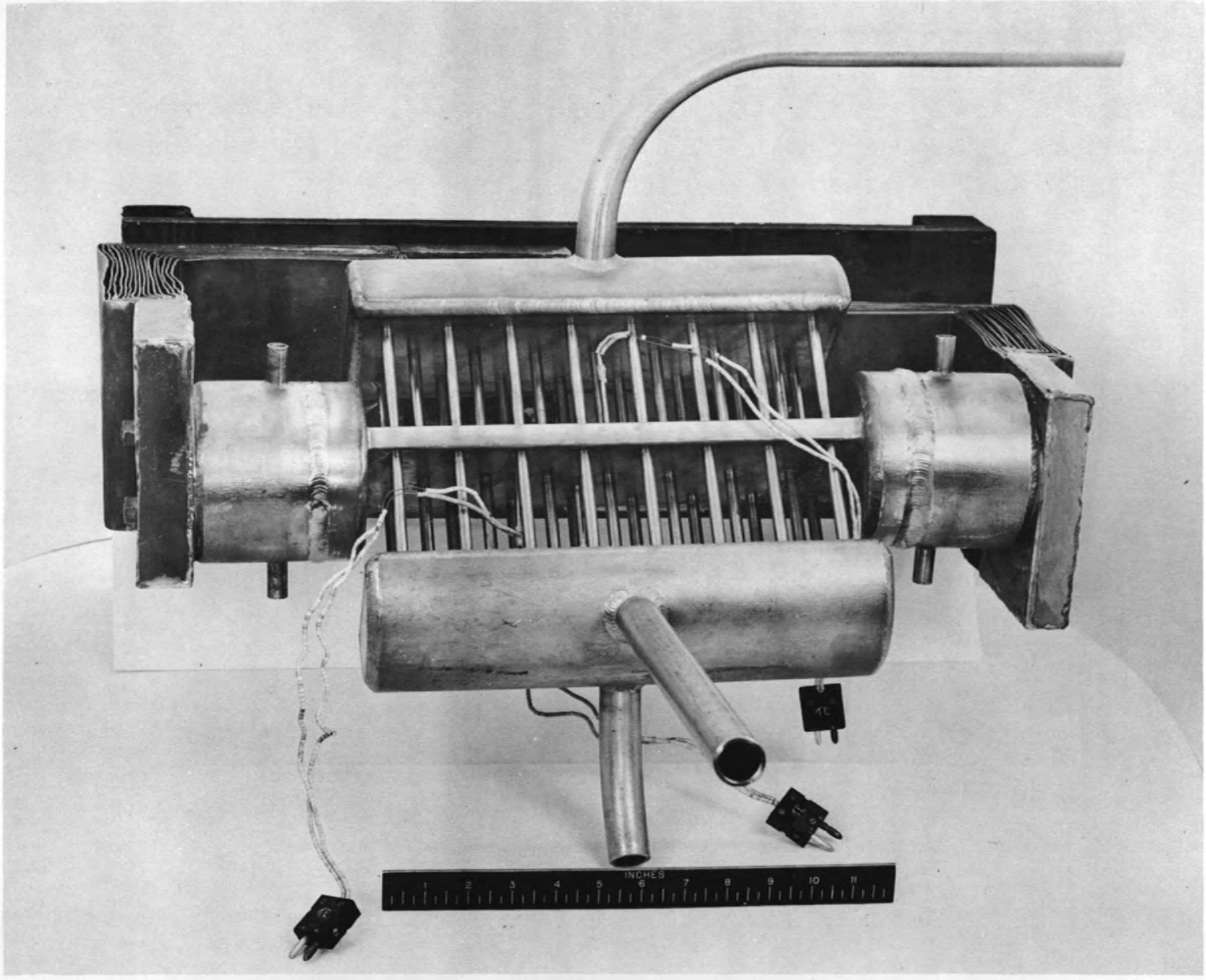

Fig. 65 (Y-12546) Heating Assembly from Beryllium Thermal Stress Test. Unclassified.

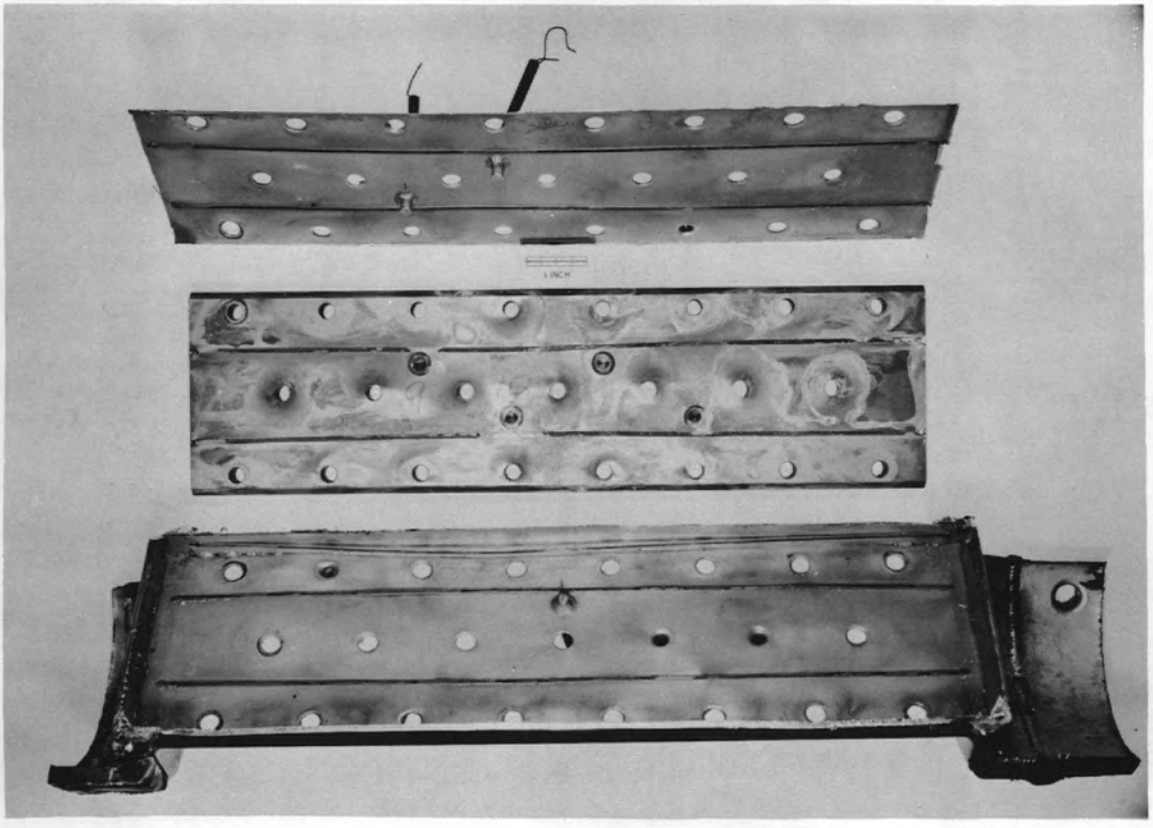

Fig. 66 (T-6132) Beryllium Block and Protection Can from Beryllium Thermal Stress Test after 1000 Hr of Operation. Unclassified.

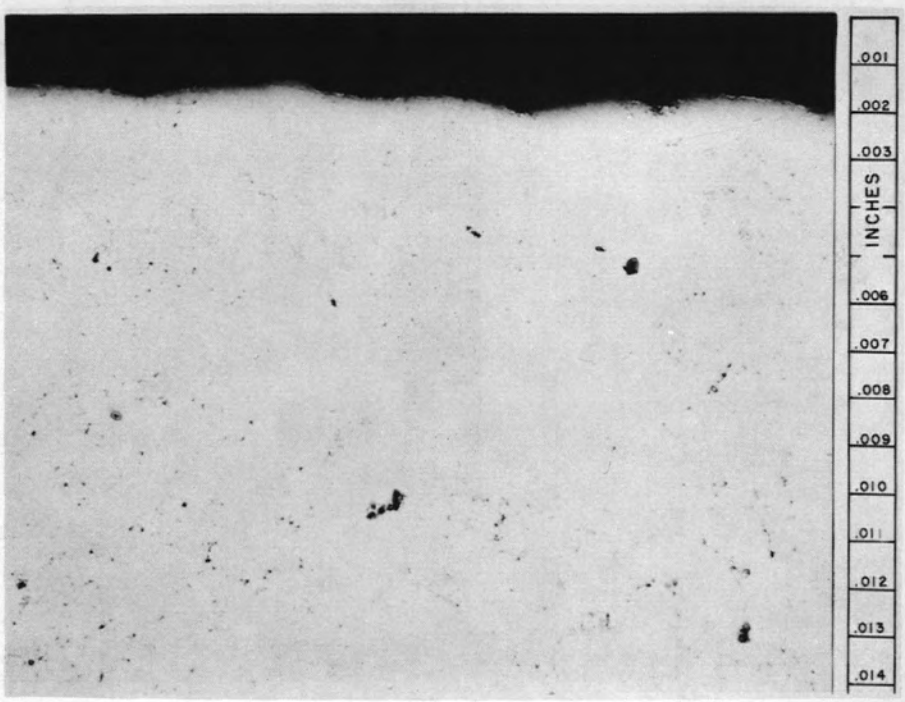

Fig. 67 (T-6564) Inside Surface of Cooling Hole of Beryllium Block after 100-Hr Beryllium Thermal Cycle Test. 250X. Unclassified.

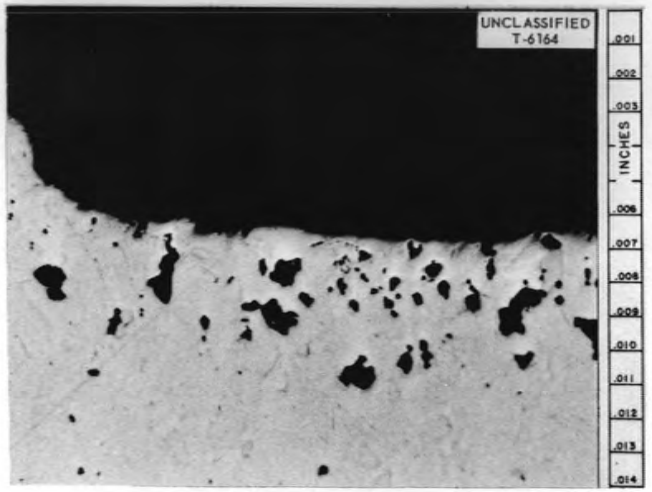

UNDER SPACER

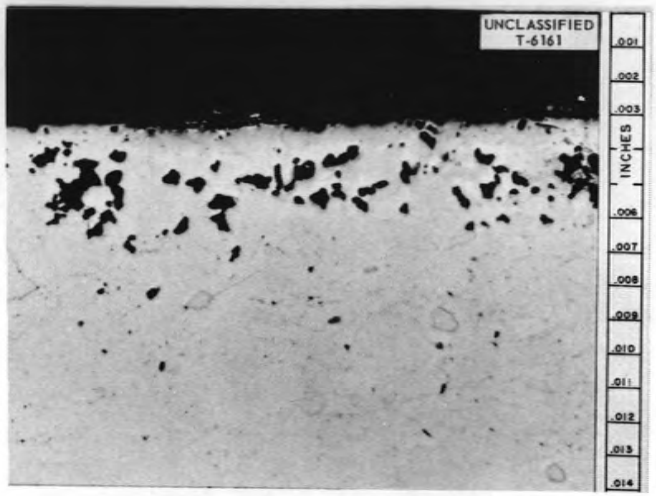

UNDER SPACER

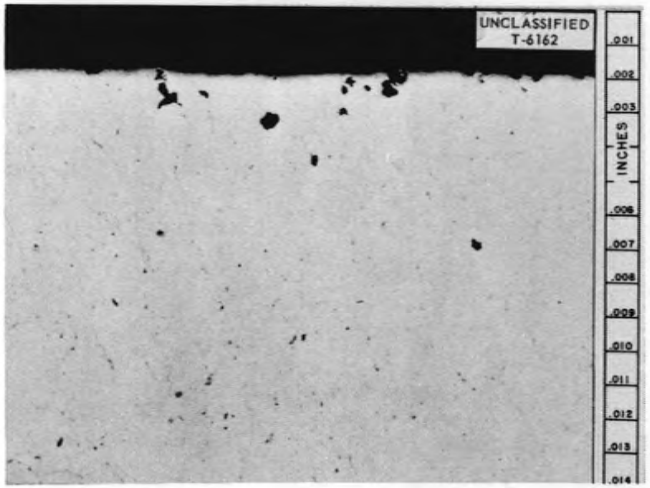

SURFACE OF BLOCK

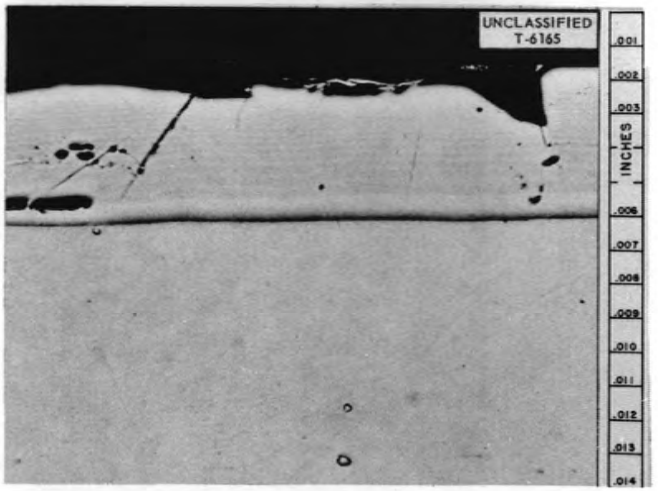

SPACER

COMPATABILITY OF Na, Be AND INCONEL

Fig. 68 Attack Found on Various Areas of the Surface of the Beryllium Block from the Beryllium Thermal Cycle Test. (Mag. 250X)

In none of these tests were we able, either visually or metallographically, to perceive corrosion layers in cold zones of the loops; however, chemical analysis has revealed the presence of traces of beryllium at the Inconel-sodium interface in the cold zone. The Oak Ridge National Laboratory, Analytical Chemistry Division is developing a microdrilling and spectrographic technique for such analyses. The method is still being investigated and no reliable data obtained in this manner can be reported at this time. Preliminary results indicate very low beryllium concentrations of about 100 micrograms per square centimeter of cold-leg surface in both the thermal and the pump loops.

In conclusion, these tests have shown that it will be possible to cool a beryllium moderator and reflector with sodium without cladding at temperatures of 1200°F, or less. It actually seems likely that because of alloy formation, cladding might do more harm than good. At 1200°F, some attack on the beryllium possibly will occur, but it will not be severe enough to cause trouble. Mass transfer due to differences in temperature does not seem to be excessive in this system; therefore, the chances of plugging small-diameter tubes in the cold zone does not appear to be large.

The major difficulty in this system will come from the Inconel can necessary to protect the beryllium from the fluorides. In many areas only a thin annulus of sodium will separate the two metals. Even at 1200°F, some attack and layer formation caused by dissimilar-metal mass transfer will be found in such areas. More work is needed, and is being done, to furnish better data on the effect of the distance of separation. Further research is also needed to separate the effect of distance between the Inconel and the beryllium from any possible effect of sodium velocity upon corrosion, since in all tests reported, whenever a close spacing was found it was accompanied by slow moving sodium.

[redacted]

CONTAINER MATERIALS FOR CIRCULATING FUEL REACTORS

W. D. Manly, H. Inouye, G. M. Adamson

As has been explained[6], Inconel was the choice of a structural material for the first high-temperature circulating-fuel reactor known as the ARE. The choice of Inconel for this application was made with a minimum amount of corrosion experience, mechanical-properties test data, and over-all fabrication data for its construction; however, the completion of the test run of the ARE has shown that Inconel was a successful container material. For future circulating-fuel reactors it is hoped that a material having increased strength and corrosion resistance can be developed.

When the following requirements of a material for this application are examined, they seem somewhat formidable.

1. It must have corrosion resistance to the fused salts.
2. It must have corrosion resistance to sodium and NaK.
3. It must have resistance to temperature-gradient mass transfer in both media (fused salts and alkali metals), and the material should exhibit a minimum amount of dissimilar-metal transfer between itself and beryllium with sodium as the coupling liquid.
4. The material should have tolerable oxidation resistance, since it will also probably be used in the radiator to minimize the amount of dissimilar mass transfer that would occur if one material were used for the core and another for the radiator.
5. The material should have good high-temperature creep strength, which it retains in the various environments such as fused salts and sodium.
6. The material should possess good high-temperature ductility to withstand the high thermal stresses and vibratory stresses that will be imposed on it in

(6) A. J. Miller, ORNL P and WA Program, CF 55-1-87.

addition to the static stresses.

7. The material should be easy to weld, so that the complicated heat exchangers described by Mr. P. Patriarca[7] and illustrated in Fig. 69 (Y-9060) can be constructed.
8. The material should be easily formable into various intricate shapes, so that all the necessary pieces of plumbing that are needed to construct a circulating fuel reactor, as seen in Fig. 70 (Dwg. 22342) can be fabricated. These include a whole gauntlet of material from extremely small tubing to a 2-in.-thick pressure shell.
9. If at all possible, this alloy should be commercially available so there will be considerable fabrication experience to produce the various sizes and shapes, and so there will be some backlog of information on the stability of this alloy, in addition to the tests that will be conducted by the Laboratory.
10. The material should be free of structural changes under operating conditions, so the creep properties would not be adversely affected and so close tolerances can be maintained. This is quite important since the material will be stressed at a high temperature for a long period of time under an intense field of neutron radiation. Alloys of the austenitic stainless steel type, which are metastable, could transform under these conditions.
11. The material should not have a prohibitive cross section so the critical mass will be reasonable and, if at all possible, elements giving rise to strong capture gamma rays with a long half-life should be avoided, so that the reactor can be approachable within a reasonable length of time after shutdown.

Many materials have been examined for this application and some evidence of their strength properties can be seen by examining Fig. 71 (Y-13508). As is shown, attractive materials for consideration from the strength standpoint are Inconel X, columbium, molybdenum, Hastelloy B, and the Nimonics, whose strengths are quite similar to Inconel X. Inconel has by far the least desirable creep properties for this application.

The most important characteristic the material must have is corrosion resistance in the fused salts, and this information was developed in tests described by

---

(7) P. Patriarca, "Heat Exchanger Fabrication," (p 35, this report) The Welding Journal, 36, No. 12, pp 1172 – 1178 (December, 1957).

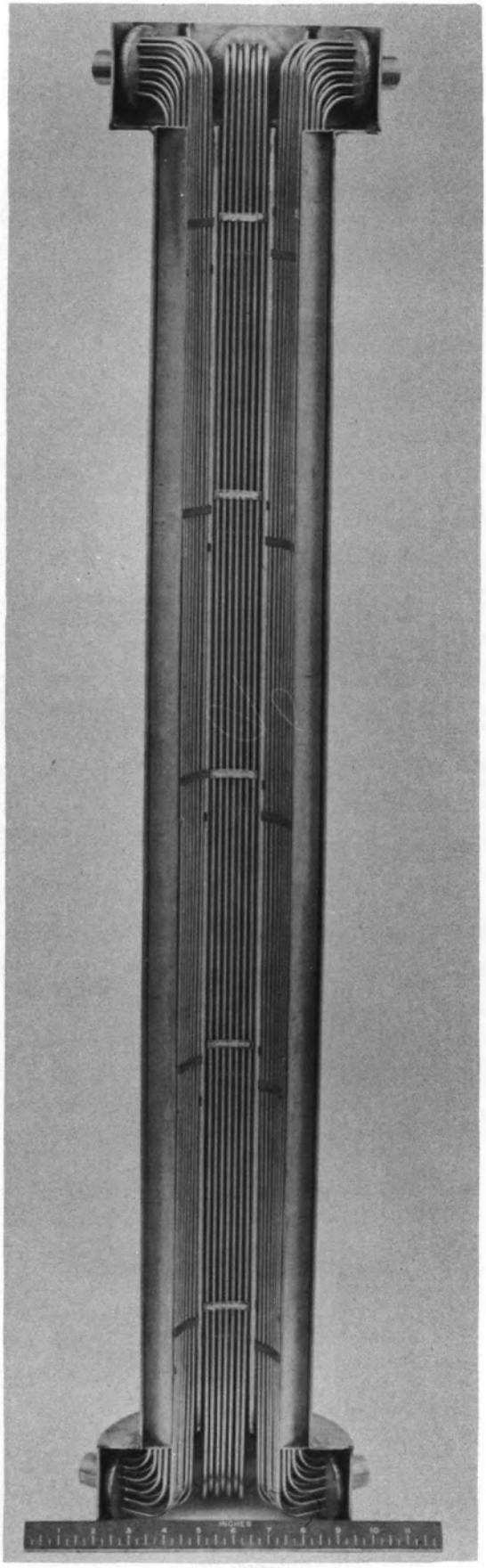

Fig. 69 (Y-9060) Intermediate Heat Exchanger. Unclassified.

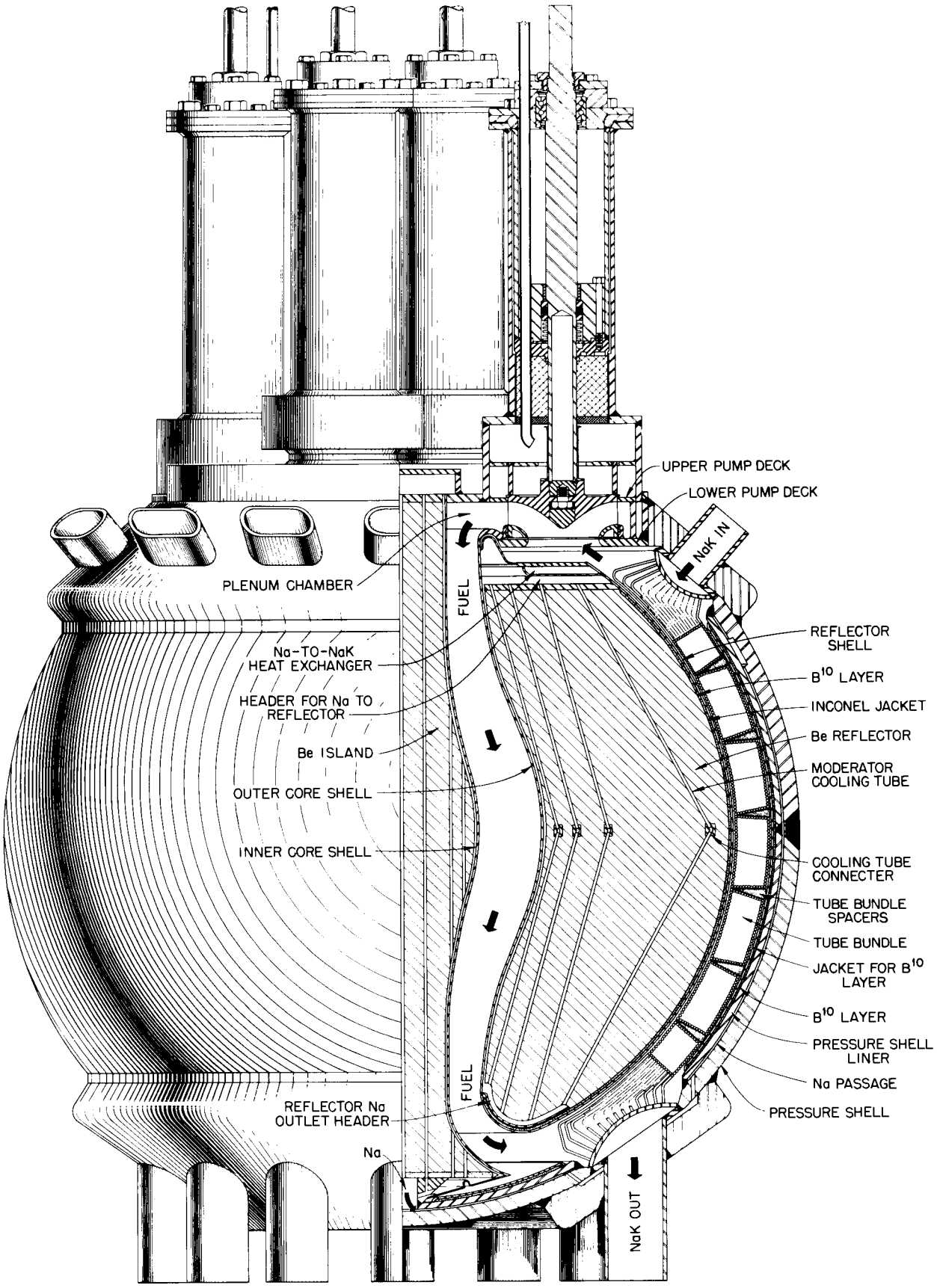

Fig. 70 (Dwg. 22342) Cutaway View of Circulating Fuel Reactor.
Classification [redacted]

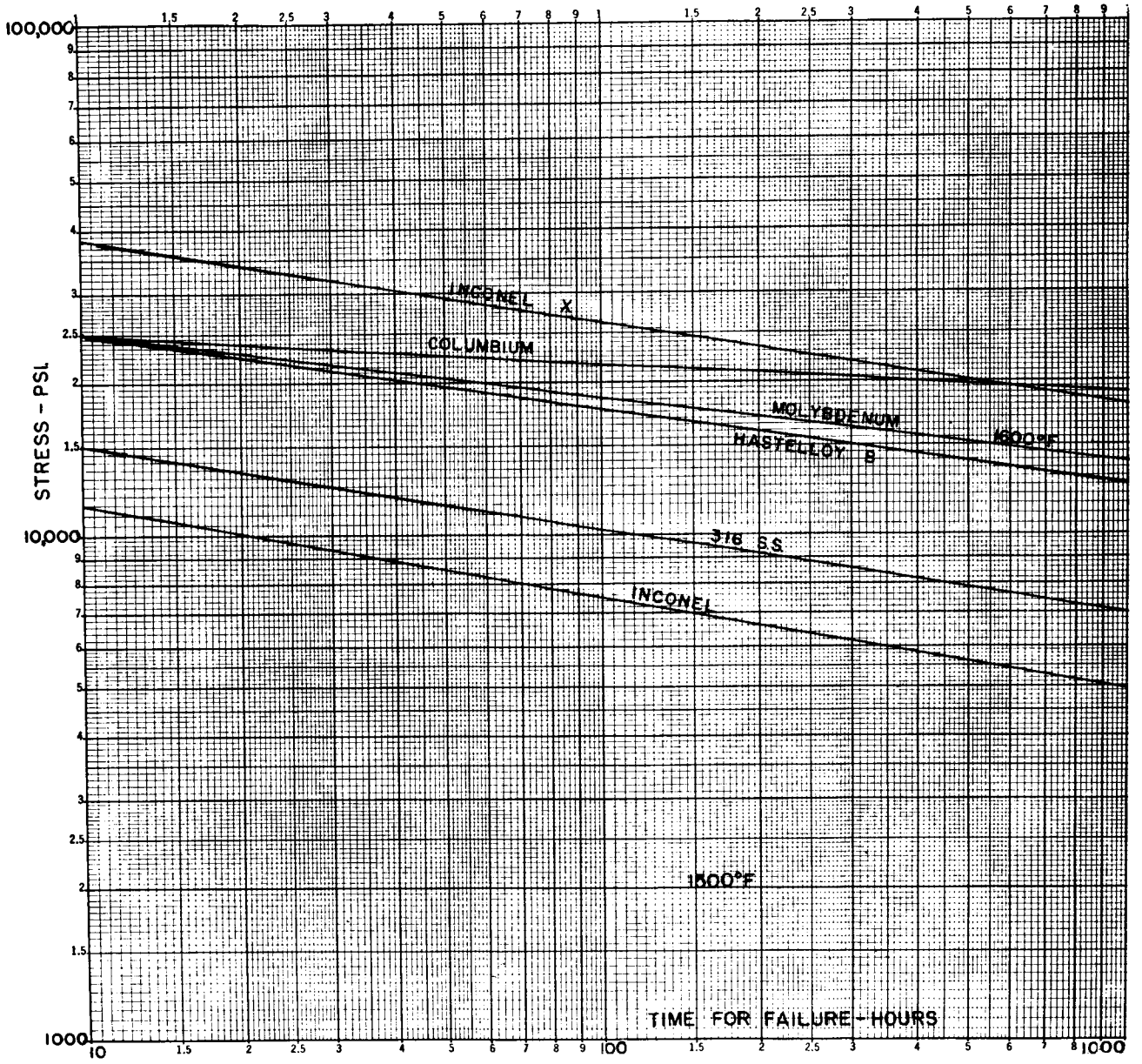

Fig. 71 (Y-13508) Creep Data of High Temperature Alloys for 1500°F Service. Unclassified.

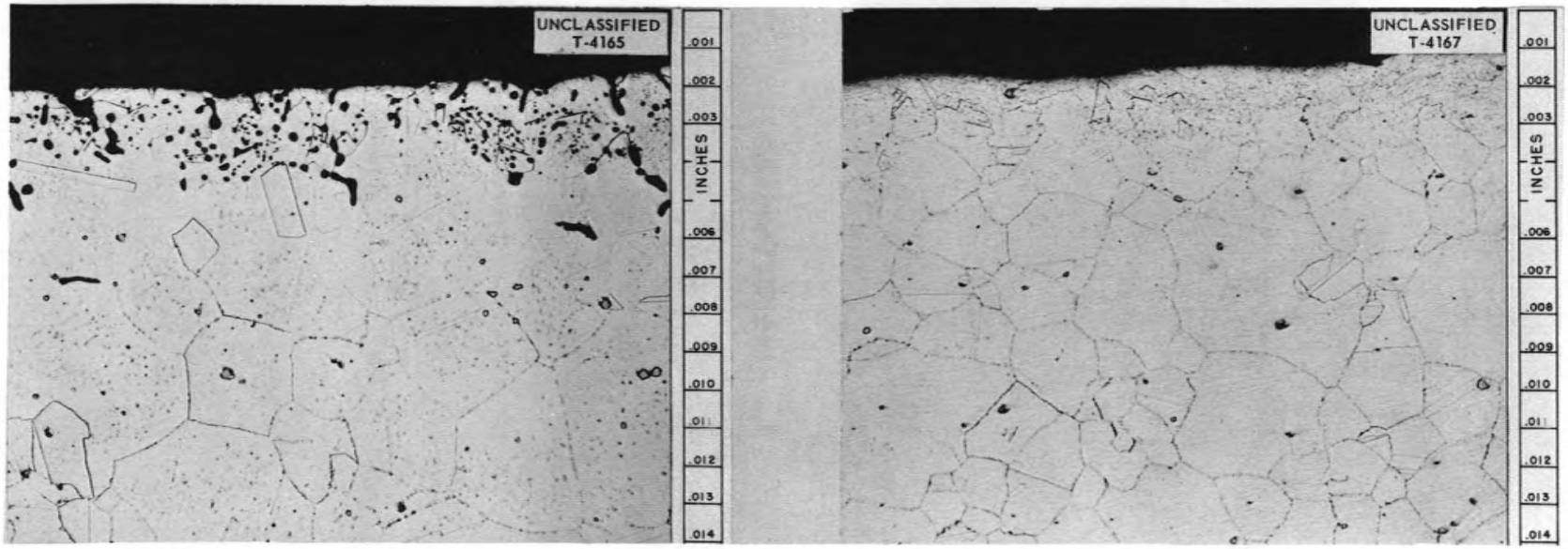

HOT LEG

COLD LEG

Fig. 72 Corrosion of Inconel in FUZRNA 30-500 hr at 1500°F. Etchant-modified aqua regia. (Mag. 250X)

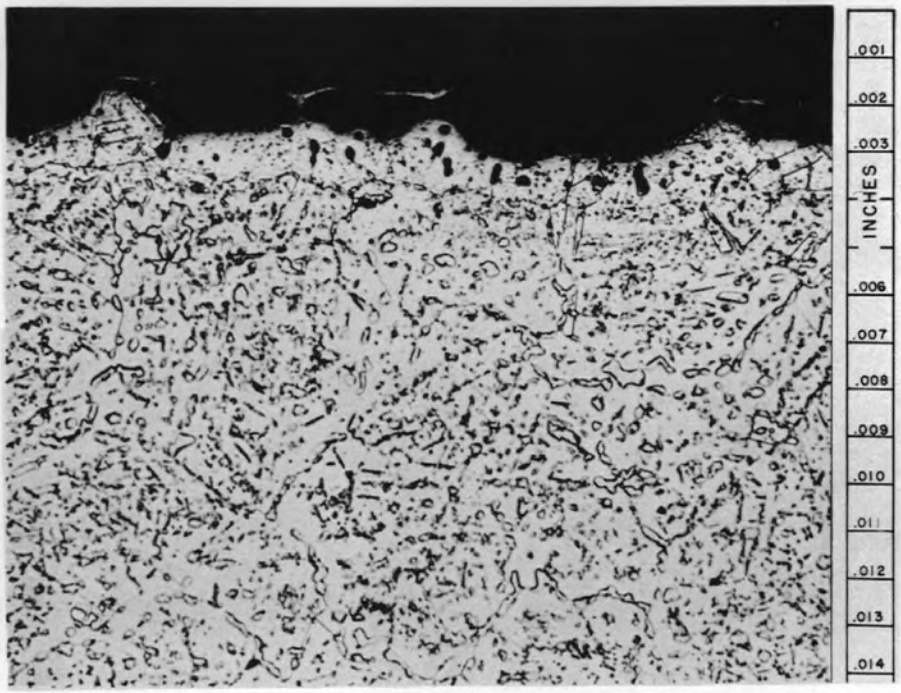

Fig. 73 (T-6084) Hot Leg of Hastelloy-B Loop after 1000 Hr at 1500°F. Unclassified.

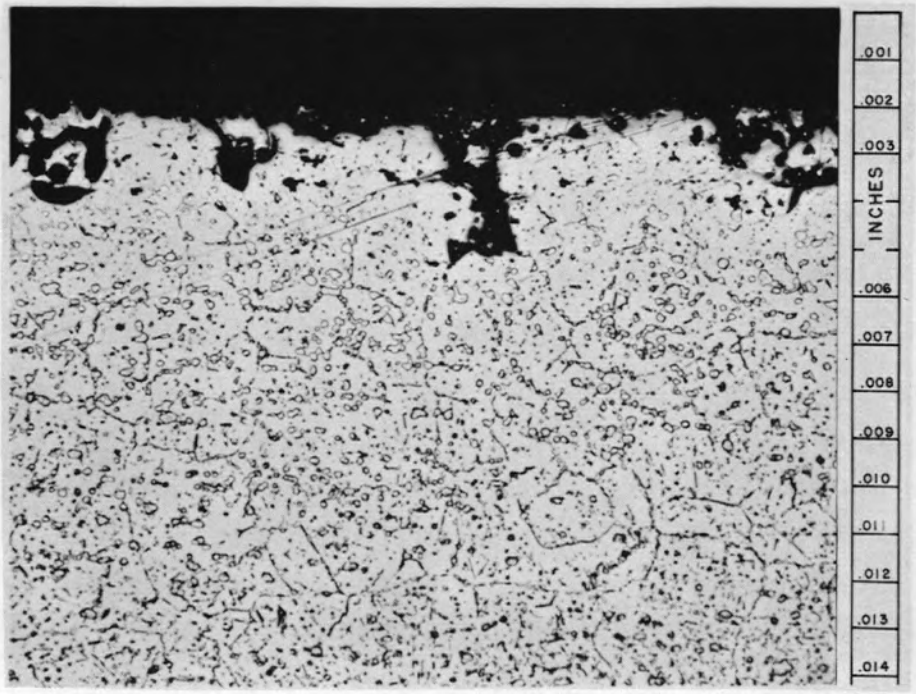

Fig. 74 (T-6100) Hot Leg of Hastelloy-C Loop after 1000 Hr at 1500°F. Unclassified.

[redacted]

Mr. G. M. Adamson.[8] In Fig. 72 (T-4361) is presented the type of corrosion experienced with Inconel in the fused salts at 1500°F after 500 hr. The material in the hot leg is attacked to a depth of 3 to 6 mils, and the amount of material transferred to the cold leg is negligible. Tests of much longer duration show that chromium can be transferred to the cold zone in small quantities, but from a corrosion standpoint Inconel is passable.

The type of corrosion found with Hastelloy B in the fused salts is seen in Fig. 73 (T-6084) after 1000 hr at 1500°F. This and additional data on the corrosion behavior of Hastelloy B, presented in the paper by Mr. G. M. Adamson[8], show it to have good corrosion resistance in the fluorides. Hastelloy B has some severe limitations and they are as follows:

1. Seamless tubing is not commercially available.
2. The material has very low ductility in the temperature range of interest.
3. Weld cracking has been experienced with this material.
4. Hastelloy B has poor oxidation resistance.
5. There is evidence of temperature gradient mass transfer of Hastelloy B in contact with sodium.

The corrosion resistance of Hastelloy C has been determined in the fused fluorides; and in examining Fig. 74 (T-6100) it is seen that the corrosion behavior is not as good as Hastelloy B, but is somewhat better than Inconel. Hastelloy C also has some limitations, such as availability of seamless tubing, weld cracking, and low ductility in the temperature range of interest.

Since the austenitic stainless steels are interesting from a fabrication standpoint and 316 stainless steel has the best creep strength, its corrosion behavior was determined. Figure 75 (T-4541) depicts the corrosion behavior of 316 stainless

---

(8) G. M. Adamson, Dynamic Corrosion Studies of Fused Fluorides in Thermal Convection Loops, ORNL-2337, (in press).

[redacted]

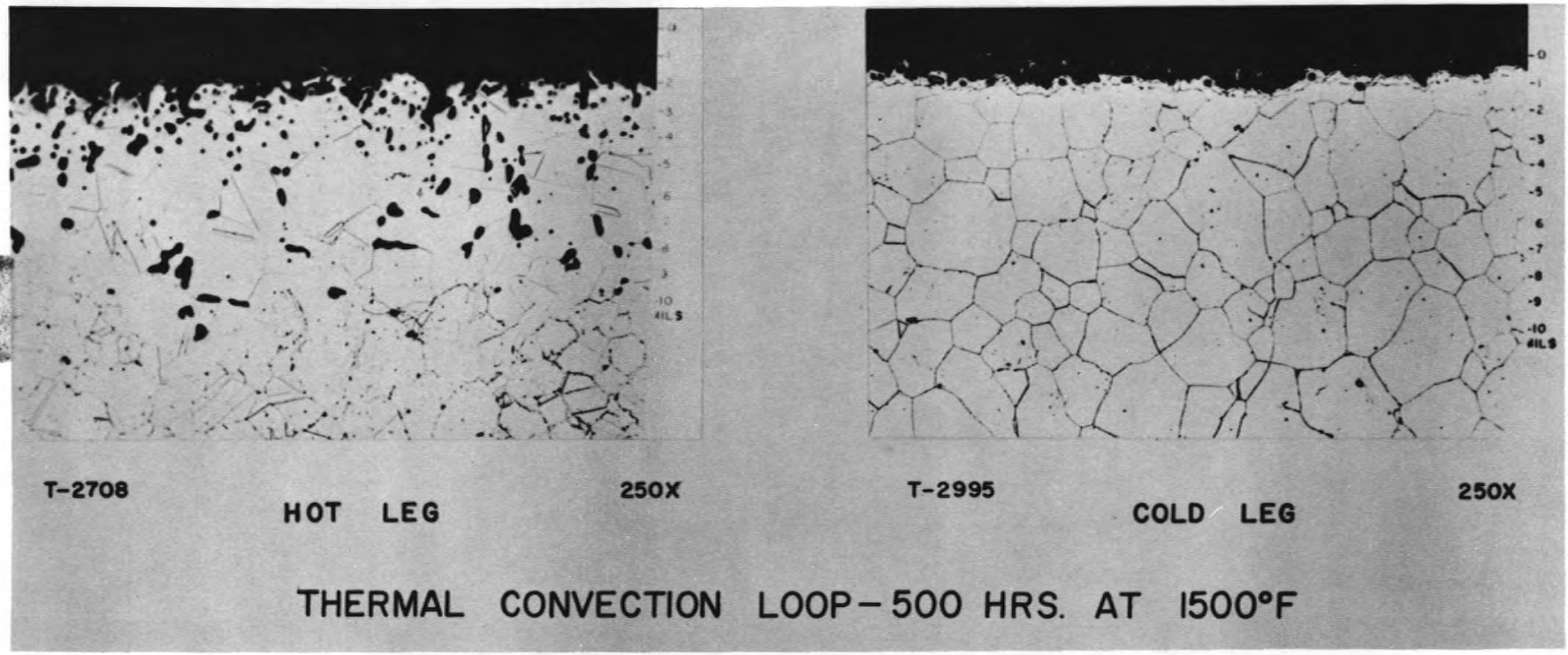

Fig. 75 (T-4541) Corrosion of 316 S.S. By ZR Base Fluorides.
Classification [redacted]

steel in zirconium-base fluorides after 500 hr at 1500°F. The 10-mil attack in the hot leg is not as detrimental to the application of 316 stainless steel as is the 1 to 2 mils of alpha iron deposited in the cold leg of the system. Any large amount of mass transfer in this complicated piping system would interfere with heat transfer and would immediately rule out an alloy showing this type of behavior.

To round out the picture of the various alloys, the 400 stainless steels were examined in contact with the fused fluorides. Figure 76 (T-6566) illustrates the large quantity of mass transfer that was obtained with 410 stainless steel and 446 stainless steel during 500-hr operation at 1500°F.

The refractory metals, such as columbium and molybdenum, have long been considered for this application; however, corrosion data are just now being obtained on these materials because of the difficulty in getting them fabricated and the necessity of oxidation protection for the material so that thermal-convection loops can be operated. To date, a columbium thermal-convection loop has not been operated; but thermodynamic studies by the Battelle Memorial Institute[9] throw considerable skepticism on the application of columbium in the fluorides. The first molybdenum thermal-convection loop was terminated after 286 hr of operation due to a weld failure. The hot leg from this loop was examined and no attack was discernible nor was mass transfer found in the cold leg. A photomicrograph of a section from the hot leg of this loop is presented in Fig. 77 (Y-6657). The refractory metals will only be used when the operating temperature of the reactor is beyond the limit of conventional structural metals. Molybdenum, as a container material in the core of the reactor, will necessitate the use of duplex tubing in the intermediate heat exchanger; so that the oxidation-resistant material would be in the NaK circuit on

(9) BMI-936, Thermodynamic Evaluation of Materials in Contact with Fluoride Fuels, (August, 1954).

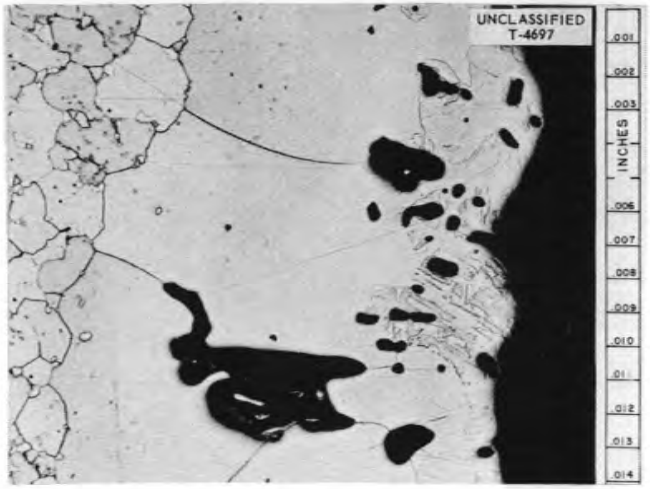

HOT LEG 250X

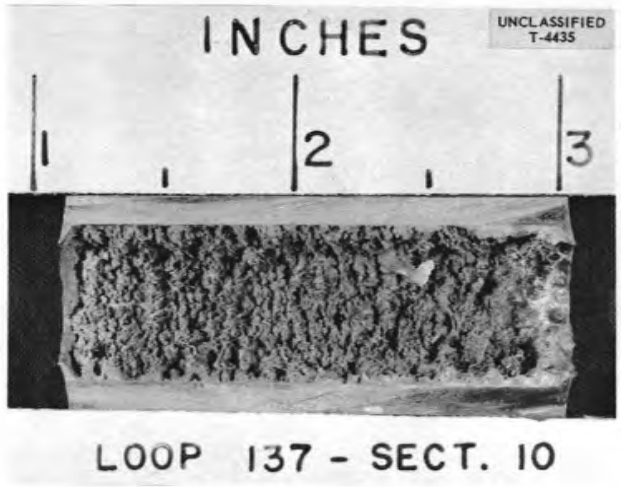

COLD LEG 2X

446 S. S. THERMAL CONVECTION LOOP 137

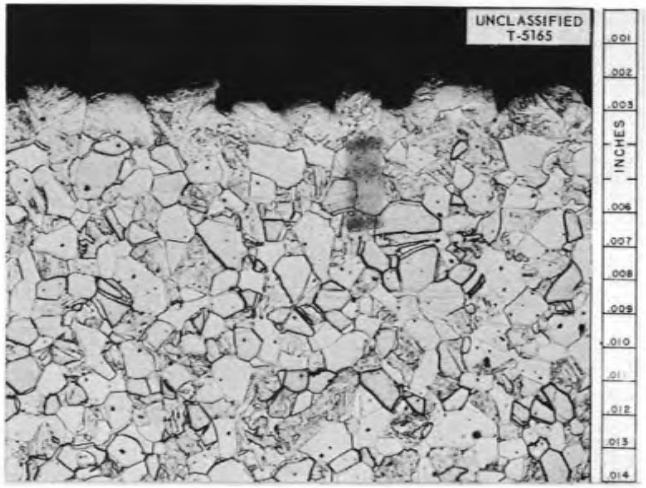

HOT LEG 250X

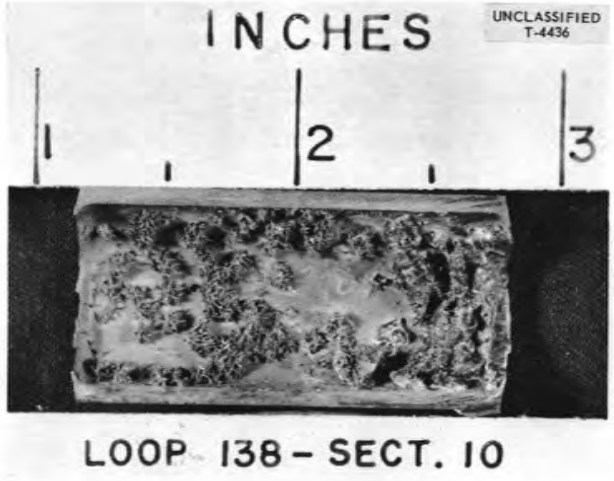

COLD LEG 2X

410 S. S. THERMAL CONVECTION LOOP 138

Fig. 76 Corrosion of 400 Series S. S. in Molten Fluorides.

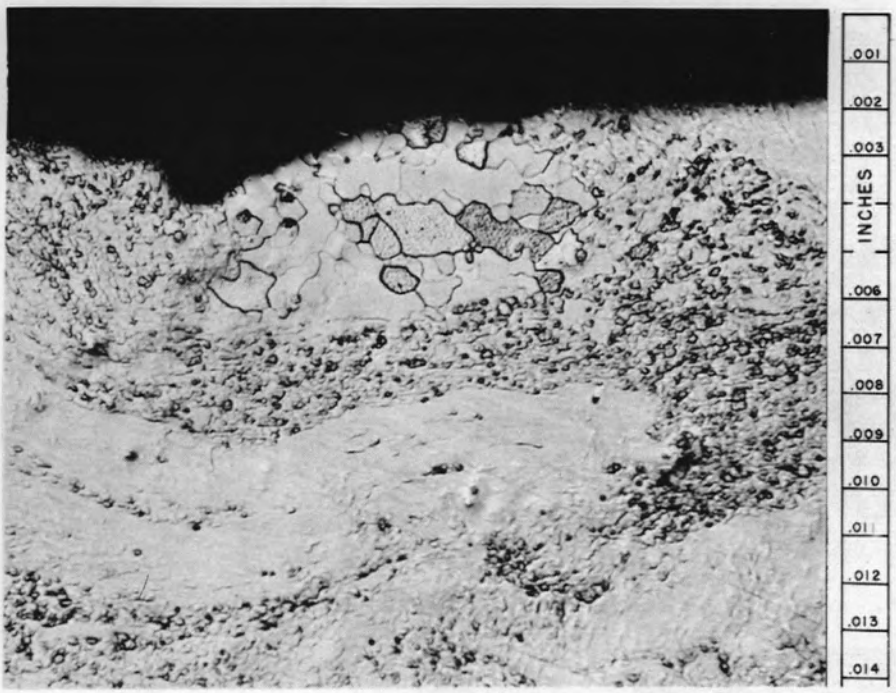

Fig. 77 (Y-6657) Hot Leg of Molybdenum Thermal-Convection Loop After 286-Hr Operation at 1500°F in Zirconium-Base Fluorides. Unclassified - [redacted] with caption.

the air side. The transition from molybdenum to an oxidation-resistant material would have to be made in the heat exchanger, because in high-temperature liquid plumbing systems a uni-metal construction must be used throughout to prevent dissimilar metal transfer.

Dissimilar-metal transfer is best seen in Fig. 78 (Y-2772) which illustrates the alloying of nickel with molybdenum, which occurred by the nickel being transported through sodium to the molybdenum surface, then coming out of solution and diffusing into the molybdenum. Both nickel and molybdenum, by themselves, have good corrosion resistance to sodium, but the dissimilar-metal transfer occurred due to the decrease in the chemical potential of the nickel and molybdenum in forming an alloy. Dissimilar-metal transfer has also been observed in large plumbing systems circulating the fused fluorides. Figure 79 (T-6565) shows the transfer of iron to the cold leg of an Inconel loop having a 316 stainless steel pump bowl. This transferred material caused a gradual increase in the pressure drop in the loop due to restriction of flow. This experimental result justifies the conclusion that only one alloy should be used throughout the plumbing system or that the transition of one metal to another should be made in the heat exchanger, so that each liquid is in contact with only one metal.

In addition to looking at conventional materials, modifications of the various high-temperature alloys have been made and are in process of being corrosion tested to find an alloy that better meets the eleven requirements for a container material. The first tests were aimed at determining the effect of carbon content on the corrosion resistance of Inconel. Figure 80 (T-4708) compares the corrosion resistance of low-carbon Inconel to commercially available Inconel. Changing the carbon content by a factor of seven has little or no effect on the corrosion resistance.

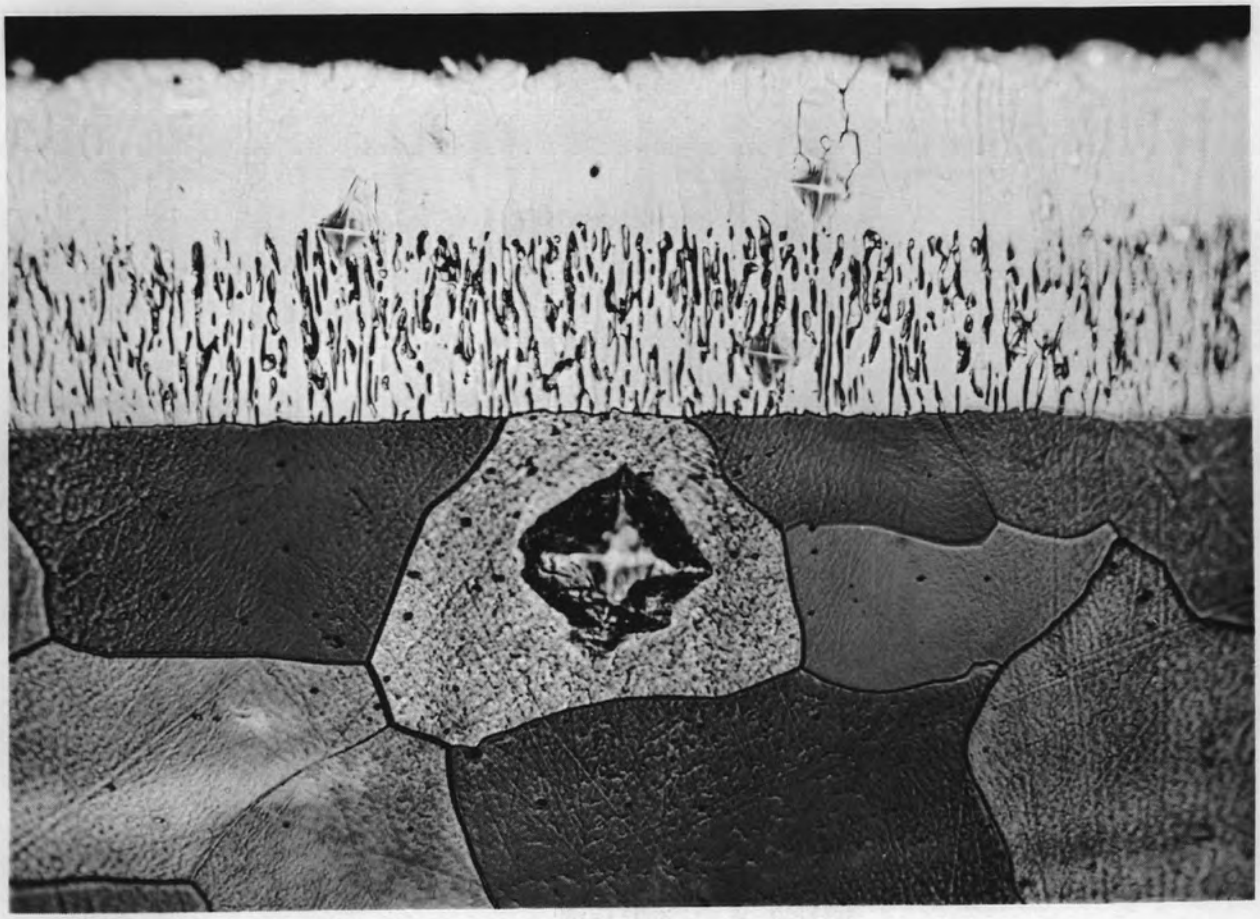

Fig. 78 (Y-2772) Photomicrograph of Nickel Deposited on Molybdenum Due to Dissimilar Metal Transfer. Unclassified.

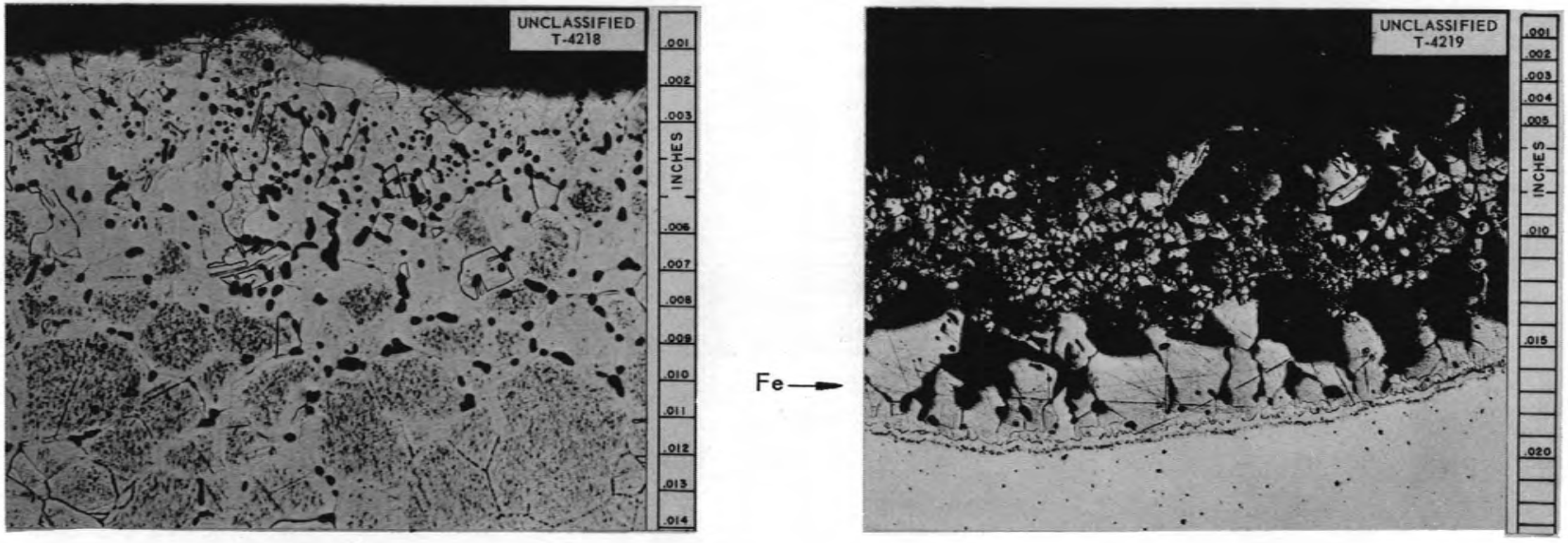

250X

150X

HOT SECTION

COLD SECTION

HEAT EXCHANGER LOOP
500 hr AT 1500°F VELOCITY = 8 ft/sec $\Delta T = 300°F$

Fig. 79 Dissimilar Metal Mass Transfer.

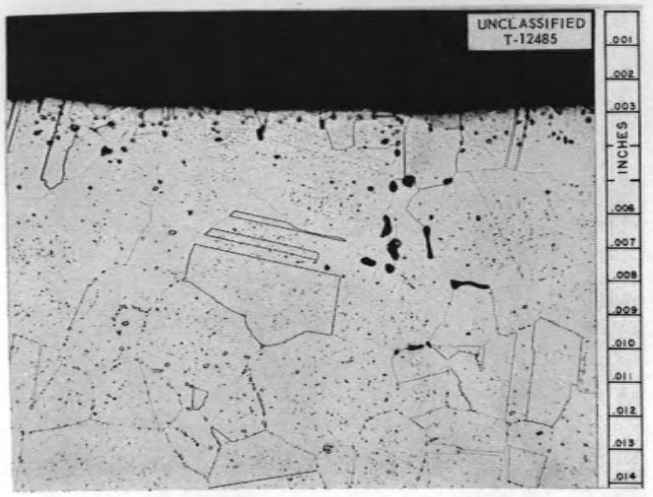

250X

COMMERCIAL TUBING - 0.08C

250X

SPECIAL TUBING - 0.013C

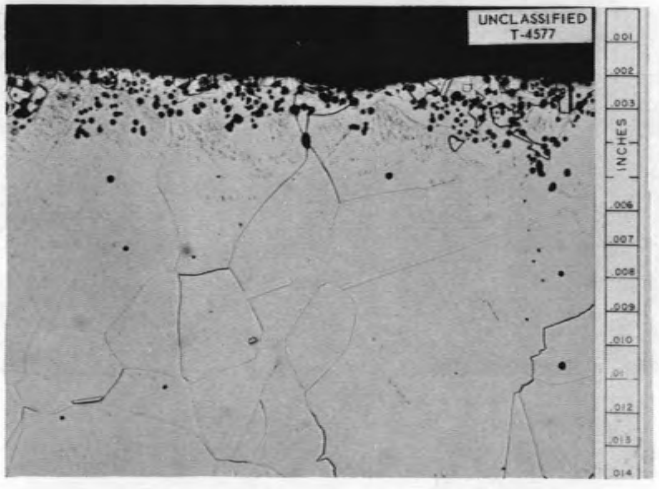

250X

SPECIAL TUBING - 0.014C + 0.3 Ti

THERMAL CONVECTION LOOPS - 1/2" TUBING 500 hr AT 1500°F

Fig. 80 Corrosion of Low Carbon Inconel.

Modifications in the Fe-Cr-Ni ratios of Inconel have shown that if the chromium content is approximately 5% to 6% the corrosion of Inconel can be markedly decreased. (Fig. 81)(T-6575).

In summation, it might be said that at present the best container material for the circulating-fuel system is some type of nickel-base alloy. High-temperature creep strength in nickel-base alloys can be obtained by two methods: One is by the age hardening response found by the precipitation of intermetallic compounds of nickel, titanium, and aluminum, which results from additions of titanium and aluminum to the basic Ni-Cr alloy. High-temperature strength can be achieved in the Ni-Mo-base alloys by the age-hardening response inherent in this system. Nickel-base alloys with large additions of titanium and aluminum, such as Inconel X and the Nimonics, show inferior corrosion resistance in both sodium and the fused fluorides as compared to Inconel, and Hastelloy-B alloy is inferior to chromium-containing alloys in molten sodium. Therefore, at this time, it seems that the best alloy for circulating fuel reactors would come from the Ni-Mo-Cr system with the chromium content not in excess of 5%, so it will not corrode quickly in the fused fluorides. It is postulated that 5% chromium would give the alloy resistance to mass transfer in sodium. With this in mind, research at the Oak Ridge National Laboratory is continuing on Hastelloy B, Inconel, Inconel X, the Nimonic alloys, and modifications of all these alloys.

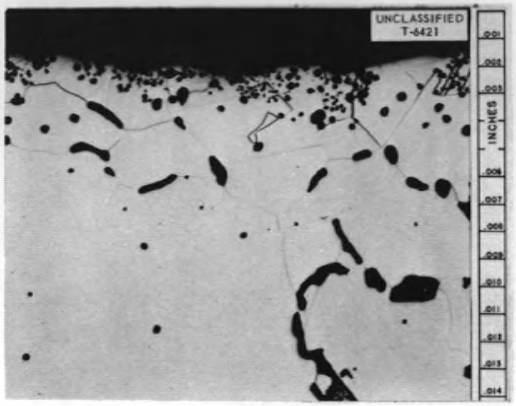

ALLOY 5

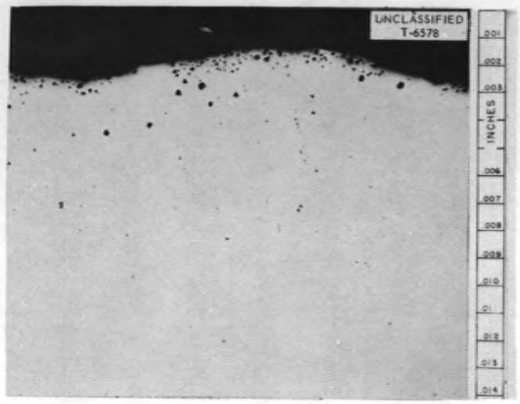

ALLOY 7

ALLOY	COMPOSITION (%)			
	Cr	Fe	Ni	Mo
5	17.6	6.8	75.6	
7	4.8	19.8	75.4	
9	6.0	10.0	74.0	10.0
INCONEL	15.0	5.0	80.0	

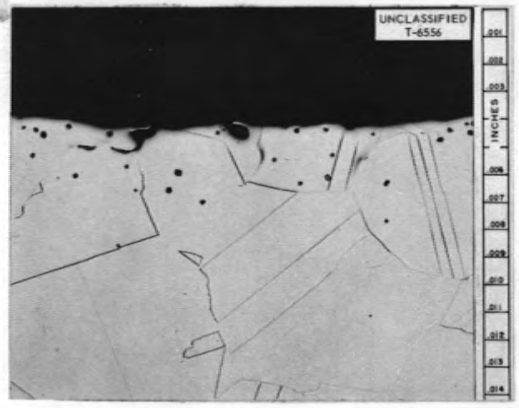

ALLOY 9

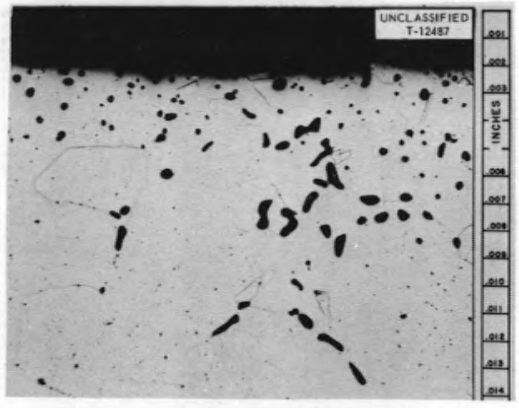

COMMERCIAL INCONEL

Fig. 81 Special Alloys Run Under Standard Test Conditions.

CORROSION BY MOLTEN FLUORIDES

G. M. Adamson, W. D. Manly and R. S. Crouse

This paper covers briefly a portion of the corrosion studies being carried out as a part of the program leading to the development of an aircraft reactor using molten fluorides as the fuel carrier. It is intended as a progress report, not a final presentation. This work is a joint effort of the Metallurgy, Materials Chemistry, and Experimental Engineering Divisions of Oak Ridge National Laboratory. While the corrosion program consists of three parts, (1) bench tests, (2) thermal loops, and (3) pump loops, only the intermediate or thermal loop tests will be discussed here. Unless specifically stated otherwise, all loops were of Inconel and were filled with a molten fluoride mixture of NaF, ZrF_4, UF_4 (50, 46, 4 M%).

A group of thermal loops similar to those used in this study are shown in Fig. 82. The development and operation of this equipment has been reported previously and will only be briefly reviewed here. A loop consists of a length of pipe, or tube, bent in the shape of a parallelogram about 3 ft high and 2 ft wide. Two sides are heated with nichrome-wound heaters covered with insulation while the other two sides are bare. Circulation is achieved by the density differences of the liquid caused by the temperature gradient. Loops are filled, while hot, with molten fluorides using inert gas pressure to accomplish the fluoride transfer.

A photomicrograph from the top of the hot leg of an Inconel loop in which NaF, ZrF_4, UF_4 (50, 46, 4 M%) has been circulated for 500 hr at 1500°F is presented in Fig. 83. These conditions have been established as base or standard conditions in this study, and this figure is typical of the attack found in these loops.

The corrosive attack results in unconnected holes beneath the Inconel surface. The holes are found primarily, but not exclusively, in the grain boundaries and in a few boundaries they extend to a depth of 8 mils below the surface. No evidence of

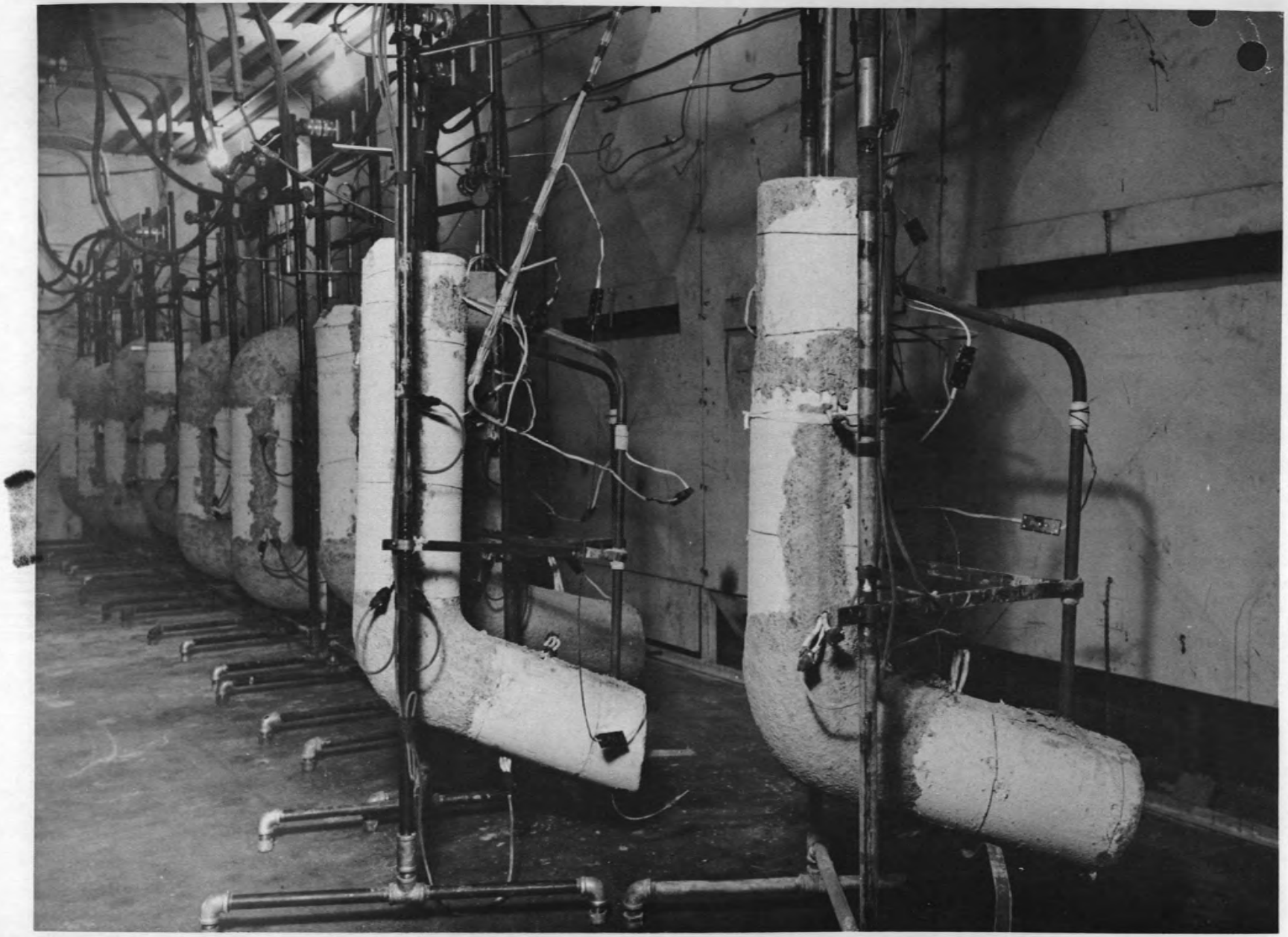

Fig. 82 (21341) Group of Thermal-Convection Loops in Operation. Unclassified.

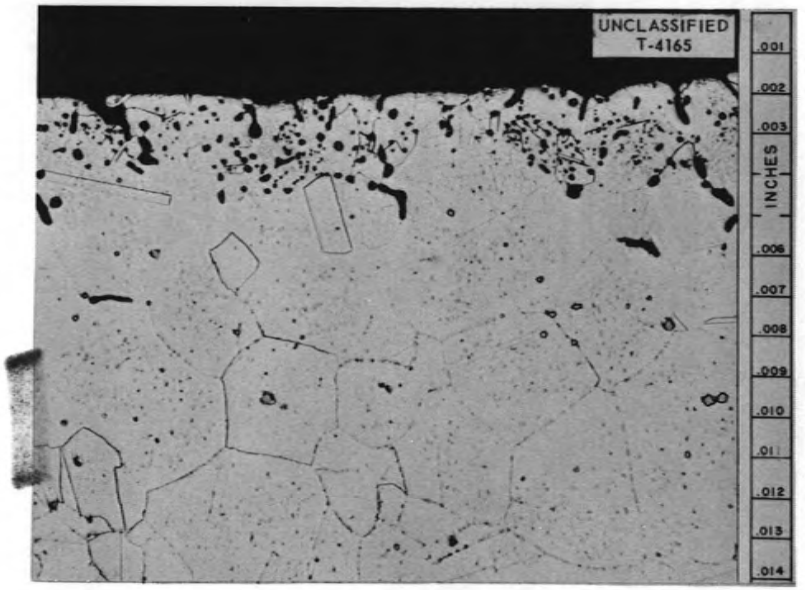

HOT LEG

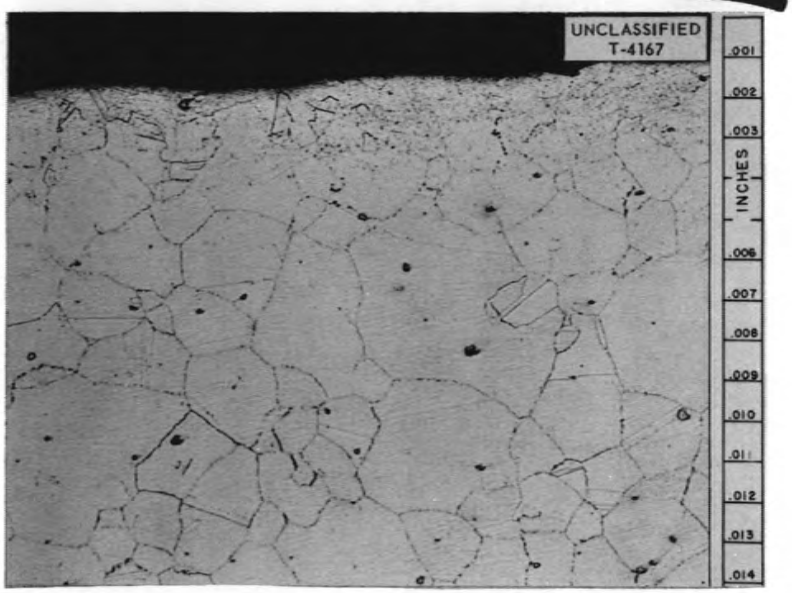

COLD LEG

Fig. 83 Corrosion of Inconel in FUZRNA 30-500 hr at 1500°F. Etchant-modified aqua regia. (Mag. 250X)

general surface removal or the usual types of intergranular attack have been noted. The second picture in this figure is from the cold leg of the same loop and it is apparent that no layer or deposit is present.

The mechanism of formation of the voids has been covered in detail at previous meetings. The major steps in this mechanism are:

1. The chromium is removed from the inner surface of the pipe either by corrosion or mass transfer. These terms are used in the same sense that has been explained in previous papers.(10)
2. Because of the concentration gradient some of the internal chromium atoms diffuse to the surface.
3. Nothing is diffusing inward so a subsurface concentration of vacancies occurs.
4. The vacancies precipitate at sites of disregistry such as grain boundaries and inclusions.
5. The vacancies collect and form discontinuous voids.
6. The voids concentrate and grow with increasing time or temperature.

The first step in this process is the one that appears to be easiest to control. This step will be discussed in considerable detail in this paper and in another by the Materials Chemistry Division.(10)

Considerable controversy has existed as to whether the holes are actually voids. That they are voids has been shown by liquid penetrants, hot-helium leak-detector tests, and metallographic studies.

One of the most important variables in any corrosion test is time. For the system being discussed, time is shown in Fig. 84 to be a two-stage effect. For about the first 200 hr there is a rapid increase in depth of attack with an increase in time. This attack will be shown to be primarily from the effects of impurities. After 200 hr the depth of attack continues to increase with increasing time but at a slower

(10) W. R. Grimes, Chemical Equilibria in Molten Fluorides (unpublished).

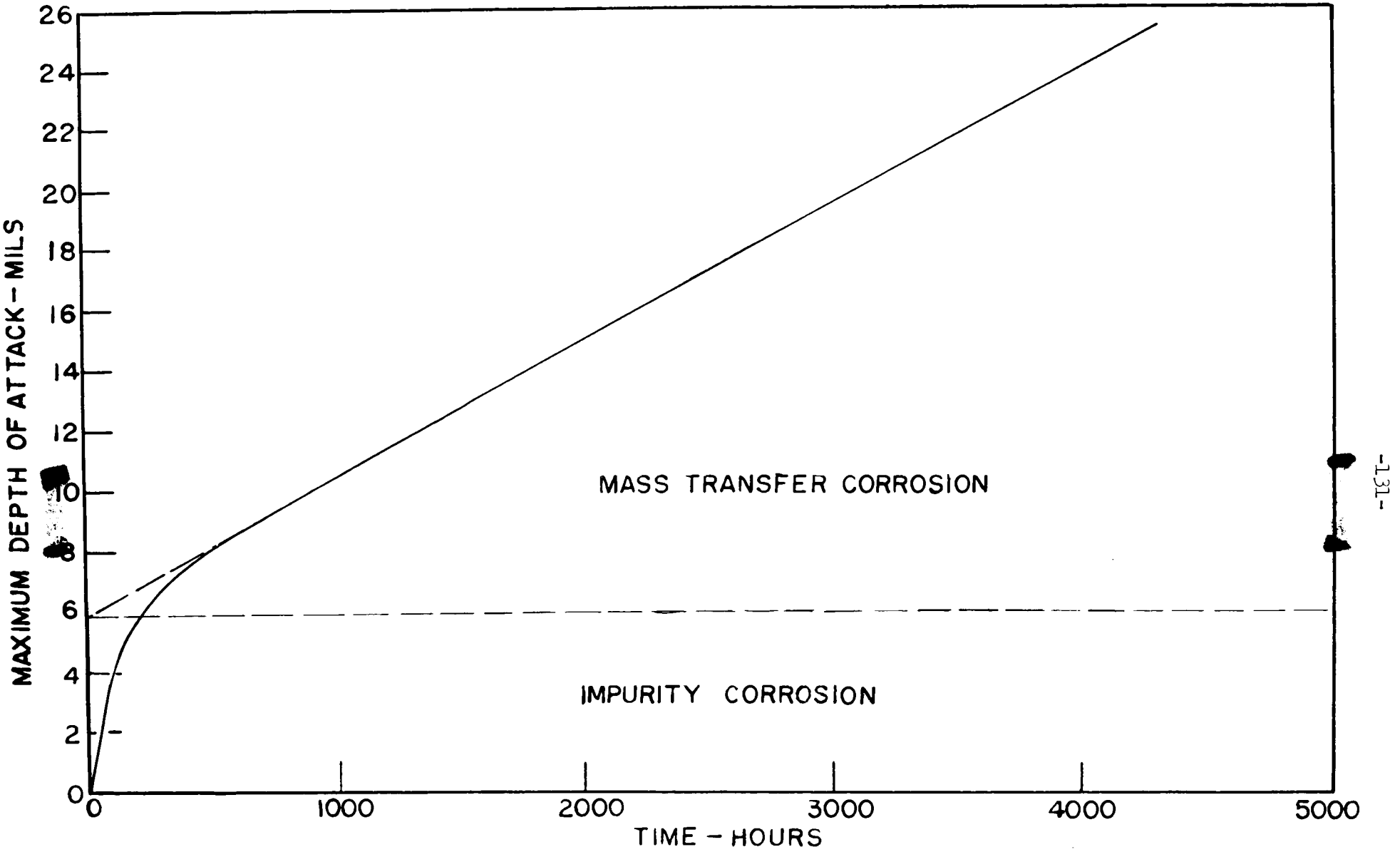

Fig. 84 (T-6550) Effect of Time on Corrosion Depth-Molten Fluorides in Inconel. Unclassified.

[redacted]

rate than is found initially. Within the accuracy of the results, this second stage is linear and is the mass-transfer portion of the attack.

The four photomicrographs in Fig. 85 are offered as evidence of the effect of impurities. All are from 500-hr loop tests filled with similar fluorides, but of varying purity. The results are tabulated below.

T Number	Total Ni + Fe ppm	HF Content Moles per Liter Purging Gas	Maximum Hot-Leg Attack Mils
4485	1850	-	15
3322	710	-	8
4410	120	$<2 \times 10^{-4}$	5-1/2
3920	600	5×10^{-4}	14

The chemical reactions by which these impurities remove the chromium from the surface are as follows:

$$NiF_2 + Cr \rightarrow CrF_2 + Ni$$

$$FeF_2 + Cr \rightarrow CrF_2 + Fe$$

$$2HF + Ni \rightarrow NiF_2 + H_2$$ -- The NiF_2 then removes the Cr.

These reactions will be discussed in greater detail from a chemical viewpoint in a paper by Mr. Warren Grimes of our Materials Chemistry Division.[11] Other evidence of the effects of these impurities has been obtained from tests with double fluoride loadings and from tests in which additions have been made.

The chemical reactions causing the second stage of the attack are not as well understood or as well substantiated as are those discussed above. During this stage the chromium is removed by mass transfer, or the movement of metal from the hotter to the colder portion of the system. The most likely reactions by which such a

[11] Ibid.

[redacted]

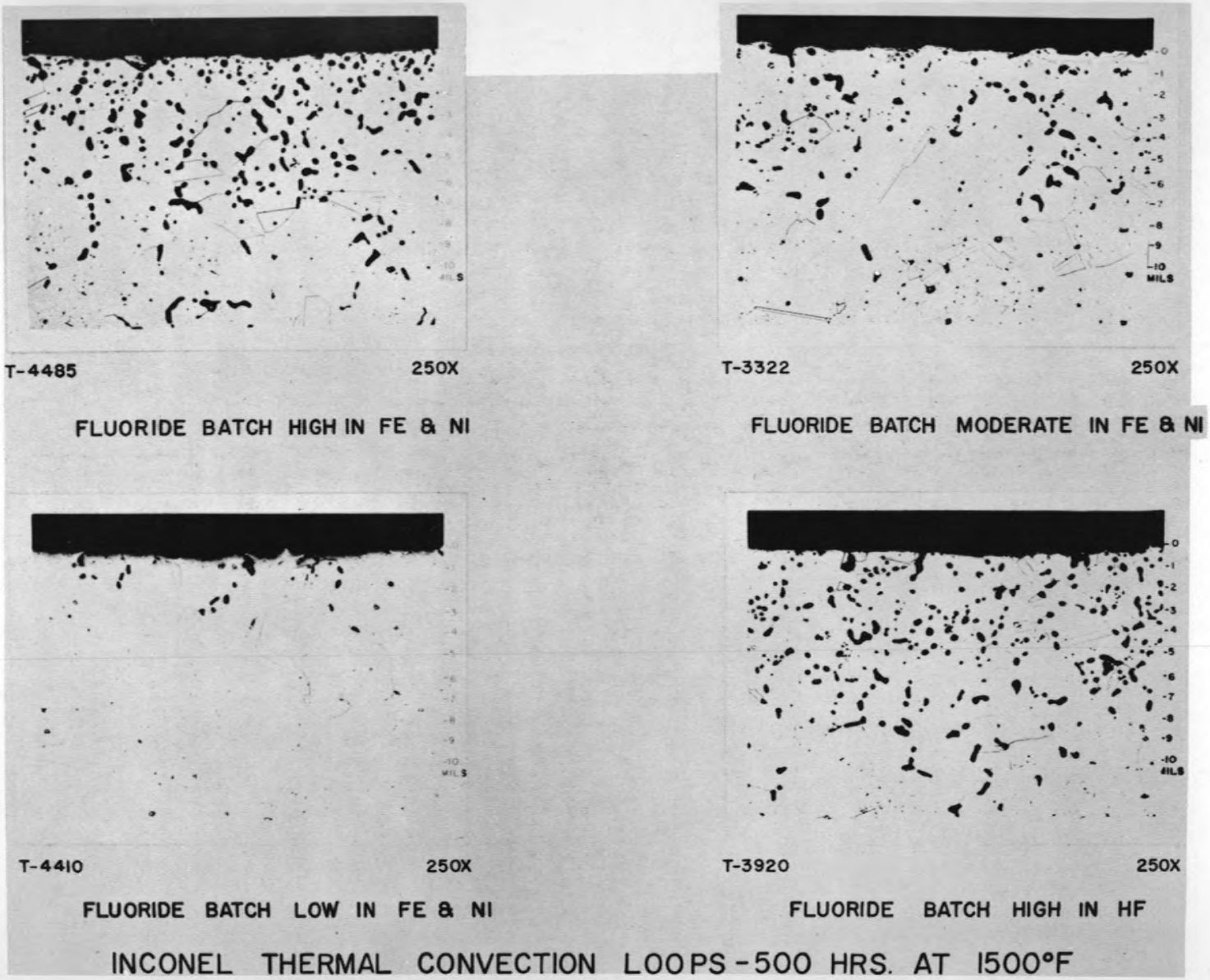

Fig. 85 (T-4544) Effect of Fluoride Batch Purity. Unclassified.

process takes place are as follows:

$$2UF_4 + Cr \underset{\text{cold}}{\overset{\text{hot}}{\rightleftharpoons}} CrF_2 + 2UF_3$$

$$2CrF_3 + Cr \underset{\text{cold}}{\overset{\text{hot}}{\rightleftharpoons}} 3CrF_2$$

$$2ZrF_4 + Cr \underset{\text{cold}}{\overset{\text{hot}}{\rightleftharpoons}} 2ZrF_3 + CrF_2$$

$$2NaF + Cr \underset{\text{cold}}{\overset{\text{hot}}{\rightleftharpoons}} CrF_2 + Na$$

Mass transfer, as found in the thermal loops, is actually a very slow chemical process. For movements of the required amounts of metal, a change in equilibrium concentration in the above reactions of as little as one ppm for the 200°F difference in temperature would be sufficient.

In the curve presented previously, the major portion of the attack resulted from impurities present in the molten fluorides. This may not be the case in a pumped loop. Mass transfer should properly be expressed as a linear function of the number of cycles, which in a pumped loop would be tremendous. The rate of the impurity reactions might vary, but ultimately the depth should be dependent primarily upon the amount of the impurities and the surface area-to-volume ratio of the system.

Even with the expected increased attack in the pump loops, the item of most concern is not the depth of attack in the hot leg but what happens to the deposited metal in the cold leg. In the proposed reactors, the heat exchangers will consist of a large number of small-diameter tubes which will be very easy to plug. A layer of chromium-metal crystals from a 5000-hr loop is shown in Fig. 86. This layer was found in the trap at the bottom of the cold leg just above a liquid-solid interface. While exact material balances are almost impossible to make, the amount of chromium found in the layer plus the increase in concentration of the fluorides do not appear to be enough to balance that lost in the hot leg. It is thought that some of the chromium attaches itself to the cold-leg surface and diffuses into the metal.

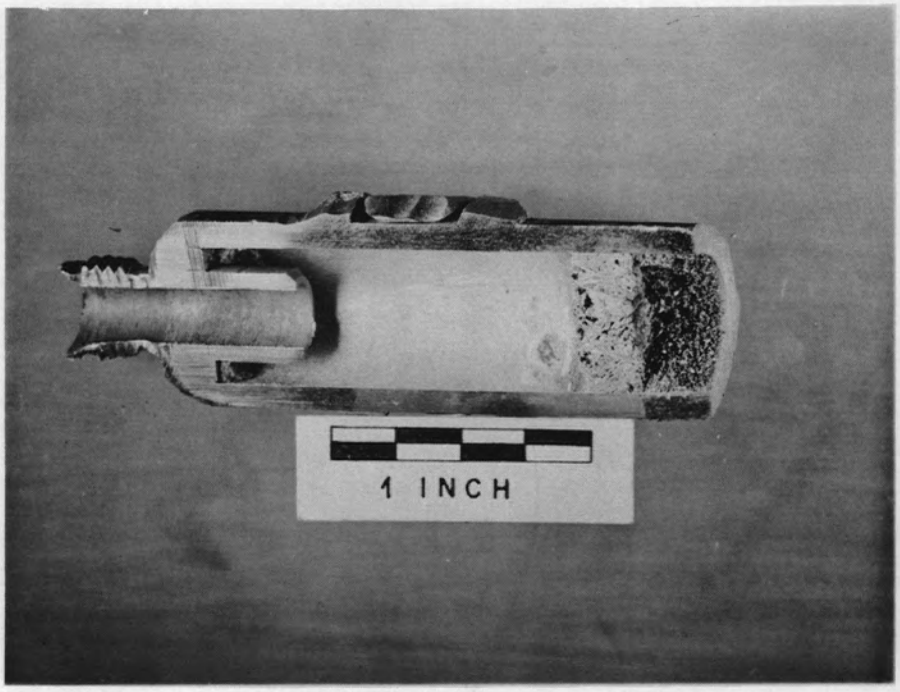

Fig. 86 (T-5211) Layer of Chromium Crystals Found in the Trap of an Inconel Loop after Circulating Fused Fluorides for 5000 Hr at 1500°F. Unclassified - Secret with caption.

The resulting change in composition of the metal is not enough to be picked up by present sampling techniques.

Another very important factor in both reactor design and in corrosion testing is temperature. As shown by the panel in Fig. 87, a fairly wide change in temperature does not affect the depth of attack found after 500 hr. The depths measured at 1350, 1500 and 1650°F are all similar. Temperature does, however, affect the size and distribution of the holes. At low temperatures they are small and evenly distributed, while at the higher temperatures they are large and are located primarily in the grain boundaries. This would be expected from the proposed corrosion mechanism since the rate of diffusion increases rapidly with temperature.

With longer times, or with mass transfer, temperature does seem to have an effect. Results from three loops filled from the same batch of fluorides and operated 2000 hr at varying temperatures are tabulated below:

Loop No.	Temp. °F	Maximum Penetration Mils	Hot-Leg Attack	Cold Leg
449	1250	6	Intergranular, moderate to heavy.	No deposit.
392	1400	8	Heavy general attack to 4 mils with occasional deeper intergranular penetrations.	Intermittent metallic deposit.
393	1600	13	Intergranular moderate to heavy, large voids.	Thin but continuous metallic deposit.

In this case an increase in depth with increasing temperature may be noted. These tests are now being confirmed.

One other variable that must be considered in corrosion work, and especially when different tests are compared, is the surface area-to-volume ratio of the

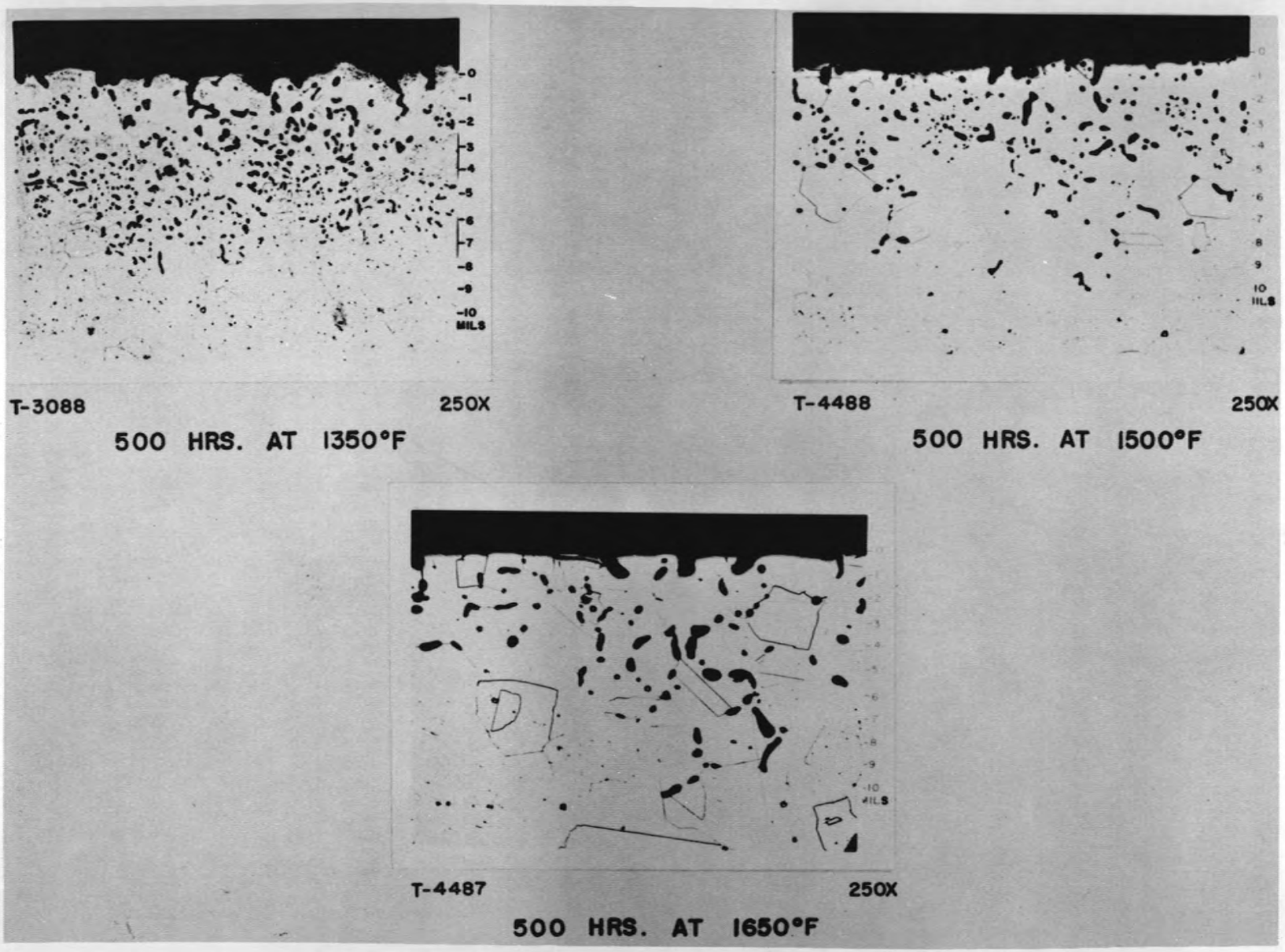

Fig. 87 (T-4542) Effect of Temperature on Corrosion of Inconel by Zirconium-Base Fluorides. Unclassified.

apparatus. Three loops with different diameters were filled from the same batch of fluorides and circulated for 500 hr yielding the following results:

Loop No.	Pipe Size	I.D. Inches	Surface Area-to-Volume Ratio. in^2/in^3	Hot-Leg Attack
359	1/2-in. tubing	0.43	10.5	Moderate to heavy to 4 mils.
352	1/2-in. pipe	0.62	6.5	Moderate to 5-1/2 mils.
349	1-in. tubing	0.87	4.6	Light to moderate to 9 mils.

Plotting depth of attack against the surface area-to-volume ratio results in a nearly linear relationship. The variation from linearity is probably due to changes in velocity and temperature drop which unavoidably accompany any changes in loop diameter.

In the case of mass transfer it is possible that an increase in the amount of attack will be found with an increase in surface area.

The large variation in test results, with varying surface area-to-volume ratios, points out the danger of comparing corrosion results from various tests. It also shows that care must be used in extending the corrosion data to cover large systems with different surface area-to-volume ratios. Mr. Douglas has also discussed the large effect this variable has on the results that are being obtained in the physical testing work.(12)

While the corrosion penetration reported here was allowable for the first low power reactor, further reduction of this corrosion is desirable. Two lines of

(12) R. B. Oliver, D. A. Douglas, and J. H. DeVan, "Effect of Environment on Creep Properties of High Temperature Alloys, (p 17, this report).

endeavor are being followed in an attempt to obtain lower rates of attack: (1) the search for better container materials is continuing, and (2) we are still working to obtain better fluoride mixtures. The search for better alloys will be covered in a paper by W. D. Manly[13] and the work on improving the fluorides by W. R. Grimes.[14] Both efforts will be discussed briefly in this paper.

The most promising new container material is Hastelloy B. Figure 88 shows the hot legs of such loops operated for 1000 and 2000 hr. It is apparent that much less attack is found with this material than is found with Inconel. A most encouraging point is that there does not seem to be an increase in attack with increasing time. The other optimistic feature is that in all loops, the molybdenum analysis in the fluorides after circulation has been very low. The one corrosion feature that requires caution in using this alloy is the surface condition. The surface of the as-received tubing is very rough and it is difficult to say if this roughness has been increased by a general surface type of attack. This question is being resolved by testing thermal loops with machined sections welded into the hot leg.

Figure 89 shows the hot leg of a Hastelloy-B loop after 1000 hr at 1650°F. Again the results are encouraging with very little attack and a low molybdenum concentration in the fluorides. A duplicate loop showed what appears to be a layer in one of the hot-leg sections and this discrepancy must yet be resolved.

The work in modifying the fluorides that shows the most promise is the replacing of the UF_4 with UF_3. Figure 90 shows the hot leg of an Inconel loop that operated 2000 hr with a zirconium fluoride-base mixture with the uranium present as UF_3. There is none of the usual subsurface-void type of attack; instead, the hot-leg surface is covered by a thin metallic layer identified by spectrographic

---

[13] W. D. Manly, Container Materials for Circulating Fuel Reactors, (p 108, this report).

[14] W. R. Grimes, Chemical Equilibria in Molten Fluorides (unpublished).

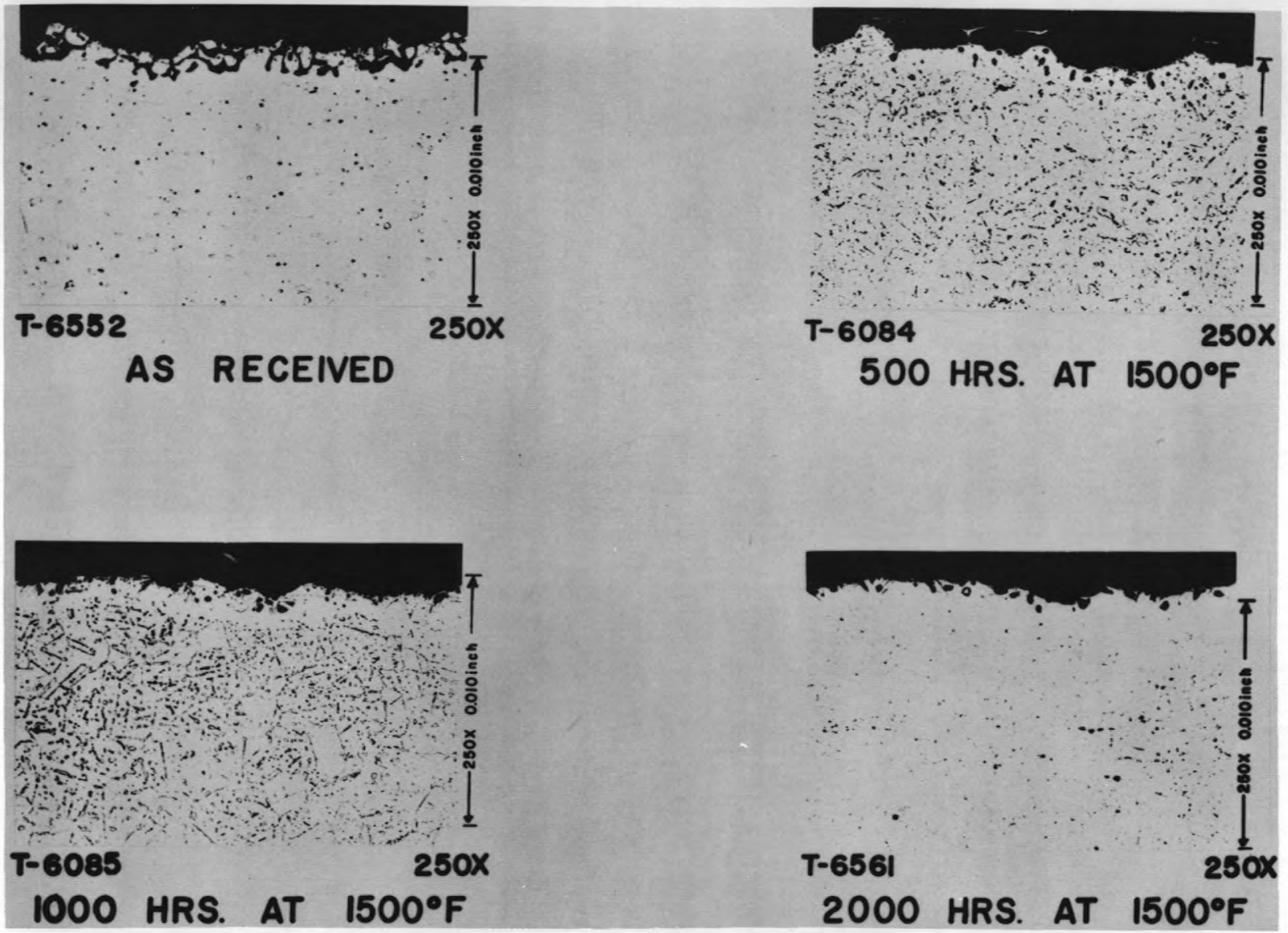

THERMAL CONVECTION LOOPS

Fig. 88 (T-6572) Corrosion of Hastelloy-B by Molten Fluorides.
Unclassified.

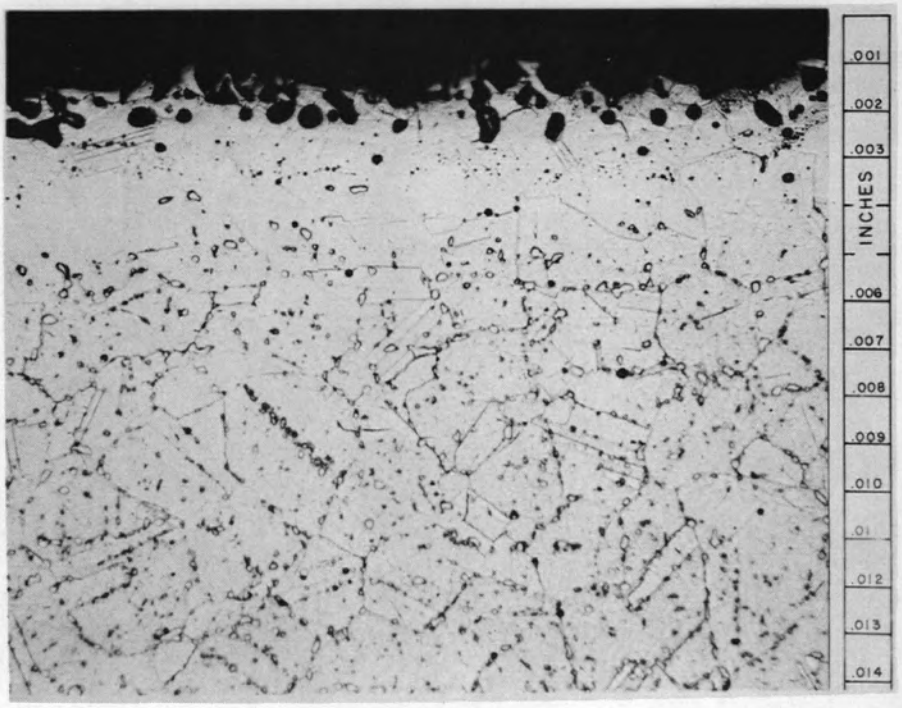

Fig. 89 (Y-6433) Hot Leg of Hastelloy-B Loop after Circulating Fused Fluorides for 1000 Hr at 1650°F. 250X. Unclassified [redacted] with caption.

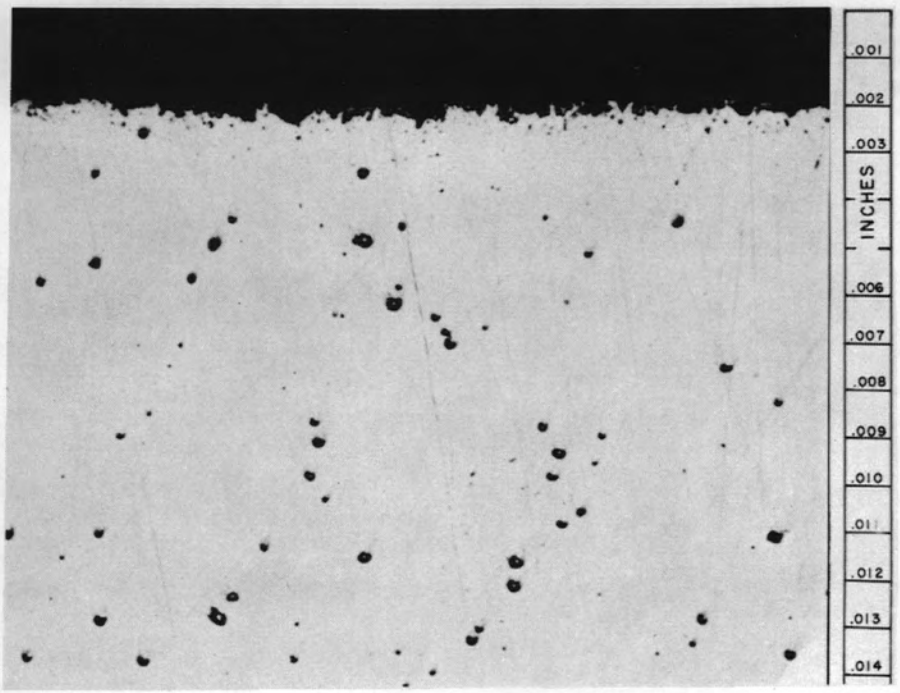

Fig. 90 (T-5708) Hot Leg of Inconel Loop after Circulating Zirconium Fluoride-Base Fluoride Mixtures Containing UF_3 for 2000 Hr at 1500°F. 250X. Unclassified [redacted] with caption.

means as being zirconium metal. The major disadvantage of this system is the fact that only about 2 M% UF_3 may be used without encountering excessively high melting points. Mixtures with various combinations of UF_3 and UF_4 will permit a reduction in depth of attack from that found with all UF_4 mixtures, but they will not eliminate it completely.

By using fluoride mixtures of the alkali metals (sodium, lithium, and potassium) it is possible to obtain useful amounts of UF_3 in solution. With this system, considerable difficulty has been encountered by Materials Chemistry in the production step and we have not been able to obtain reproducible mixtures. Figure 91 shows the hot leg of one of the least-corroded Inconel loops after circulating an alkali-metal-base mixture containing both UF_3 and UF_4 for 500 hr. This loop shows practically no attack and no visible surface layer. While this preliminary investigation produced encouraging results, we have not been able to reproduce these results and a supposedly duplicate loop might have an attack as deep as 13 mils. It is hoped, however, that when the production problems have been solved that the depth of attack in all the loops will compare to the better values now being obtained.

In conclusion it can be stated that: (1) we are beginning to understand the corrosion mechanisms in the Inconel– molten-zirconium fluoride-base system, (2) the depths of attack and amounts of mass-transferred metal are more than we would like, but they can be tolerated, and (3) both Hastelloy B and alkali-metal fluoride mixtures with the uranium as UF_3 offer promise of lower rates of attack.

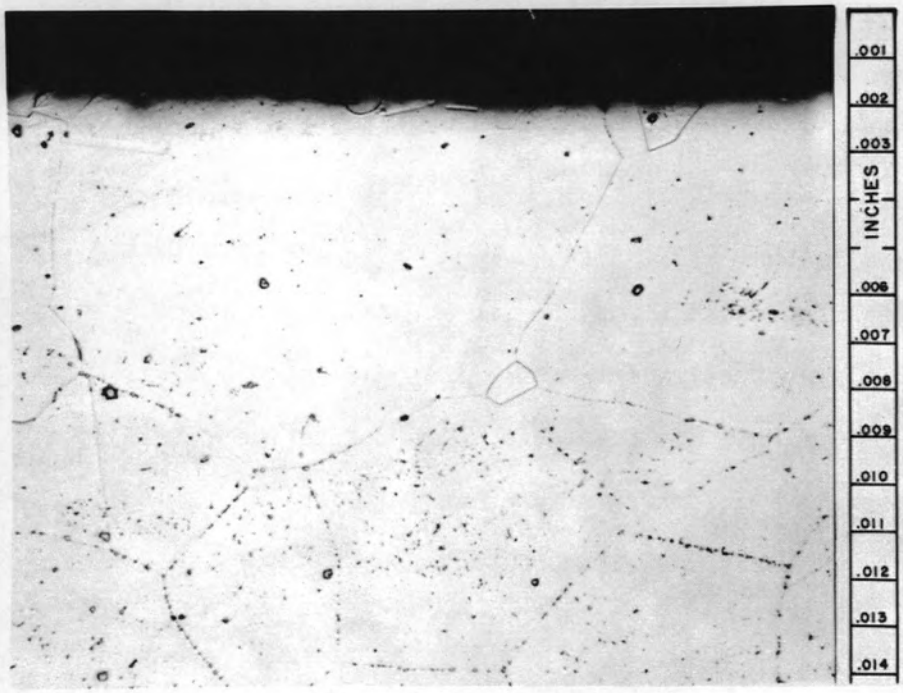

Fig. 91 (T-6562) Hot Leg of Inconel Loop after Circulating Alkali Metal-Base Fluoride Mixtures Containing both UF_3 and UF_4 for 500 Hr at 1500°F. 250X. Unclassified [redacted] with caption.

CORROSION AND MASS TRANSFER IN LIQUID LEAD

J. V. Cathcart
W. D. Manly

A study has been made of the mass transfer and corrosion characteristics of a number of metals and alloys in liquid lead. The object of this research was to obtain a comparison of the resistance to mass transfer in liquid lead of a number of structural metals. In order to obtain an insight into the role played by individual metals, tests were carried out not only on structural alloys themselves, but also on their components. For example, in addition to testing several stainless steels, the mass-transfer characteristics of such pure metals as iron, chromium and nickel were also investigated.

The test apparatus was a small thermal-convection loop (Fig. 92). The loop itself was made of 1/2-in. quartz tubing. Six-inch tubes of the test metals were mounted in the hot and cold legs of the loops where they were held in place by indentations in the quartz tubing. Attached above the loop and separated from it by a fritted quartz filtered disk was a large quartz bulb, 80 mm in diameter. This bulb was used for the deoxidation of the lead prior to the loading of the loop. Two side arms, one above the deoxidation bulb and the other below the fritted disk, were attached to hydrogen and vacuum lines through a suitable system of stop-cocks. Eight-inch, split-core, clam-shell heaters were used to heat the loop, one such heater being suspended by stainless steel clamps around each arm of the loop. The deoxidation bulb was heated with an electric tape heater. Temperatures were measured by thermocouples placed around the loop and tied in place by wire. The temperature of the hot leg was controlled with a Leeds and Northrup Micromax-DAT unit.

With the loop set up in operating position, the lead in the deoxidation bulb was heated to 425°C, the hydrogen was allowed to pass through the fritted quartz disk and bubble up through the lead. During the deoxidation process, which lasted

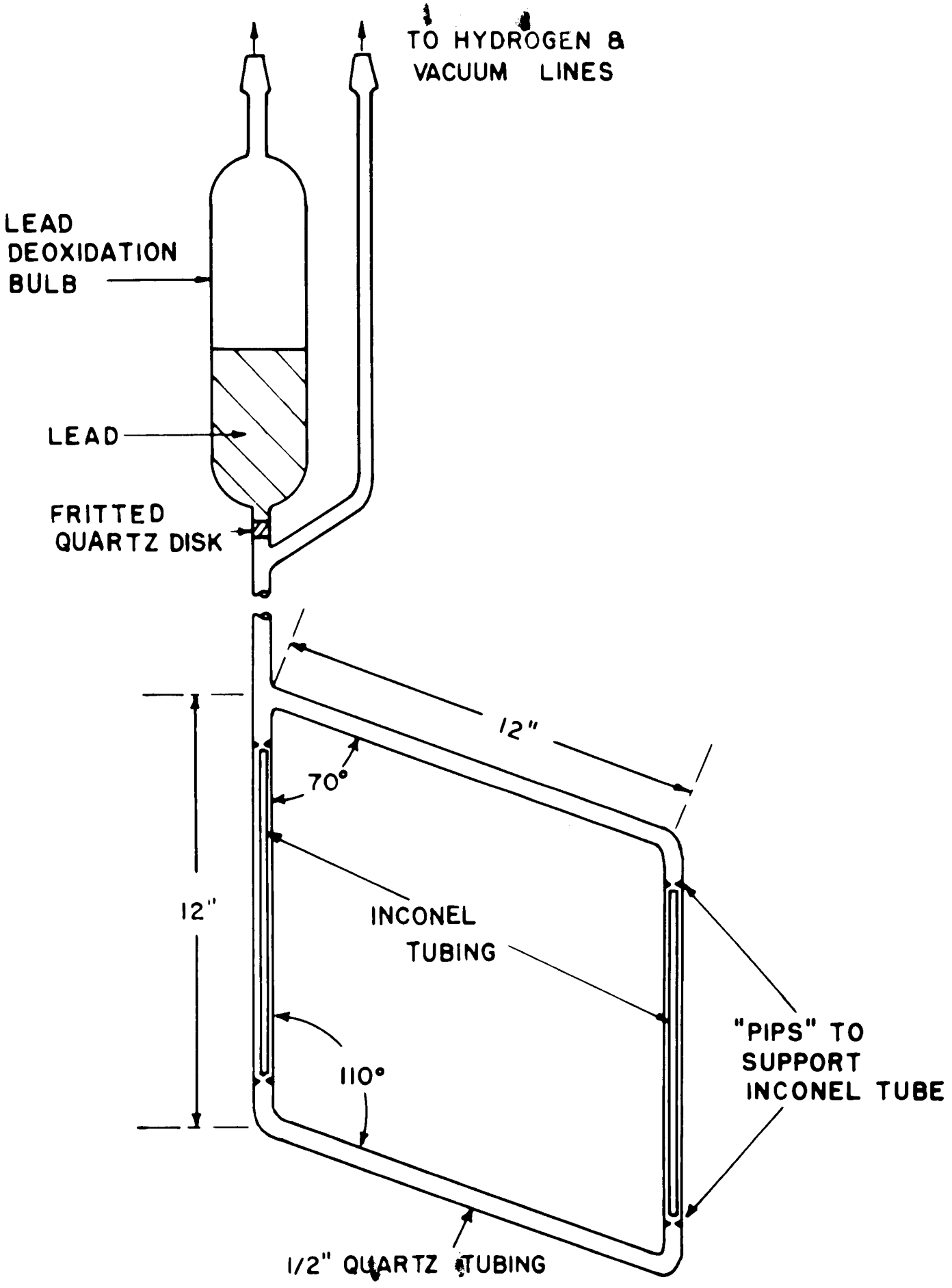

Fig. 92 (Y-8067) Quartz Thermal Convection Loop. Unclassified.

about 48 hr, surface tension forces prevented the liquid lead from passing through the fritted disk. When the deoxidation was complete, the loop was evacuated and hydrogen admitted into the deoxidation bulb. This caused the lead to flow through the fritted disk and into the loop.

The procedure assured that the oxide content of the lead was reduced to a minimum, and, in addition, prevented reoxidation of the lead during the loading of the loop. The technique offered several other advantages. Each loop required only a small amount of metal tubing, a factor of some importance in cases where the test metal was expensive or in short supply. No bending or welding of the test metal was required so that such hard-to-fabricate metals as chromium and molybdenum could be studied without difficulty. The fact that the test specimens were completely enclosed in the quartz tubing of the loop eliminated any necessity for protecting the outer surface of the test metal from air oxidation. This fact greatly facilitated the testing of such metals as molybdenum or columbium which are very reactive at high temperatures. The detection of leaks in a quartz loop prior to operation was also much easier than in conventional metal loops.

The relative resistance to mass transfer of one test metal, as compared to another, was obtained by measuring the time required for the build-up, in the cold leg of the loop, of a sufficient quantity of mass-transferred material to cause a stoppage in the circulation of the liquid lead. The plugs thus formed always consisted of porous matter of fine dendritic needles and platelets.

After a test had been completed, the loop was cut into short sections. Each section was placed in a tube such as is shown in Fig. 93. These tubes were divided into two compartments by fritted glass filter disks, and each compartment was connected to hydrogen and vacuum lines through a side arm. With the tube filled with hydrogen, the lead in a section from the loop was melted. By the proper manipulation of hydrogen pressure and vacuum, the molten lead was then filtered into the bottom

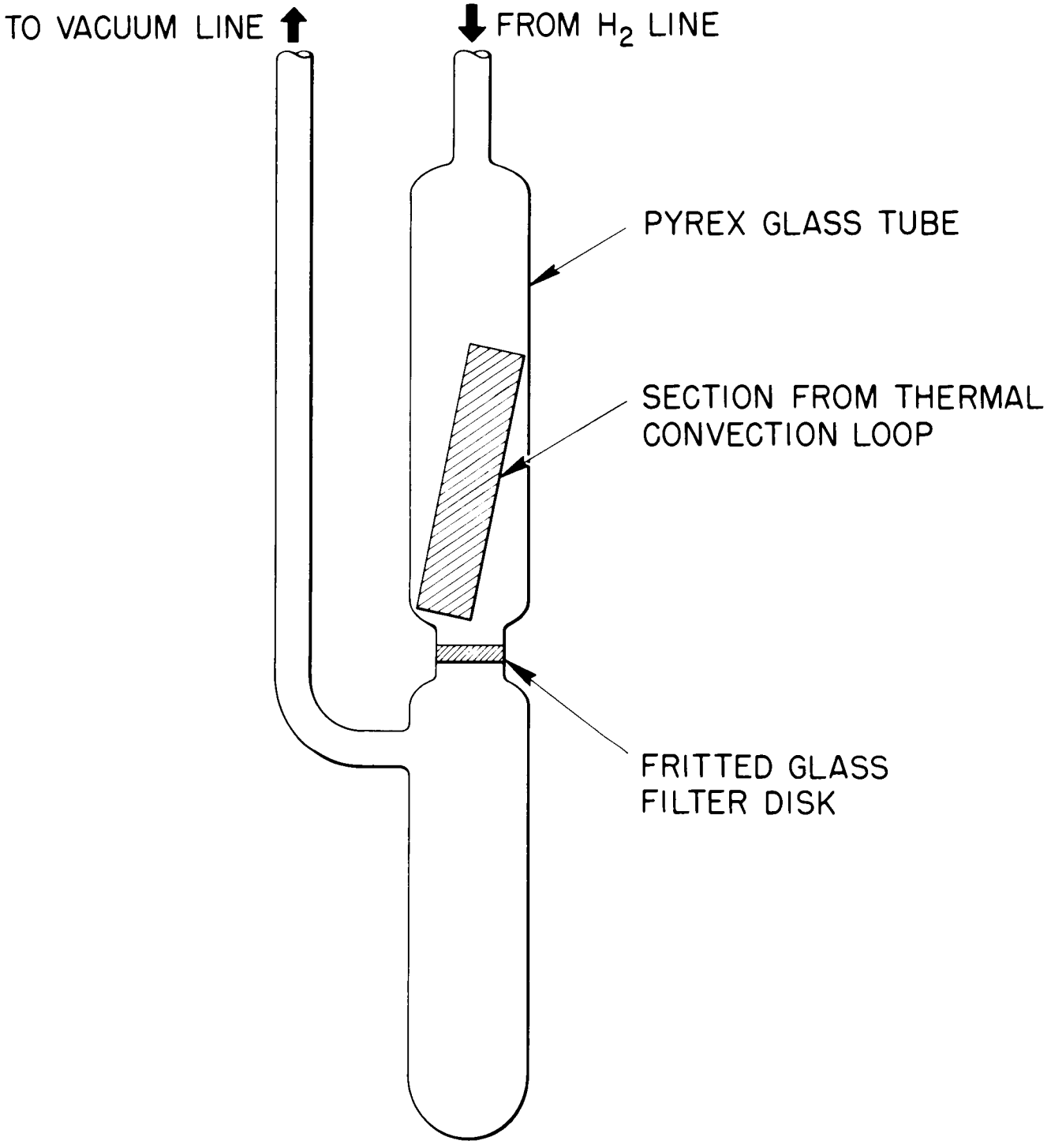

Fig. 93 (Y-12456) Apparatus for Removing Excess Lead from Loop Sections. Unclassified.

compartment. In this manner any mass-transferred material could be recovered and its position in the loop located.

A total of 23 metals and alloys have been tested. The results obtained are summarized in Fig. 94. Almost all of the tests were run in duplicate and the numbers which appear at the end of each of the bars on the figure indicate the average length of the test for the metal in question. In all cases, the hot- and cold-leg temperatures were about 800 and 500°C, respectively. In most experiments the loops were allowed to run until complete plugging occurred. However, in some cases involving metals having a relatively high resistance to mass transfer, the tests were stopped after 500 - 800 hr. These tests are indicated by a "delta" on the chart. Except for columbium and molybdenum, which did not exhibit mass transfer, small amounts of mass-transferred material were found in all these loops. It is presumed that complete plugging would have occurred had the loops been allowed to run long enough.

The metals which have been tested can be divided into three groups on the basis of their relative resistance to mass transfer and, in the case of the alloys, on their structural characteristics.

Group I: Metals in this group showed no mass transfer or corrosion in liquid lead under the test conditions. Only molybdenum and columbium fell into this category. Figure 95 shows a transverse section of the hot-leg specimen from a molybdenum loop. As may be seen, the surface of the metal was unattacked.

Group II: This category consists of all of the alloys which contain intermetallic compounds or whose compositions are relatively close to those corresponding to intermetallic compound formation. The materials in this group were types 410 and 446 stainless steels, Hastelloy B, 25% Mo-75% Ni, 2% Si-14% Cr-Fe, 45% Cr-55% Co, 50% Mo-50% Fe, 50% Cr-50% Fe, and 16% Ni-37% Cr-47% Fe (sigma and ferrite). With the exception of

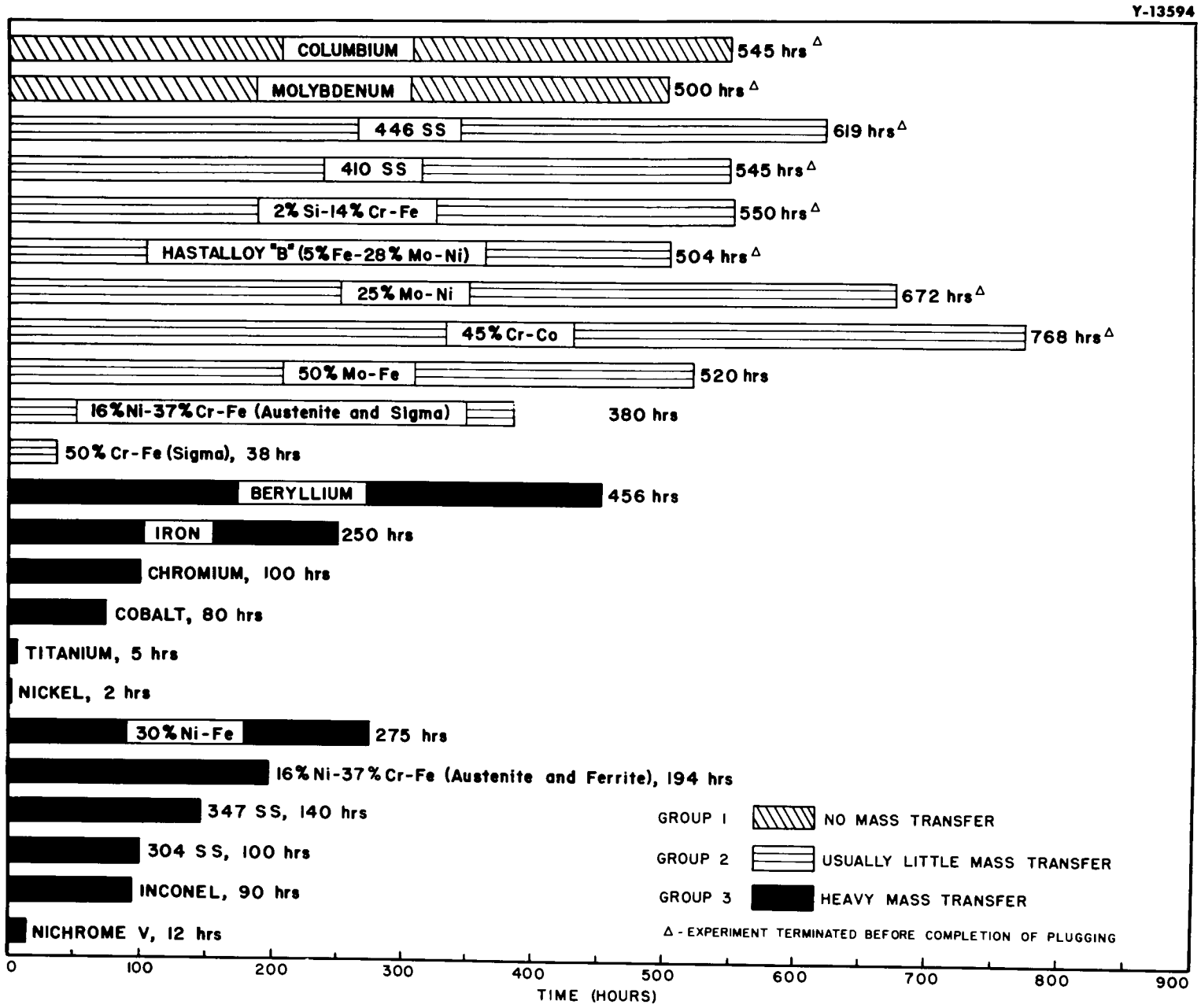

Fig. 94 (Y-13594) Mass Transfer in Liquid Lead. Unclassified.

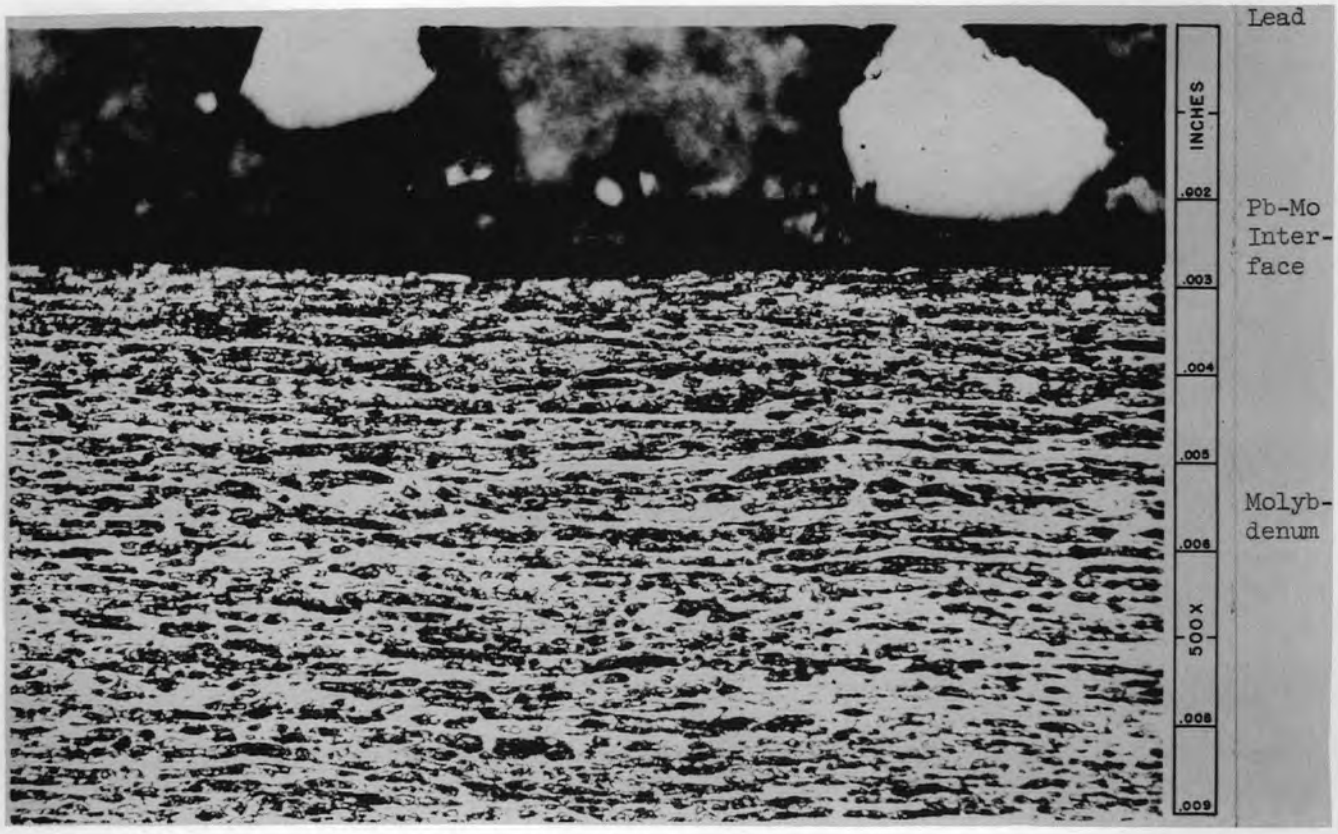

Fig. 95 (Y-8899) Transverse Section of Hot-Leg Specimen, Pb-Mo Loop. 500X. Unclassified.

the 50% Cr-50% Fe alloy, these metals all showed a much greater resistance to mass transfer in liquid lead than their individual components.

The corrosive attack on these materials varied considerably. Figure 96 shows shows a transverse section of the hot-leg specimen from a type 446 stainless steel loop where the corrosive attack was relatively light. On the other hand, the 25% Mo-Ni alloy suffered severe intergranular penetration as shown in Fig. 97.

Group III: Metals and alloys in this group include iron, nickel, chromium, titanium, beryllium, cobalt, types 347 and 304 stainless steels, 30% Ni-Fe and 16% Ni-37% Cr-47% Fe (ferrite and austenite) alloys, Nichrome V, and Inconel. These materials all showed relatively low resistance to mass transfer in liquid lead. The plugging times for the alloys were roughly those to be expected from the plugging times of their individual constituents. It should be noted that intermetallic compound formation is either impossible for the alloys of this group or else the compositions of the alloys are far removed from intermetallic phases.

A comparison of the data for the various metals tested thus indicates clearly that a tendency toward intermetallic compound formation in an alloy is associated with an increase in resistance to mass transfer in liquid lead. The only exception found to this general rule was the 50% Cr-50% Fe alloy. One possible explanation for the anomalous results obtained with the 50% Cr-50% Fe loops is based on the extensive system of cracks in the original test specimens (Fig. 98). These cracks no doubt increased the surface area-to-volume ratio to such an extent as to appreciably accelerate mass transfer. However, the amount of mass transferred material found in these loops was only about one-fourth of that observed in the normal loop. Thus, while it is conceivable that such small plugs could indeed have produced the failure of the loops, it seems more likely that the stoppages were caused in some other manner. When the test specimens were removed from the loops,

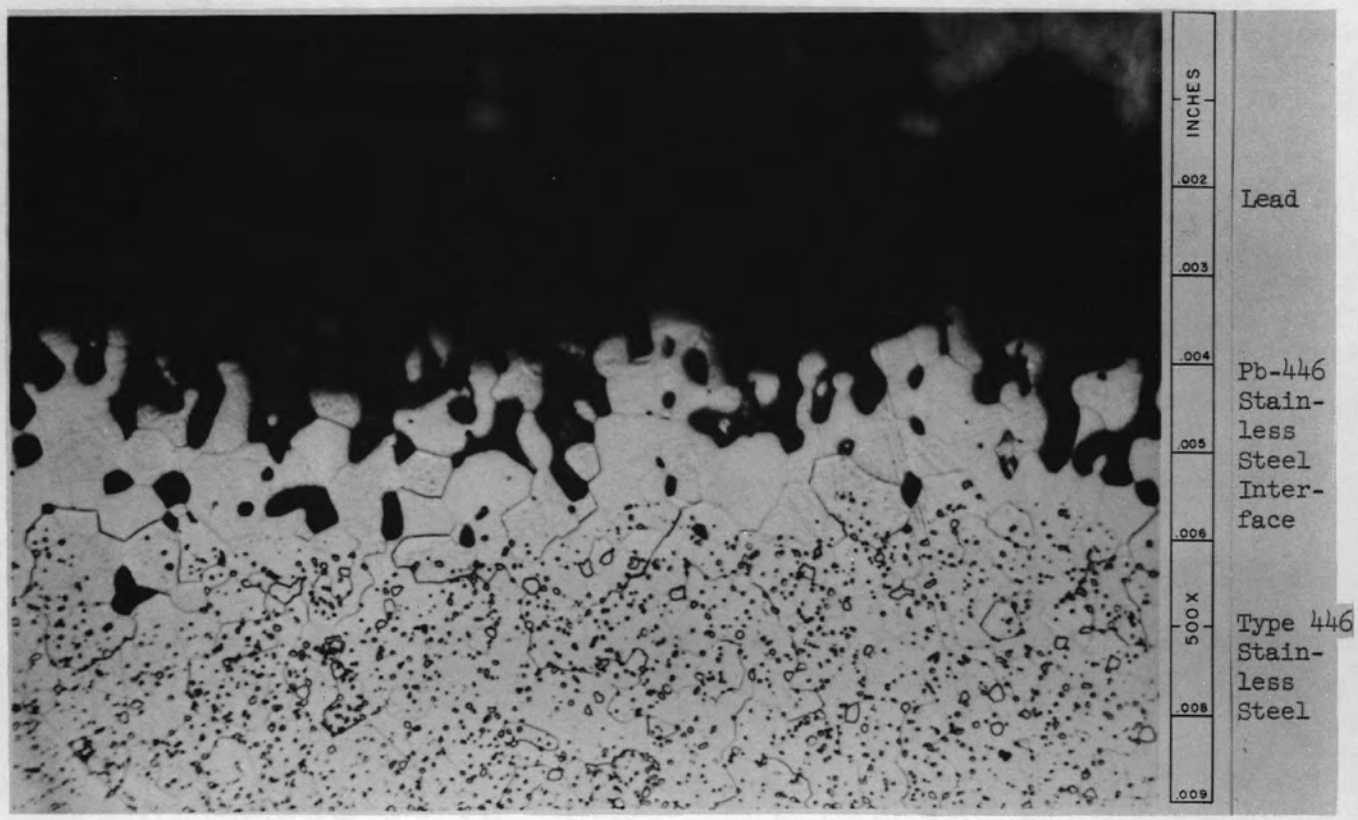

Fig. 96 (Y-9357) Transverse Section of Hot-Leg Specimen, Pb-446 Stainless Steel Loop. 500X. Unclassified.

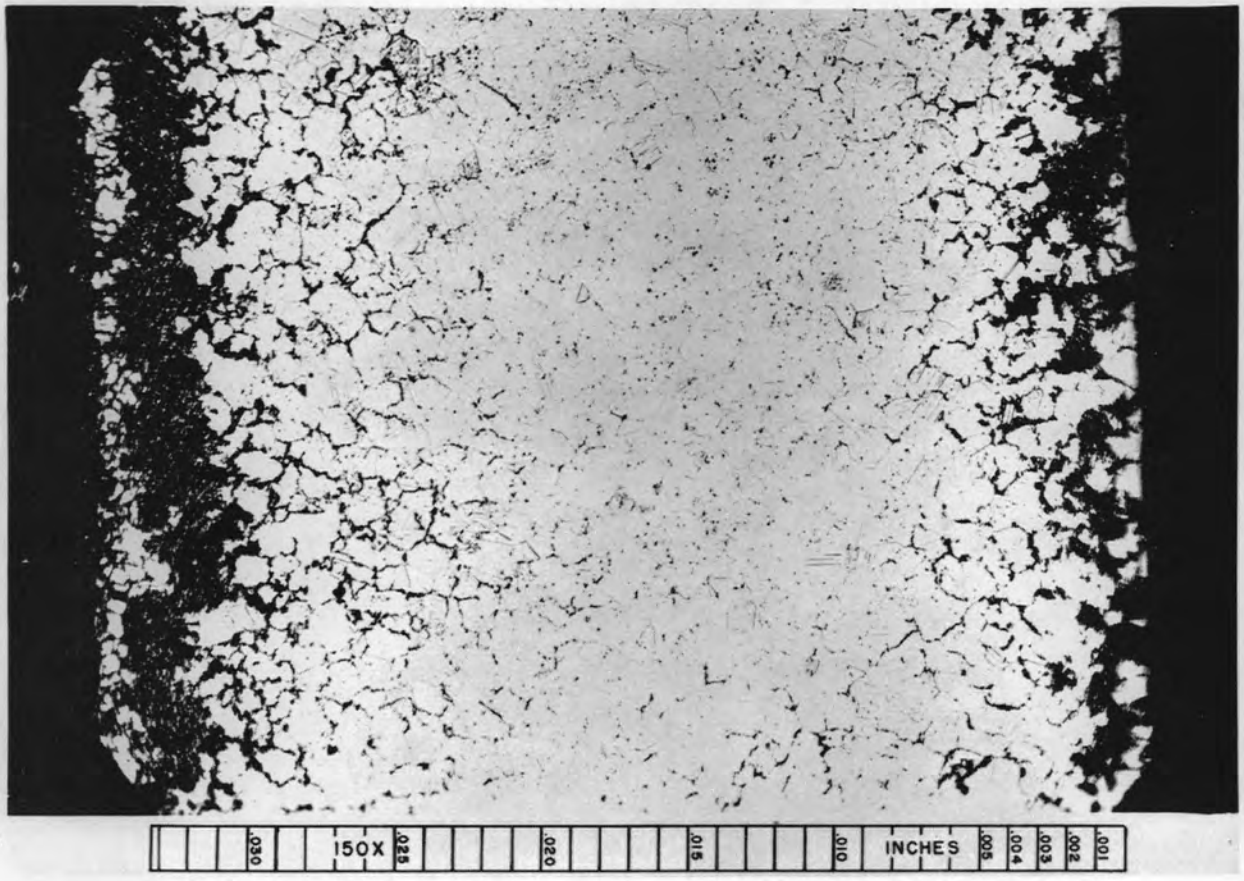

Fig. 97 (Y-10392) Transverse Section of Hot-Leg Specimen, Pb-25% Mo-Ni Loop. 150X. Unclassified.

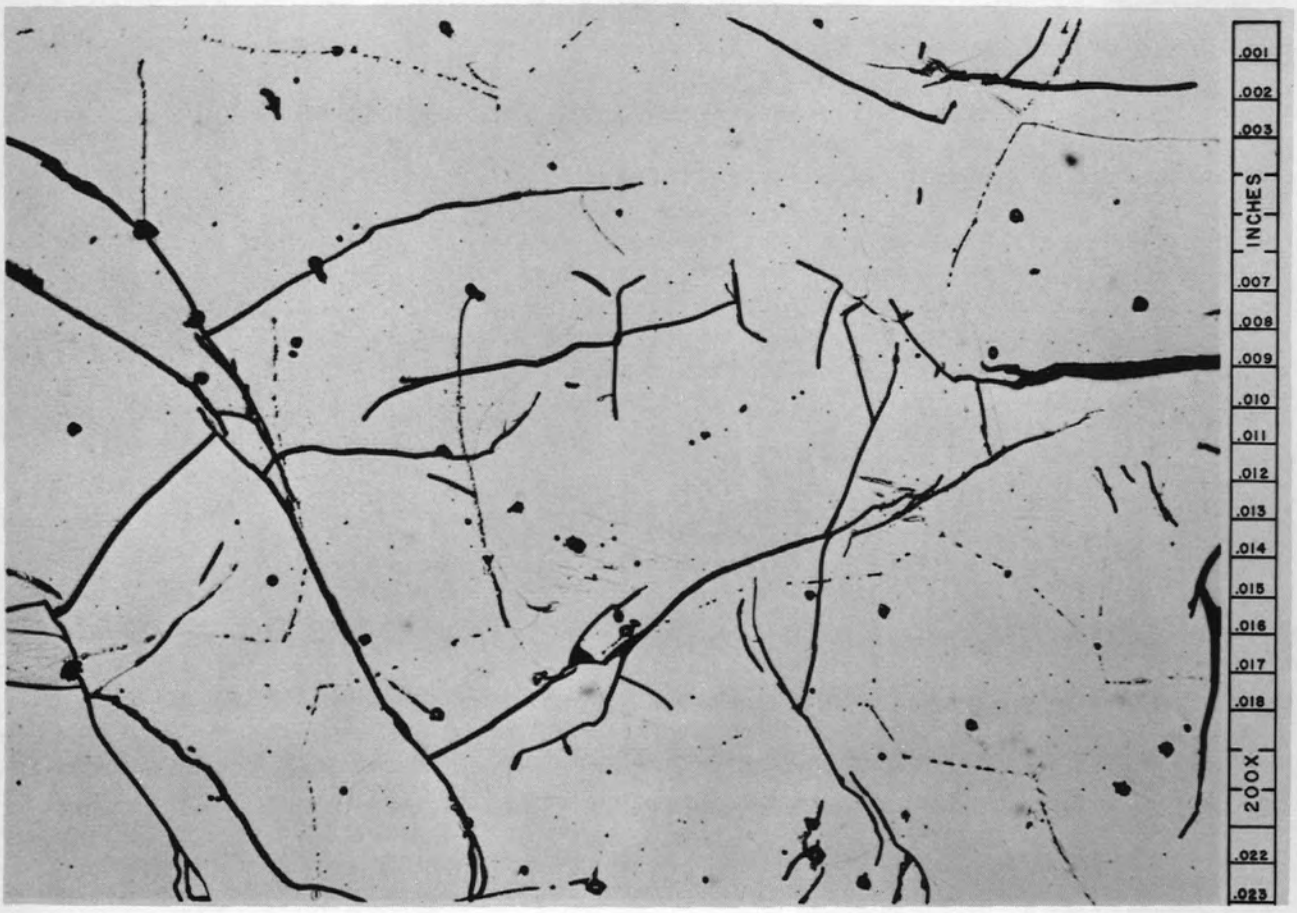

Fig. 98 (Y-13216) Transverse Section of a 50% Fe-50% Cr Specimen Before Contact with Lead Showing Extensive Crack Formation. 200X. Unclassified.

it was observed that they were exceedingly friable, crumbling into small pieces almost at the touch. If a small chunk of the test specimen had been completely or partially dislodged during the operation of the loop, it could have been caught in either the hot- or cold-leg specimen tubes and caused a sufficient slowing down of the lead circulation to produce premature failure of the loop. Because of the excessive brittleness of the test specimens, it was not possible to remove them from the loops without cracking them slightly; therefore, it is not possible to state unequivocably that this explanation is a valid one. However, the extensive cracking of the test specimens and their excessive friability would appear to justify the belief that the results obtained with the 50% Cr-50% Fe alloy may not be comparable to those obtained with other alloys in which intermetallic compound formation is possible.

LIST OF TABLES

LIST OF ILLUSTRATIONS

ORNL-2685
Reactors-Special Features
of Aircraft Reactors

INTERNAL DISTRIBUTION

1. C. [illegible] Center
2. Biolo[illegible] Library
3. Health [illegible]hysics Library
4. Metallurg[illegible] Library
5-6. Central Res[illegible]arch Library
7. Reactor Expe[illegible]mental Engineering Lib[illegible]ry
8-12. Laboratory Record[illegible] Department
13. Laboratory Records, [illegible]RNL R.C.
14. A. M. Weinberg
15. L. B. Emlet (K-25)
16. J. P. Murray (Y-12)
17. J. A. Swartout
18. E. D. Shipley
19. M. L. Nelson
20. W. H. Jordan
21. R. S. Livingston
22. R. R. Dickison
23. F. L. Culler
24. A. H. Snell
25. A. Hollaender
26. K. Z. Morgan
27. C. S. Harrill
28. C. E. Winters
29. D. S. Billington
30. A. J. Miller
31. R. A. Charpie
32. M. J. Skinner
33. A. L. Boch
34. H. G. MacPherson
35. W. R. Grimes
36. W. E. Browning
37. A. P. Fraas
38. W. B. McDonald
39. [illegible] W. Keilholtz
40. J. C. Wilson
[illegible]. H. W. Savage
42. J. H. Frye, Jr.
43. W. D. Manly
44. J. E. Cunningham
45. W. H. Cook
46. E. E. Hoffman
47. D. A. Douglas, Jr.
48. J. H. DeVan
49. P. Patriarca
50. G. M. Slaughter
51. J. H. Coobs
52. C. O. Smith
53. G. M. Adamson, Jr.
[illegible] R. S. Crouse
55. [illegible]. V. Cathcart
56. [illegible] Hikido
57. M. [illegible]. Hill
58. H. [illegible]buye
59. T. K. [illegible]oche
60. J. H. K[illegible]enig (consultant)
61. H. Leidhe[illegible]ser, Jr. (consultant)
62. C. S. Smit[illegible] (consultant)
63. H. A. Wilhel[illegible] (consultant)
64. ORNL - Y-12 T[illegible]hnical Library, Document Refere[illegible]ce Section

EXTERNAL DISTRIBUTION

65-68. Air Force Ballisti[illegible] Missile Division
69. AFPR, Boeing, Sea[illegible]le
70. AFPR, Boeing, Wic[illegible]ita
71. AFPR, Douglas, L[illegible]ng Beach
72-74. AFPR, Douglas, S[illegible]nta Monica
75-76. AFPR, Lockheed, Marietta
77. AFPR, North Am[illegible]rican, Canoga Park
78. AFPR, North A[illegible]erican, Downey
79-80. Air Force Spe[illegible]ial Weapons Center
81. Air Materiel Command

82-83. Air Research and Development Command (RDZN)
84. Air Technical Intelligence Center
85-87. ANP Project Office, Convair, Fort Worth
88. Albuquerque Operations Office
89. Argonne National Laboratory
90. Armed Forces Special Weapons Project, Sandia
91. Armed Forces Special Weapons Project, Washington
92-93. Army Ballistic Missile Agency
94. Army Rocket and Guided Missile Agency
95. Assistant Secretary of the Air Force, R&D
96-101. Atomic Energy Commission, Washington
102. Atomics International
103. Battelle Memorial Institute
104-106. Bettis Plant (WAPD)
107. Brookhaven National Laboratory
108. Bureau of Aeronautics
109. Bureau of Aeronautics General Representative
110. BAR, Aerojet-General, Azusa
111. BAR, Chance Vought, Dallas
112. BAR, Convair, San Diego
113. BAR, Grumman Aircraft, Bethpage
114. BAR, Martin, Baltimore
115. Bureau of Yards and Docks
116-117. Chicago Operations Office
118. Chicago Patent Group
119. Curtiss-Wright Corporation
120. Curtiss-Wright, Quehanna
121. Director of Naval Intelligence
122. duPont Company, Aiken
123. Engineer Research and Development Laboratories
124-131. General Electric Company (APPD)
132-133. General Electric Company, Richland
134. GE Company, San Jose (AT(30-3)-502)
135. General Nuclear Engineering Corporation
136. Hartford Aircraft Reactors Area Office
137. Idaho Test Division (LAROO)
138-139. Knolls Atomic Power Laboratory
140. Lockland Aircraft Reactors Operations Office
141. Los Alamos Scientific Laboratory
142. Marquardt Aircraft Company
143. Martin Company
144. National Advisory Committee for Aeronautics, Cleveland
145. National Advisory Committee for Aeronautics, Washington
146. National Bureau of Standards
147. Naval Air Development Center
148. Naval Air Material Center
149. Naval Air Turbine Test Station
150. Naval Research Laboratory

151. New York Operations Office
152. Nuclear Development Corporation of America
153. Nuclear Metals, Inc.
154. Oak Ridge Operations Office
155. Office of Naval Research
156. Office of the Chief of Naval Operations
157. Patent Branch, Washington
158-159. Phillips Petroleum Company (NRTS)
160-163. Pratt and Whitney Aircraft Division
164. San Francisco Operations Office
165. Sandia Corporation
166-167. School of Aviation Medicine
168. Sylvania-Corning Nuclear Corporation
169. Technical Research Group
170. USAF Headquarters
171. USAF Project Rand
172. U. S. Naval Radiological Defense Laboratory
173-174. University of California Radiation Laboratory, Livermore
175-186. Wright Air Development Center
187-211. Technical Information Service Extension
212. Division of Research and Development, AEC, ORO